

**THEORETICAL ANALYSIS OF THE
COMPLEXATION OF Ln(III) WITH
GLUTATHIONE/ Mg(II) : ITS THERMODYNAMICS
AND BIOLOGICAL PROPERTIES**

by

MHASIRIEKHO ZIEKHRÜ

Registration No: 786/2017



Submitted to

NAGALAND UNIVERSITY

In Fulfillment of Requirements for the Degree

of

DOCTOR OF PHILOSOPHY IN CHEMISTRY

DEPARTMENT OF CHEMISTRY

NAGALAND UNIVERSITY

LUMAMI-798627

NAGALAND, INDIA

2022



नागालैण्ड विश्वविद्यालय NAGALAND UNIVERSITY

(केंद्रीय विश्वविद्यालय) / (A Central University)

मुख्यालय : लुमामी, जिला : जुन्हेबोटो (नागालैण्ड) – 798 627

Hqrs: Lumami, Dist: Zunheboto, Nagaland – 798 627

Department of Chemistry

DECLARATION

I, Mr. Mhasiriekho Ziekhrü bearing Ph.D. Registration No. 786/2017 with effect from 30th August 2016, hereby declare that the subject matter of my Ph.D. thesis entitled “**Theoretical Analysis of the Complexation of Ln(III) with Glutathione/Mg(II): Its Thermodynamics and Biological Properties**” is the record of work done by me and also that the contents of this thesis did not comprise of the basis for the award of any previous degree/diploma to me or to anybody else in any other University/Institute, to the best of my knowledge.

This Ph.D. thesis is submitted in compliance with the UGC Regulation 2016 dated May 05, 2016 (Minimum Standard and Procedure for Award of M. Phil./Ph.D. Degree) to the Nagaland University for the degree of Doctor of Philosophy in Chemistry

Mhasiriekho
(Mhasiriekho Ziekhrü)

Upasax
15/12/22
Head

Department of Chemistry
Nagaland University

Indira Devi 15/12/2022
(Prof. M. Indira Devi)

Supervisor



नागालैण्ड विश्वविद्यालय NAGALAND UNIVERSITY

(केंद्रीय विश्वविद्यालय) / (A Central University)

मुख्यालय : लुमामी, जिला : जुन्हेबोटो (नागालैण्ड) – 798 627

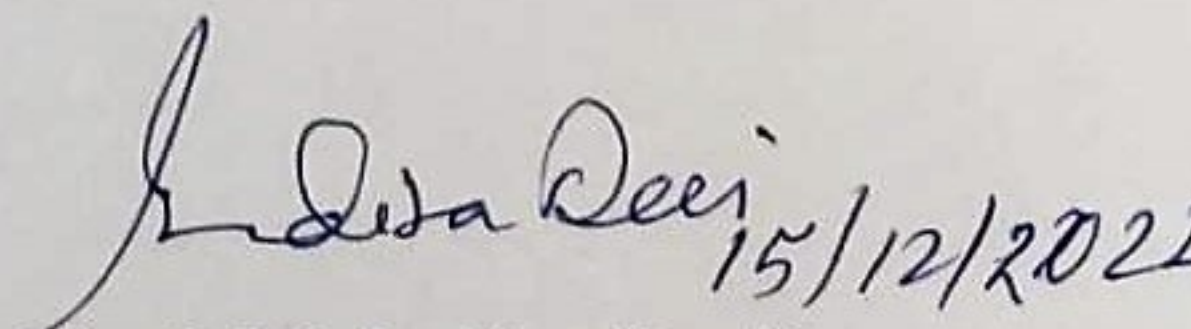
Hqrs: Lumami, Dist: Zunheboto, Nagaland – 798 627

Department of Chemistry

CERTIFICATE

This is to certify that **Mr. Mhasiriekho Ziekhrü**, a registered Research Scholar for Ph.D. degree in Chemistry under Nagaland University has carried out his research work under my guidance and supervision. His thesis entitled “**Theoretical Analysis of the Complexation of Ln(III) with Glutathione/Mg(II): Its Thermodynamics and Biological Properties**” embodies the original research work and has fulfilled all the requirements according to the rules/regulations of Nagaland University.

Further, to the best of my knowledge, the present research work has not been submitted to any University/Institution for the award of any degree or diploma.


(Prof. M. Indira Devi)
Supervisor



नागालैण्ड विश्वविद्यालय NAGALAND UNIVERSITY

(केंद्रीय विश्वविद्यालय) / (A Central University)

मुख्यालय : लुमामी, जिला : जुन्हेबोटो (नागालैण्ड) – 798 627

Hqrs: Lumami, Dist: Zunheboto, Nagaland – 798 627

Department of Chemistry

CERTIFICATE

This is to certify that **Mr. Mhasiriekho Ziekhrü**, a registered Research Scholar for Ph.D. degree in Chemistry under Nagaland University, bearing Ph.D. Registration No. **786/2017**, has satisfactorily completed all the courses offered in the Pre-Ph.D. Course Work Programme in the Department of Chemistry, Nagaland University, Hqrs. Lumami.

The course includes:

CHEM-601 Research Methodology

CHEM-602 Advance in Chemistry

CHEM-603 Literature Review, Report Writing and Presentation.


U. Saha
15/12/22

Head

Department of Chemistry

Nagaland University

Ph.D. COURSE WORK CERTIFICATES

**NAGALAND UNIVERSITY**

Sl. No. : 16- **59054**

STATEMENT OF MARKS

Ph. D COURSE WORK EXAMINATION, 2017


DEPARTMENT OF CHEMISTRY


The following are the marks secured by Mhasiriekho Ziekhriü

Roll No. 05/16 of Ph.D Course Work Examination held in 2017

Subject(s)/Paper(s)	Max. Marks	Minimum Qualifying Marks	Marks Secured
Paper No. Chem-601 Research Methodology	100	35	78
Paper No. Chem-602 Advance in Chemistry	100	35	68
Paper No. Chem-603 Literature Review, Report Writing and Presentation	100	35	76
Total Aggregate Marks			222
Average Pass Mark – 55 %			

Result	Division	Percentage
Passed	I Division	74 %

Marks compared by  H.Q. LUMAMI

COE/Dy. Reg./AR (Exams) 

NAGALAND UNIVERSITY

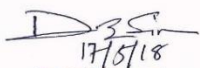
HEAD QUARTERS : LUMAMI

Ph. D COURSE WORK EXAMINATION


This is to certify that Mr/Ms. Mhasiriekho Ziekhriü

of Nagaland University bearing Roll No. 05/16 is qualified in the Ph.D Course Work Examination

in the Department of CHEMISTRY Nagaland University held in the Year 20. 17


17/05/18
Head of Department

Head
Department of Chemistry
Nagaland University


17/05/18
Dean,
School of Sciences
Nagaland University
H.Q. Lumami Nagaland

ACKNOWLEDGEMENTS

Thanks to the Almighty God for giving me the strength and ability to understand, learn and complete this work.

I have many people to thank for their help but words will probably fall short.

*I would like to thank my supervisor, **Prof. M. Indira Devi**, Department of Chemistry, Nagaland University, Headquarters – Lumami, for her valuable guidance, knowledge, advice and involvement in helping me complete my work successfully.*

I am thankful to the Department of Chemistry, Nagaland, University, Lumami, for providing laboratory facilities to carry out my Ph.D. thesis work. I would like to respectfully thank all the teaching and non-teaching staff in the Department of Chemistry for their assistance and cooperation. I also express my gratitude to my labmates and all my fellow research scholars for their constant support, love and help.

I thank the Ministry of Tribal affairs, India, for financial support through NFST fellowship.

Thank you to my family and friends for all your support throughout my studies at Nagaland University.

I stay grateful!

Date.....

(Mhasiriekho Ziekhru)

DEDICATIONS

This Ph.D. thesis is dedicated to my family. To my parents and sisters, for supporting me and believing that I could accomplish anything I put my mind to. Thank you for all of your support along the way. Thank you for being so patient with me and bringing out the best in me, even when research took turns for the worse. I couldn't have done this without you.

List of Figures

Figure 1.1	Shape of 4f-orbitals.	6
Figure 1.2	Typical Lanthanide Emission Spectra. (A) Eu(III)($^5D_0 \rightarrow ^7F_J$) f-f transitions ($J = 0-4$) of a triple-stranded helicate with approximate D_3 symmetry showing in the right insert the crystal-field splitting of the 7F_1 state. (B) Ce(III)($^2D_{3/2} \rightarrow ^2F_{7/2,5/2}$) d-f emission band in $Y_3Al_5O_{12}:Ce^{III}$ (0.33%) showing the spin-orbit splitting of the $4f^1$ configuration into $^2F_{7/2}$ and $^2F_{5/2}$.	14
Figure 1.3	Inert and labile forms of metal ions <i>in vivo</i> .	17
Figure 1.4	Chemical structures of (a) glutathione reduced (GSH) and (b) glutathione oxidized (GSSG).	23
Figure 1.5	Hypothetical reaction profile of the variation of concentration of reactants and products with time.	26
Figure 1.6	A plot between $\log k$ and $1/T$.	28
Scheme 1.1	Biosynthesis of glutathione.	23
Figure 2.1	Comparative absorption spectra of Pr(III), Pr(III):GSH and Pr(III):GSH:Mg(II) in DMF at pH 2.	71
Figure 2.2	Comparative absorption spectra of Pr(III), Pr(III):GSH and Pr(III):GSH:Mg(II) in DMF at pH 4.	71
Figure 2.3	Comparative absorption spectra of Pr(III), Pr(III):GSH and Pr(III):GSH:Mg(II) in DMF at pH 6.	72
Figure 2.4	Comparative absorption spectra of Pr(III), Pr(III):GSH and Pr(III):GSH:Mg(II) in CH_3CN at pH 2.	72
Figure 2.5	Comparative absorption spectra of Pr(III), Pr(III):GSH and Pr(III):GSH:Mg(II) in CH_3CN at pH 4.	73
Figure 2.6	Comparative absorption spectra of Pr(III), Pr(III):GSH and Pr(III):GSH:Mg(II) in CH_3CN at pH 6.	73
Scheme 2.1	Probable structure of (a) Pr(III):GSH and (b) Pr(III):GSH:Mg(II) complex.	59
Figure 3.1	Comparative absorption spectra of Pr(III), Pr(III):GSH and Pr(III):GSH:Mg(II) in DMF.	94
Figure 3.2	Comparative absorption spectra of Pr(III), Pr(III):GSH and	94

	Pr(III):GSH:Mg(II) in CH ₃ CN.	
Figure 3.3	Comparative absorption spectra of Pr(III), Pr(III):GSH and Pr(III):GSH:Mg(II) in dioxane.	95
Figure 3.4	Comparative absorption spectra of Pr(III), Pr(III):GSH and Pr(III):GSH:Mg(II) in methanol.	95
Figure 3.5	Comparative UV-Vis absorption spectra of Pr(III):GSH:Mg(II) complex in DMF at 303K at different hours.	96
Figure 3.6	Comparative UV-Vis absorption spectra of Pr(III):GSH:Mg(II) complex in DMF at 308K at different hours.	96
Figure 3.7	Plot of P_{obs} vs time (hr) of the $^3H_4 \rightarrow ^3P_2$ transition of Pr(III):GSH:Mg(II) at 303K, 308K, 313K and 318K.	97
Figure 3.8	Plot of $\log k$ vs $(1/T) \times 10^3$ of Pr(III):GSH:Mg(II) complex in DMF-water solvent.	97
Figure 4.1	Comparative absorption spectra of Pr(III), Pr(III):GSH and Pr(III):GSH:Mg(II) in CH ₃ CN.	117
Figure 4.2	Comparative absorption spectra of Pr(III), Pr(III):GSH and Pr(III):GSH:Mg(II) in CH ₃ OH.	117
Figure 4.3	Comparative absorption spectra of Pr(III), Pr(III):GSH and Pr(III):GSH:Mg(II) in DMF.	118
Figure 4.4	Comparative absorption spectra of Pr(III), Pr(III):GSH and Pr(III):GSH:Mg(II) in dioxane.	118
Figure 4.5	Comparative absorption spectra of Pr(III), Pr(III):GSH and Pr(III):GSH:Mg(II) in DMF at pH 2.	119
Figure 4.6	Comparative absorption spectra of Pr(III), Pr(III):GSH and Pr(III):GSH:Mg(II) in DMF at pH 4.	119
Figure 4.7	Comparative absorption spectra of Pr(III), Pr(III):GSH and Pr(III):GSH:Mg(II) in DMF at pH 6.	120
Figure 5.1	FTIR spectra of (A) Pr(III):GSH complex and (B) Glutathione.	125
Figure 5.2	Probable structure of Pr(III):GSH complex.	125
Figure 5.3	XRD pattern of Pr(III):GSH complex.	127
Figure 5.4	SEM micrography for the praseodymium(III) complex.	128
Figure 5.5	TGA curve of the Pr(III):GSH complex.	129

Figure 5.6	Mechanism of DPPH scavenging.	131
Figure 5.7	DPPH free radical scavenging activity in the presence of different concentrations of (A) Trolox and (B) sample.	132
Figure 5.8	Antioxidant activity of standard (Trolox) and the sample using FRAP assay.	134
Figure 5.9	Estimation of antimicrobial activity by agar plate diffusion experiment (A) <i>Escherichia coli</i> (B) <i>Bacillus subtilis</i> (C) <i>Staphylococcus aureus</i> and (D) <i>Klebsiella pneumoniae</i> .	136

List of Tables

Table 1.1	Discovery of the lanthanide elements.	3
Table 1.2	The electronic configurations of lanthanides along with their ground states.	5
Table 1.3	Physical Properties of Lanthanide Elements La-Eu.	9
Table 1.4	Physical Properties of Lanthanide Elements Gd-Lu.	10
Table 1.5	Salient properties of calcium and lanthanide.	16
Table 1.6	The critical roles of Glutathione.	24
Table 1.7	Experimentally observed hypersensitive transitions of Ln(III) ions in optical spectra.	33
Table 2.1	The zero-order energies and partial derivatives with respect to F_k and ζ_{4f} parameters for Pr(III).	55
Table 2.2	Matrix elements $U^{(\lambda)}$ for Pr(III) aquo.	57
Table 2.3	Computed values of various energy interaction parameters: Slater-Condon F_k (cm^{-1}), Lande ζ_{4f} (cm^{-1}), Racah E^k (cm^{-1}), nephelauxetic effect (β), bonding ($b^{1/2}$) and covalency (δ) for the different Pr(III) systems in aquated organic solvents (DMF:H ₂ O, MeCN:H ₂ O) at pH 2, 4 and 6	67
Table 2.4	Observed and computed values of energies (cm^{-1}) and RMS values of the different Pr(III) complexation systems in different solvents (DMF:H ₂ O, MeCN:H ₂ O) at pH 2, 4 and 6.	68
Table 2.5	Observed and computed values of oscillator strength (P), and Judd-Ofelt (T_λ) parameters of the different Pr(III) systems in aquated organic solvents (DMF:H ₂ O, MeCN:H ₂ O) at pH 2, 4 and 6.	69-70
Table 3.1	Computed values of the energy interaction parameters: Slater-Condon factor F_k (cm^{-1}), Lande spin-orbit interaction ζ_{4f} (cm^{-1}), Racah E^k , Nephelauxetic ratio (β), bonding ($b^{1/2}$) and percent covalency (δ) parameter of Pr(III) and its complexes in 50% (v/v) aquated solvents of CH ₃ OH, C ₄ H ₈ O ₂ , CH ₃ CN and DMF.	88
Table 3.2	Observed and computed values of oscillator strengths ($P \times 10^6$) and Judd-Ofelt ($T_\lambda \times 10^{10}$) parameters of Pr(III) and its complexes in 50% (v/v) aquated solvents of CH ₃ OH, C ₄ H ₈ O ₂ , CH ₃ CN and DMF.	89

Table 3.3	Observed and calculated oscillator strengths ($P \times 10^6$) and Judd-Ofelt intensity parameters ($T_\lambda \times 10^{10}$) parameters for Pr(III):GSH:Mg(II) complex at 303K (30°C) at different hours.	90
Table 3.4	Observed and calculated oscillator strengths ($P \times 10^6$) and Judd-Ofelt intensity parameter ($T_\lambda \times 10^{10}$) parameters for Pr(III):GSH:Mg(II) complex at 308K (35°C) at different hours.	91
Table 3.5	Observed and calculated oscillator strengths ($P \times 10^6$) and Judd-Ofelt intensity parameter ($T_\lambda \times 10^{10}$) parameters for Pr(III):GSH:Mg(II) complex at 313K (40°C) at different hours.	92
Table 3.6	Observed and calculated oscillator strengths ($P \times 10^6$) and Judd-Ofelt intensity parameter ($T_\lambda \times 10^{10}$) parameters for Pr(III):GSH:Mg(II) complex at 318K (45°C) at different hours.	93
Table 3.7	Rate constants at different temperatures (303K, 308K, 313K, 318K) and activation energy (E_a) of Pr(III):GSH:Mg(II).	98
Table 3.8	Thermodynamic parameters (ΔH^0 , ΔG^0 and ΔS^0) of Pr(III):GSH:Mg(II) complexation at different temperatures.	98
Table 4.1	The zero-order energies and partial derivatives with respect to F_k and ζ_{4f} parameters for Nd(III).	105
Table 4.2	Computed values of energy interaction parameters; Slater-Condon F_k (cm^{-1}), Lande ζ_{4f} (cm^{-1}), Racah (E^k), Nephelauxetic ratio (β), bonding ($b_{1/2}$) and percent covalency (δ) parameters of Nd(III) and its complexes with GSH and Mg(II) in 50% (v/v) aquated solvents of CH_3OH , $\text{C}_4\text{H}_8\text{O}_2$, CH_3CN and DMF.	113
Table 4.3	Computed and observed values of energies (cm^{-1}) and RMS values of Nd(III), Nd(III):GSH, Nd(III):GSH:Mg(II) in different solvents.	114
Table 4.4	Computed values of energy interaction parameters: Slater-Condon F_k (cm^{-1}), Lande ζ_{4f} (cm^{-1}), Racah (E^k), Nephelauxetic ratio (β), bonding ($b_{1/2}$) and percent covalency (δ) parameters of Nd(III) and its complexes in 50% (v/v) aquated DMF at pH 2, 4 and 6.	115
Table 4.5	Computed and observed values of energies (cm^{-1}) and RMS values of Nd(III), Nd(III):GSH, Nd(III):GSH:Mg(II) in DMF solvent at pH 2, 4 and 6.	116
Table 5.1	Powder XRD data praseodymium(III) complex with glutathione.	127

Table 5.2	DPPH radical scavenging activity, IC ₅₀ values of the standard Trolox and the sample.	132
Table 5.3	Zone of inhibition (mm) of Pr(III):GSH in comparison with the standard streptomycin.	135
Table 5.4	Minimum inhibitory concentration of Pr(III):GSH in mg/ml in comparison with the standard streptomycin.	135

CONTENTS

Declaration

Certificates

Acknowledgment

Dedication

List of Figures

List of Tables

Chapter 1

1-49

Introduction

1.1 Lanthanides: General Features

1.1.1 End Uses of Lanthanides

1.2 Review on Lanthanide Coordination Chemistry and its Biological Relevance

1.3 Glutathione - The Basics

1.4 Chemical kinetics

1.4.1 Factors that affect reaction rates

1.4.2 Activation energy and the rate of the reaction

1.4.3 Arrhenius rate equation

1.5 Spectroscopic Features of Lanthanides

1.5.1 Hypersensitive transitions

1.6 Purpose of the research

References

Chapter 2

50-73

Spectral analysis of the complexation of Pr(III) with GSH in the presence and absence of Mg(II) at different pH

2.1 Introduction

2.2 Experimental

2.3 Methods

2.4 Results and discussions

References

Tables

Figures

Chapter 3

74-98

Spectral analysis of the complexation of Pr(III) with GSH in the presence and absence of Mg(II) in different solvents and kinetics for the complexation of Pr(III):GSH with Mg(II)

3.1 Introduction

3.2 Experimental

3.3 Methods

3.4 Results and discussions

References

Tables

Figures

Chapter 4

99-120

Spectral analysis of the complexation of Nd(III) with GSH in the presence and absence of Mg(II) in different solvents and pH

4.1 Introduction

4.2 Experimental

4.3 Methods

4.4 Results and discussions

References

Tables

Figures

Chapter 5

121-140

Synthesis, characterization, antioxidant and antibacterial studies of praseodymium complex with glutathione

5.1 Introduction

5.2 Experimental

5.2.1 Materials and methods

5.2.2 Preparation of the complex

5.2.3 *In vitro* Antioxidant assays

5.2.4 *In vitro* Antibacterial activity

5.3 Results and discussions

5.3.1 Fourier transform infrared spectroscopy (FTIR)

5.3.2 X-ray diffraction (XRD)

5.3.3 Scanning Electron Microscopy (SEM)

5.3.4 Thermogravimetric analysis (TGA)

5.3.5 *In vitro* Antioxidant activity

(a) Radical scavenging assay (DPPH)

(b) Reducing power assay

5.3.6 *In vitro* Antibacterial activity

References

Chapter 6

141-143

Summary and conclusions

Appendix

CHAPTER 1

INTRODUCTION

The lanthanides are a series of fifteen chemical elements from lanthanum (La) to lutetium (Lu) with atomic number 57 to 71. The 15 elements, together with their chemical symbols, are lanthanum (La), cerium (Ce), praseodymium (Pr), neodymium (Nd), promethium (Pm), samarium (Sm), europium (Eu), gadolinium (Gd), terbium (Tb), dysprosium (Dy), holmium (Ho), erbium (Er), thulium (Tm), ytterbium (Yb) and lutetium (Lu). The series takes the name of “rare earths” when Scandium and Yttrium are added to it. The Group 3 elements namely scandium (Sc), yttrium (Y), lanthanum (La) and actinium (Ac) are as a matter of fact the first elements of their corresponding d-transition series (3d, 4d, 5d and 6d). The remaining lanthanides i.e., Cerium-Lutetium aren't included in the main frame of the periodic table of elements, thus they are usually written separately towards the bottom, primarily to make the chart more compact. This is a reflection of the fact that the name lanthanide comes from the Greek word *lanthanein* which means “to escape notice” [1]. The position of lanthanides in the periodic table has been and continues to be a source of contention, with numerous new periodic classifications lately proposed, some of which mix the d- and f-block elements [2]. The term “lanthanide” was coined by Victor Goldschmidt in the year 1925 [3,4]. The lanthanide series of chemical elements resemble each other in their chemical and physical properties. They are characterized by the gradual filling up of electrons in the 4f-shell. The lanthanides are referred to as 4f elements because their 4f shells are partially occupied by the electrons. The f electrons of lanthanides are well

shielded by the 5s, 5p and 6s subshells. The general electronic configuration of lanthanides is $(n-2)f^{1-14} (n-1)d^{0-1} ns^2$. The most stable oxidation state of the lanthanide elements is +3 since their 4f- electrons are only relatively involved in bonding. But oxidation number +2 exists for all lanthanides (except radioactive and short-lived Pm), at least in the form of organometallic complexes. Furthermore, cerium has a relatively stable +4 oxidation state with configuration [Xe], whereas the other ions have far less access to this state (except in some Pr and Tb inorganic compounds such as LnF_4). At atomic number 57, there is a sharp reduction in the energy of the 4f atomic orbitals (below that of the 5d orbitals) which causes progressive filling of these orbitals after La. The filled 5s, 5p and 6s sub-shells significantly shield the f orbitals that penetrate the xenon core. As a result, there is very little interaction with ligand orbitals. The stereochemistry of the lanthanide complexes is guided by the ligands' steric features and the ligand-field effects are minimal, hence the surroundings of the metal ion has little effect on its spectroscopic and magnetic characteristics [5].

The lanthanides were discovered after more than a century of research, beginning in the late 1700s. The first rare earth to be discovered was sesquioxide yttria, Y_2O_3 in 1794 but was only separated and characterized after more than 100 years, lutetium being the last one (1907) and promethium which is radioactive was synthesized in 1947 [6]. Although discovered in 1794, they were not characterized until a century later because of their scarcity in pure form and high insolubility. Johan Gadolin (1760-1852), a Finnish scientist, investigated ytterbia, an impure form of yttrium oxide, in 1794, believing it to be a new element. Sir Humphry Davy (1778-1829), an English chemist, demonstrated that ytterbia was a combination made up of oxygen and a metal, rather than an element, more than a decade later. Berzelius and Klaproth isolated the first Cerium compound in 1803. Moseley later proved that there were fourteen elements between Lanthanum and Hafnium by using

x-ray spectra of the elements [7,8]. The remaining elements were extracted from the same mineral afterwards. Table 1.1 presents an overview of lanthanide history [9]. Separating the lanthanides was difficult for nineteenth-century chemists since several of them occur together in the same minerals and have close chemical similarities. This made separation and purification of lanthanides difficult and caused a lot of confusion because it was hard

Table 1.1: Discovery of the lanthanide elements.

Lanthanide	Year	Discoverer	Origin of Name
Lanthanum (La)	1839	Mosander	Lanthanum: Greek for “to lie hidden”
Cerium (Ce)	1803	1. Berzelius and Hisinger 2. Klaproth	Ceres, an asteroid discovered in 1801
Praseodymium (Pr)	1885	Von Welsbach	From Greek: <i>prasios</i> - green; <i>dymium</i> -twin
Neodymium (Nd)	1885	Von Welsbach	From Greek: <i>Neo</i> - new; <i>dymium</i> - twin
Promethium (Pm)	1947	1. Marinsky 2. Glenenine 3. Coryell	Prometheus, the Greek God who stole fire from Heaven for men’s use.
Samarium (Sm)	1879	De Boisbaudran	From its ore, Samarskite, named after the Russian engineer Samarski
Europium (Eu)	1889	Crookes	Europe
Gadolinium (Gd)	1880	Marignac	After the Finnish chemist Gadolin
Terbium (Tb)	1843	Mosander	After the town of Ytterby in Sweden
Dysprosium (Dy)	1886	De Boisbaudran	From Greek: <i>Dysprositors</i> - hard to get at
Holmium (Ho)	1879	1. Cleve 2. Soret	Holmia, Latinized version of Stockholm
Erbium (Er)	1843	Mosander	After the town of Ytterby in Sweden
Thulium (Tm)	1878	Cleve	After Thule, the roman name for the northernmost region of the inhabitable world
Ytterbium (Yb)	1878	Marignac	After the town of Ytterby in Sweden
Lutetium (Lu)	1908 1907	1. Von Welsbach 2. Urbain	Lutetia, Latin for Paris

to tell one element from another or from its mineral precursor. Due to the fact that they are obtained from relatively rare minerals, these elements were first categorized as "rare earth." This can however be deceiving because the Lanthanide elements have a practically infinite abundance.

1.1 Lanthanides: General Features

The Lanthanides, like any other series in the periodic table, such as the Alkali metals or Halogens, have a lot of similarities. The following are some of these characteristics [10]:

- Physical properties are similar throughout the series.
- The +3 oxidation state is primarily adopted. It is most commonly seen in crystalline compounds.
- They can also be in the +2 or +4 oxidation states, while some lanthanides are more stable in the +3 state.
- Compounds with coordination numbers more than 6 (typically 8-9).
- Across the series, there is a tendency for the coordination number to decrease.
- Binding preference for more electronegative elements (such as O or F).
- Effects of crystal fields is small.
- Very less dependence on ligands.
- Rapid ligand-exchange occurs in ionic complexes.

The electronic configuration of the lanthanides are shown in Table 1.2.

Table 1.2: The electronic configurations of lanthanides along with their ground states and valences.

Lanthanide element	Atomic number	Symbol	Neutral atom electronic configuration	Possible valence state	<u>Trivalent atom</u>	
					Electronic configuration	Ground state
Lanthanum	57	La	[Xe] 4f ⁰ 5d ¹ 6s ²	3	[Xe] 4f ⁰	¹ S ₀
Cerium	58	Ce	[Xe] 4f ¹ 5d ¹ 6s ²	3, 4	[Xe] 4f ¹	² F _{5/2}
Praseodymium	59	Pr	[Xe] 4f ³ 6s ²	3	[Xe] 4f ²	³ H ₄
Neodymium	60	Nd	[Xe] 4f ⁴ 6s ²	3	[Xe] 4f ³	⁴ I _{9/2}
Promethium	61	Pm	[Xe] 4f ⁵ 6s ²	3	[Xe] 4f ⁴	⁵ I ₄
Samarium	62	Sm	[Xe] 4f ⁶ 6s ²	2, 3	[Xe] 4f ⁵	⁶ H _{5/2}
Europium	63	Eu	[Xe] 4f ⁷ 6s ²	2, 3	[Xe] 4f ⁶	⁷ F ₀
Gadolinium	64	Gd	[Xe] 4f ⁷ 5d ¹ 6s ²	3	[Xe] 4f ⁷	⁸ S _{7/2}
Terbium	65	Tb	[Xe] 4f ⁹ 6s ²	3, 4	[Xe] 4f ⁸	⁷ F ₆
Dysprosium	66	Dy	[Xe] 4f ¹⁰ 6s ²	3	[Xe] 4f ⁹	⁶ H _{15/2}
Holmium	67	Ho	[Xe] 4f ¹¹ 6s ²	3	[Xe] 4f ¹⁰	⁵ I ₈
Erbium	68	Er	4f ¹² 6s ²	3	[Xe] 4f ¹¹	⁴ I _{15/2}
Thulium	69	Tm	4f ¹³ 6s ²	3	[Xe] 4f ¹²	³ H ₆
Ytterbium	70	Yb	4f ¹⁴ 6s ²	2, 3	[Xe] 4f ¹³	² F _{7/2}
Lutetium	71	Lu	4f ¹⁴ 5d ¹ 6s ²	3	[Xe] 4f ¹⁴	¹ S ₀

As we progress from La to Lu, the atomic size decreases with increasing atomic number. Hence, Lanthanum has the highest atomic radius while Lutetium has the smallest atomic radius among the Lanthanides. This phenomenon of a steady decrease in the atomic and ionic size of lanthanides with an increase in atomic number is termed Lanthanide

Contraction. The presence of "lanthanide contraction," is an important property of lanthanide elements. The screening effect of increased nuclear charge by inner sphere 4f-electrons is the primary cause of lanthanide contraction. This is the result of a poor shielding effect of the 4f electrons. This is in turn because of the improper shape of the f-orbitals (Fig. 1.1).

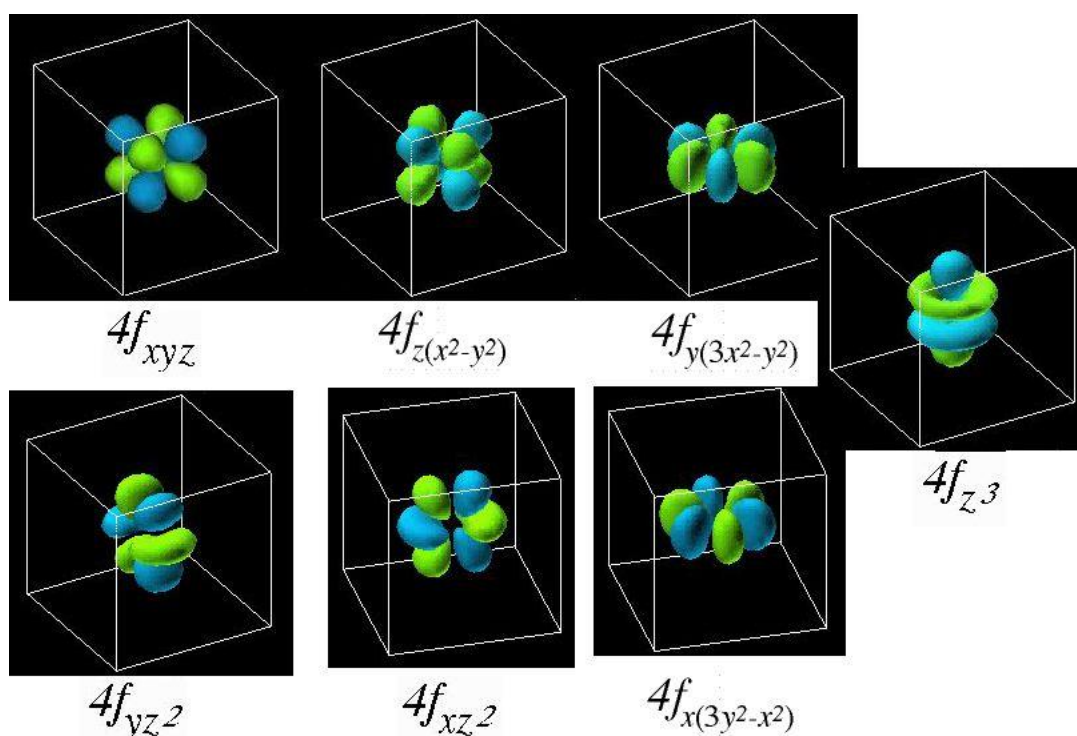


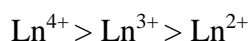
Fig. 1.1: Shape of 4f-orbitals.

The shielding effect is a phenomenon in which the inner-shell electrons shield the outer-shell electrons from the effects of nuclear charge. When the shielding isn't as good, the positively charged nucleus attracts the electrons more, decreasing the atomic radius as the atomic number rises. As the atomic number increases, so does the number of incoming electrons, and therefore the nuclear charge. The electrons are attracted to the nucleus due to inappropriate shielding, resulting in a decrease in size. The decrease in size isn't uniform all through the lanthanides and in comparison, to the rest of the elements, the first six

elements show a rapid decrease. Table 1.3 and Table 1.4 shows selected physical properties of lanthanides.

Separation of lanthanides is possible due to the reduction in size from one lanthanide to the next, however, it is difficult due to the smallness and regularity of the drop in size. The radius of Ho(III) has been lowered to the point where it is nearly identical to that of Y(III), which is why a much lighter element is associated with a heavier lanthanide [11]. The overall lanthanide contraction is comparable to the expansion observed while transitioning from the first to the second transition series, and this may hence be expected to occur while passing from the second to the third transition series. The interpolation of the lanthanides, on the other hand, almost totally cancels this projected increase, resulting in very similar sizes and properties for the second and third members of each group of transition elements.

Lanthanides have a low charge density due to their huge size; as a result, they cannot induce much polarization and so have no tendency to form complexes. They do, however, form compounds with chelating ligands like EDTA. The stability of lanthanide complexes improves as the atomic number increases when they form complexes. The best application of this characteristic is in the separation of Lanthanides. Hydrated lanthanide ions have a low tendency to form complexes, and their capacity to form complexes declines as the atomic number increases. The following is a representation of the order of complex formation in lanthanides:



Lanthanides have ionization energies that are comparable to those of alkaline earth metals, making them reactive metals.

Lanthanides, according to the Hard and Soft Acid Bases concept (HSAB), behave as typical hard acids, with a preference for fluorine (F) and oxygen (O) donor ligands for bonding. Complexes with nitrogen, sulphur, and halogen (excluding fluorine) are not stable in the presence of water, but if these donor sites are part of multidonor ligands, they are involved in strong complexation with lanthanides [12]. The lack of extensive interaction with 4f orbitals reduces the ligand field stabilization energy (LFSE). Low LFSE reduces overall stability but increases geometry and coordination number flexibility because LFSE is not lost, for example, when an octahedral complex is transformed into trigonal prismatic or square anti-prismatic geometry. Furthermore, the complexes are prone to be labile in solution.

Lanthanide bonding is primarily ionic in nature. The evidence, both theoretical and experimental, is overwhelming. Even in the most stable complexes, the bond strength is of the same order of magnitude as the Ln(III)-Water dipole interaction, according to Moeller et al. (1965) [13]. Bond distance measurements have also indicated that lanthanide bonding is ionic. Although water is a powerful ligand for Ln(III) ions, the difficulties that competing ligands have in removing water molecules from the coordination sphere severely limits the types of ligands with which Ln(III) ions can interact in aqueous solution. These ligands are known as class 'A' or hard acceptors.

One distinguishing feature of such acceptors is a preference for donor atoms in the order O>N>S and F>Cl. Lanthanides, like other metals, have a strong preference for O donor atoms. Evidence suggests that Ln(III) ions can align with S atoms in the most uncommon of circumstances.

Table 1.3: Physical Properties of Lanthanide Elements La-Eu.

Parameter	La	Ce	Pr	Nd	Pm	Sm	Eu
CAS number	[7439-91-0]	[7440-45-1]	[7440-10-0]	[7440-00-8]	[7440-12-2]	[7440-19-9]	[7440-53-1]
Atomic number	57	58	59	60	61	62	63
Atomic weight	138.91	140.12	140.908	144.24	(145)	150.36	151.96
Melting point °C	918	798	931	1021	1042	1074	822
Boiling point °C	3464	3433	3520	3074	~3000	1794	1429
Density at 25 °C in g/cm ³	6.1453	6.770	6.773	7.007	7.22	7.520	5.234
Heat of fusion in kJ/mol	6.201	5.179	6.912	7.134	8.623	9.221	
Heat of sublimation at 25°C,	431.0	422.6	355.6	327.6	~348	206.7	144.7
Conduction electrons	3	3.1	3	3	3	3	2
Crystal structure	hcp	dhcp	dhcp	dhcp	dhcp	rhomb.	bcc
Atomic radius in pm ^a	187.9	182.5	182.8	182.1	181.1	180.4	204.2
Neel point, °C	n.a	~13	n.a	n.a	n.a	15	90

^arhomb: rhombohedral.^bFor CN=12 and the α -form at room temperature.

Table 1.4: Physical Properties of Lanthanide Elements Gd-Lu.

Parameter	Gd	Tb	Dy	Ho	Er	Tm	Yb	Lu
CAS number	[7440-54-2]	[7440-27-9]	[7429-91-6]	[7440-60-0]	[7440-52- α_1]	[7440-30-4]	[7440-64-4]	[7439-94-3]
Atomic number	64	65	66	67	68	69	70	71
Atomic weight	157.95	158.9254	162.50	164.930	167.26	168.934	173.04	174.97
Melting point °C	1313	1365	1412	1474	1529	1545	819	1663
Boiling point °C	3273	3230	2567	2700	2868	1950	1196	3402
Density at 25 °C in g/cm ³	7.9004	8.2294	8.5500	8.7947	9.066	9.3208	6.9654	9.8404
Heat of fusion in kJ/mol	10.05	10.80	10.782	16.874	19.90	16.84	7.657	18.65
Heat of sublimation at 25°C, kJ/mol ^b	397.5	288.7	290.4	300.8	317.10	232.2	152.1	427.6
Conduction electrons	3	3	3	3	3	3	2	3
Crystal structure	Hcp	Hcp	Hcp	Hcp	Hcp	Hcp	fcc	hcp
Atomic radius in pm ^a	180.1	178.33	177.43	176.61	175.66	174.62	193.92	173.49
Curie point, °C	292.7	220	86	19	18	32.	n.a.	n.a
Neel point, °C	n.a.	230	178	133	84	56	n.a.	n.a

^aFor CN=12 and the α -form at room temperature.

1.1.1 End Uses of Lanthanides

- i. *Magnetic Properties and Magnets:* The magnetic characteristics of lanthanides are extraordinary. Samarium-cobalt magnets were the first high-performance magnetic materials to be mass-produced. Electronic equipment such as headphones for the famous Walkman (Sony, New York, NY), 1979, were able to be miniaturised as a result of such remarkable magnetic properties. Electric motors for hybrid and electric vehicles, wind turbines, hard disks and magnets for magnetic resonance imaging (MRI) are just a few of the many technological applications. Nd-magnets are the core of nuclear magnetic spectrometers and scanners.
- ii. *Phosphors and Scintillators:* Rare earths as light-converting materials (phosphors) with great energy efficiency and colour rendering are required in energy-saving lighting and display systems. Fluorescent tubes, compact fluorescent lamps (CFLs), plasma and liquid crystal (LCD) displays, light-emitting diodes (LEDs), electroluminescent foils and organic light-emitting diodes (OLEDs) are among the most common applications. The primary uses of scintillators include the measurement of UV radiation (200-220nm range) or x-rays in medical imaging, as well as the detection of radioactivity (medical imaging and security checks). Trivalent cerium and divalent europium are common ions used in these applications [14–17].
- iii. *Metallurgy, Alloys and Compounds:* Metallurgical uses rely on lanthanides' strong affinity for oxygen and sulphur. They improve the resistance of numerous metals and alloys to high-temperature oxidation as well as their thermomechanical qualities, e.g., hardening stainless steel. Adding Y, La, or Ce to heat-resistant alloys

improves their performance as well. Scandium is the most potent strengthener of aluminum. Electric and hybrid electric vehicles, as well as portable gadgets, use nickel-lanthanide hydride (Ni-LnH) batteries (smartphones, cameras).

- iv. *Glass Industry:* Rare earths, particularly cerium, are frequently employed in the glass industry. Glass and ceramics are coloured with Pr (green), Nd (purple) and Er (pink). Lanthanide ions are well suited as active materials for solid-state lasers emitting in the UV, visible, or NIR due to their numerous and well-defined electronic levels. Lanthanide dopants are ideal waveguide amplifiers for optical fibers in telecommunications [18,19].
- v. *Catalysts:* Rare earths are active elements in a wide range of catalytic reactions and several applications have reached industrial scale. Cerium oxide is widely used in automotive postcombustion catalysts. They are used in organic synthesis. Neodymium salts are used as a diene polymerization catalyst.
- vi. *Ceramics:* Lanthanide chemical and structural properties are also used in the ceramics industry. Tiny amounts of rare-earth oxides stabilise tetragonal or cubic zirconia. Stabilized forms of zirconia are used in sensors, cutting tools or imitation jewellery.
- vii. ***Other Uses***
Defense Applications: Rare earths are indispensable for night vision, guiding systems, laser weapons, motorization, aircraft electric generators, and light alloys for jet turbines as well as for stabilizing rocket nose cones, jamming and sonar

devices, antimissile systems, range finders, satellite power and telecommunication systems and radar systems.

Agriculture: In agriculture, rare earths are primarily used as fertilisers in the form of lanthanide salts or complexes. Most studies found that consuming rare earths improved the growth of pigs, poultry, sheep, goats, calves, horses, fish and prawns. Chlorides, nitrates, and complexes with ascorbate or citrate are the most common rare-earth-containing compounds found in these diets.

Medical Applications. Applications in bioanalysis and bioimaging are gaining traction [20,21], particularly since the advantage of luminescent immunoassays over radioactive immunoassays was recognised. In nuclear magnetic medical imaging, gadolinium complexes are used as contrast agents.

Photovoltaics: Lanthanide compounds are being studied for their ability as wavelength-converting materials. Lanthanides can be used as photocatalysts for either water splitting or organic substance degradation during water purification [22].

1.2 Review on Lanthanide Coordination Chemistry and its Biological Relevance

Even though the lanthanide and actinide transition series have no known vital role in life processes, they undoubtedly provide some of the most exciting, complex and crucial chemical and biological challenges of all inorganic elements in the periodic table. The causes for this stem primarily from the properties granted by their outer electron

configuration and associated energy levels, as well as their chemical toxicity, which is low for lanthanides but high for actinides and their radiotoxicities, which are a big issue for actinides. Lanthanides are distinguished by the shielding of the 4f orbitals by the $5s^25p^6$ subshells, which gives them an inner rather than valence orbital character. This, in turn, determines their distinct chemical, magnetic, and optical properties, which are central to a wide range of practical applications [23,24].

Due to the 4f-orbital shielding, the lanthanides' absorption and emission lines involving these orbitals are extremely sharp, with full-width-at-half-height (fwhh) values of only a few nm [25]. These spectral lines were weak and varied greatly depending on the sample purity and the inorganic matrix in which the emitting ions were buried. Broader bands (fwhh 100 nm) were occasionally seen (Fig. 1.2)

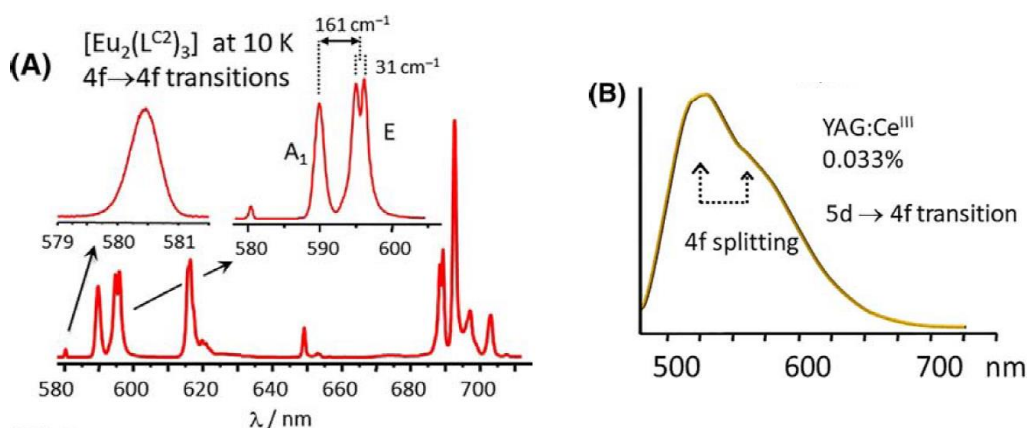


Fig. 1.2: Typical Lanthanide Emission Spectra [24]. (A) $\text{Eu(III)}(^5\text{D}_0 \rightarrow ^7\text{F}_J)$ f-f transitions ($J = 0-4$) of a triple-stranded helicate with approximate D_3 symmetry showing in the right insert the crystal-field splitting of the $^7\text{F}_1$ state. (B) $\text{Ce(III)}(^2\text{D}_{3/2} \rightarrow ^2\text{F}_{7/2,5/2})$ d-f emission band in $\text{Y}_3\text{Al}_5\text{O}_{12}:\text{Ce}^{\text{III}}$ (0.33%) showing the spin-orbit splitting of the $4f^1$ configuration into $^2\text{F}_{7/2}$ and $^2\text{F}_{5/2}$.

The paramagnetic nature of lanthanides is responsible for their higher magnetic moment due to the number of unpaired electrons in the 4f orbitals. This makes them

extremely useful in applications such as Nuclear Magnetic Resonance Spectroscopy (NMR) and Nuclear Magnetic Resonance Imaging (MRI) [26–30]. Because of their large magnetic moment and good relaxation efficiency, gadolinium(III) complexes, particularly with polyamino-polycarboxylic acids, are ideal contrast enhancing agents [31,32]. Dysprosium and Thulium chelates have been found to be good shift reagents for tracking sodium compartmentalization during an *Ischaemia* attack. The following are some other key biological and biochemical applications:

- (a) In electron microscopy and x-ray diffraction research, lanthanides can be utilised as heavy atom "stains."
- (b) Lanthanide-based lasers are mostly used in telecommunications, night vision and medicine (e.g., eye or skin treatment) [18,33].
- (c) Another distinguishing feature of f-f transitions is their slow emission kinetics, which reflects the long lifetimes of the excited f-states as a result of their forbiddance. This, in turn, offers up new possibilities. Bioapplications as lanthanide-based probes [34] considerably eases the shortcomings of optical analysis and bioimaging, in that lanthanide probes are substantially more photostable (particularly the all-inorganic ones) and their slow luminescence can be detected in time-resolved mode [35].
- (d) *In vivo* targeting and localization in tumours using appropriate lanthanide ion complexes [36].
- (e) Through competition or exchange reactions with lanthanide ions, the thermodynamic properties of metal ion binding sites, such as Ca(II), can be elucidated. This is particularly significant because calcium, one of the most important and ubiquitous essential elements, has very few properties that can be used to probe its biochemistry *in situ*. Lanthanide(III) ions are extensively used as

biomimetic agents for Ca(II) because of their functional and/or size similarities [37].

Table 1.5 lists some similarities between Ca(II) and Ln(II).

Table 1.5: Salient properties of calcium and lanthanide.

Property	Ca(II)	Ln(III)
Coordination number	6-12 reported	6-12 reported
	6 or 7 favored	8 or 9 observed
Coordination geometry	Highly flexible	Highly flexible
Preference for donor sites	O>N>S	O>N>S
Ionic radii (Å)	1.00-1.18	0.86-1.22
	(CN 6-9)	(CN 6-9)
Type of bonding	Electrostatic	Electrostatic
Hydration number	6	8 or 9
Water exchange rate constant (S ⁻¹)	~5x10 ⁸	~5x10 ⁷
Crystal field stabilization	None	Negligible
Spectroscopic behaviour	Spectroscopic silence	Abundance of spectroscopic signals both optical and magnetic
Stability of complexes	Weak complexes	Strong complexes
Diffusion coefficient (cm ² /s x 10 ⁵)	1.34	Ln(III), 1.30

(f) Kinetic aspects of biological reactions involving metal ions can also be studied to obtain mechanistic insights.

(g) Lanthanide-doped upconverting luminous nanoparticles (UCNPs) are attractive materials for optical imaging-guided drug delivery and therapy. UCNPs absorb low-energy near-infrared light (NIR) and produce high-energy photons with shorter wavelengths. The current availability of sophisticated inorganic-organic hybrid

nanomaterials has boosted interest in this field, particularly because drug delivery and bioimaging can be coupled in a method known as theranostics [38,39].

- (h) Simple devices, based on lateral flow competitive assays with lanthanide-doped nanoparticles as reporters, are being developed as the demand for quicker and better bioanalyses grows. These tests are used for quality control e.g., in agriculture or the food industry. They are also used in point-of-care medical analysis and substance addiction field testing.

Secondary disposal sites for lanthanide or actinide after entrance into the body are primarily through the plasma in the bloodstream. The f-block elements are conveniently located between three (or possibly four) fractions that are in equilibrium with one another and are responsible for transport and intracellular uptake within the bodily compartment. To demonstrate this concept, we use iron as a key fundamental element. Iron is divided into fractions that are in thermodynamic and labile equilibrium with one another. The metal is bound inertly in a fourth fraction, which is also interchangeable with the previous three fractions (Fig. 1.3). This latter fraction can be looked at as a storage area.

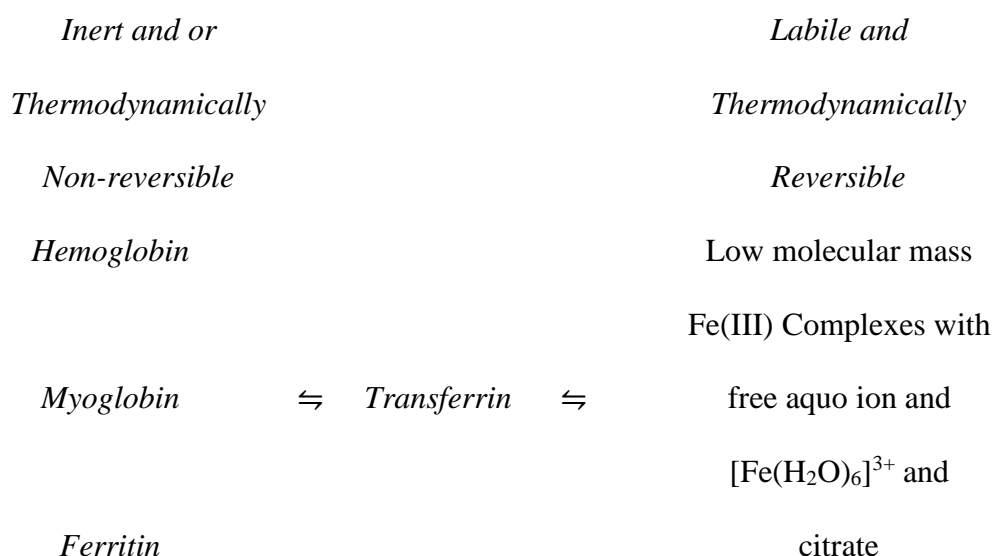


Fig. 1.3: Inert and labile forms of metal ions *in vivo*.

In terms of metal transport, the labile compartments are of particular significance. Transferrin is a blood-plasma glycoprotein (molecular weight of around 80 kDa) that transports iron into and out of the cells [40]. Transferrin is responsible for ferric-ion transport and plays a key role in the body's iron metabolism. It is the most important ferric pool in the body. It consists of two homologous lobes called N- and C- lobes with each possessing a high-affinity Fe(III) binding site. Apart from Fe(III) ion, Transferrin can bind a variety of divalent, trivalent and tetravalent metal ions which include metals from the transition, lanthanide, and actinide series [41,42]. *In vitro* and *in vivo* studies on lanthanide binding with biomolecules have been reported [43,44]. UV difference spectroscopy and other *in vitro* investigations using Pu(IV), Th(IV) and a variety of trivalent lanthanides have conclusively proven that, like iron, each transferrin molecule can bind two lanthanide or actinide ions [42,45].

Harris reported equilibrium formation constants for transferrin complexes of Nd(III) and Sm(III) using absorption difference and comparative absorption spectra [46]. Although data on the formation constants for the f-block elements are less, such findings on transferrin with lanthanides and actinides have significant consequences for actinide/lanthanide distribution in the human body. The *f*-elements have been found to participate in specific parts of iron transport pathways *in vivo* by binding to transferrin. However, no plutonium, for example, is detected in RBC after incorporation, and there is no conclusive evidence that plutonium or other actinides or lanthanides are delivered into the cell by transferrin receptor-mediated endocytosis. This aspect of *f*-element-transferrin chemistry is perplexing, and it necessitates a great deal more research. The apparent contradiction of the *f*-elements binding to transferrin and the imperfect participation in the iron metabolic pathway can be explained by a number of theories. A possible cause for this discrepancy in Fe(III)-transferrin and lanthanide/actinide transferrin may be due to

conformational changes upon binding with the metal ion. These conformational changes are crucial for the metal-transferrin complexes for subsequent binding with cell receptors before internalization. Evans has thoroughly examined the interactions of several lanthanides with a wide spectrum of proteins (1990) [47]. The enzymes *Trypsin*, *Elastase*, *Collagenase*, *Amylase*, *Nuclease*, *ATPase*, *Phospholipase-A₂* and *Acetylcholinesterase*, as well as contractile proteins *Actin* and *Myosin* and molecular oxygen carriers such as *Haemocyanin*, have all been studied. These investigations revealed that the carboxyl group is the most important ligand for the Ln(III) ion, with carboxyl or hydroxylic oxygen providing further coordination.

Studies of newer lanthanide complexes are a potential area of research in inorganic chemistry because of their promising biological properties. Schiff base lanthanide complexes have been widely studied and their resulting anticancer, antimicrobial, and antioxidant activities have been reported in literature [48–50]. Lanthanide ions are known to exhibit therapeutic properties such as antibacterial activity [51,52]. The use of cerium oxalate as an antiemetic was one of the first therapeutic applications of lanthanide(III) ions. The discovery of the antibacterial activity of lanthanides can be dated back to the 19th century when salts of Ce(III) were reportedly used as antiseptic powder due to their antibacterial properties [53]. Marydasan et al. synthesised a series of optically active heterobimetallic Eu(III) complexes using 3-trifluoroacetylcamphorate as the ligand. In addition to chiral luminescence, the complexes demonstrated promising antibacterial action against multidrug resistant *Staphylococcus aureus* and *Enterococcus faecalis* strains [54]. Deghadi et al. synthesised bioactive complexes of La, Er and Yb from 2-acetylferrocene derivative Schiff base. All of the complexes outperformed the free ligand in terms of anticancer efficacy. Additionally, most of the complexes had good antibacterial activity against *Pseudomonas aeruginosa*, *Bacillus subtilis*, *Staphylococcus aureus* and

Escherichia coli species, with inhibition zone diameters ranging from 10-15 mm/mg[50]. The Ln(III) complexes were observed to have a superior bactericidal activity than their respective bioactive parental ligands. When parent L complexes with Ln ions, the activity of the parent L is increased due to an increase in lipophilicity, which promotes antibacterial activity [55]. Though more research is required, Ln complexes could be a viable alternative to antibacterial drugs currently being used. Abu-Yamin et al. synthesized a series of Ln(III) complexes of Gd, Sm and Nd from a new schiff base. The complexes were characterized and tested for their biological properties such as antimicrobial, antifungal, antioxidant and antitumor properties. The complexes were found to possess potent antibacterial and antifungal properties, as well as antioxidant and anticancer properties [56]. Such compounds may have therapeutic applications but, more studies are needed to prove their efficacy and safety.

Microtubule stability is reportedly influenced by lanthanide compounds. Soto et al. [57] discovered that different lanthanides behaved differently, and this was attributed to Ln(III) similarity to Ca(II) or Mg(II), because Ca(II) ion was shown to disrupt microtubules, in contrast to Mg(II) strengthening of microtubule activity. Because of their larger size and hence propensity to exhibit relatively greater coordination numbers, the lower lanthanides behaved more like Ca(II). Because heavier lanthanides like Tb, Dy, and Ho are smaller in size, they behave like Mg(II) and have more potential to strengthen the microtubules. Soto et al. linked Ln(III) function and the variable behaviour of different lanthanides to their effect on tubulin GTPase activity [57]. The activities in the association of tubulin with GTP is governed by Mg(II). This process of association controls the shape and size of the microtubule. When supplied in small doses, Ln(III) could mimic the activities of Mg(II), bolstering tubulin's association. Ln(III), on the other hand, interferes with the assembly when given in excessive quantities.

Lanthanides frequently occupy Ca(II) binding sites but they are found to bind to protein sites that aren't normally known to bind Ca(II) or any other metal. Ln(III) ions have a stronger affinity for proteins than Ca(II) ions due to their higher charge to volume ratio. Lanthanide affinities vary greatly, but they generally increase when the hydration of the sequestered lanthanide ion decreases and the cationic charge of the binding site increases. In addition to protein research, *in vitro* Ln(III) binding to other types of biomolecules such as Nucleic acid, phospholipids, phospholipid membrane, porphyrins, vitamin B₁₂ and high-density lipoproteins can provide structural and other information. Such interactions of lanthanides with biomolecules are valuable as they mimic the interaction of those biomolecules with actinides and has been helpful in the understanding the biochemistry of actinides.

1.3 Glutathione - The Basics

Glutathione, also referred to as GSH, is an endogenous peptide compound that is present in cells. It was discovered in 1888 by J. de Rey-Pailhade from the extracts of yeast, animal tissues and egg white. It was initially named *philothon* by De Rey-Pailhade which in Greek means love and sulfur. Nobel laureate F. G. Hopkins also studied the philothon from animal tissue extracts and contributed greatly towards its discovery and characterization [58]. He later named it “glutathione”. Although Hopkins originally described glutathione as a dipeptide, Hunter and Eagles’ work [59] eventually led to its revision and clarification, recognizing glutathione to be a tripeptide of glutamic acid, glycine and cysteine [60]. Glutathione has many metabolic functions but primarily acts as an antioxidant in preventing oxidative stress by reducing cell damage and is also known to pique the immune system. Glutathione levels in the cell and mitochondria directly are highly associated with health and longevity.

Glutathione is a tripeptide (γ -L-glutamyl-L-cysteinyl-glycine) synthesized exclusively in the cytosol component of the cell [61]. Over 90% of it abounds in the thiol form for which it is noteworthy as the most common non-protein thiol present in cells [62,63]. It is present in millimolar concentrations of up to 10Mm in cells and is found in high concentrations in the liver. Glutathione by nature exists in two states, viz. reduced glutathione (GSH), which is the predominant form and oxidized glutathione (GSSG) shown in Fig. 1.4 [64,65]. Glutathione is a polydentate ligand with two carboxylate oxygen, an amino nitrogen, a sulphydryl group, and two amide groups as possible binding sites [61]. Because the structure of glutathione prevents all of its possible binding sites from being coordinated to the same metal ion at the same time, its coordination chemistry is characterised by protonated and polynuclear complex formation. The donor atoms of GSH can be grouped into three classes of binding sites: the glutamic (amino acid-like) set of amine and carboxylate donors, the thiol and the peptide bonds. (The isolated carboxylate of glycine can be functionally included in the first class, but often participates in coordination with the thiol donor, due to the spatial constraints). Hard metal donors prefer to interact with the glutamic moiety, whereas soft metal donors prefer the thiol. Since metal-glutathione complexes are involved in the toxicology of various metals, the coordination chemistry of glutathione is particularly essential and of considerable interest as a model system for the binding of metal ions by bigger peptides and proteins.

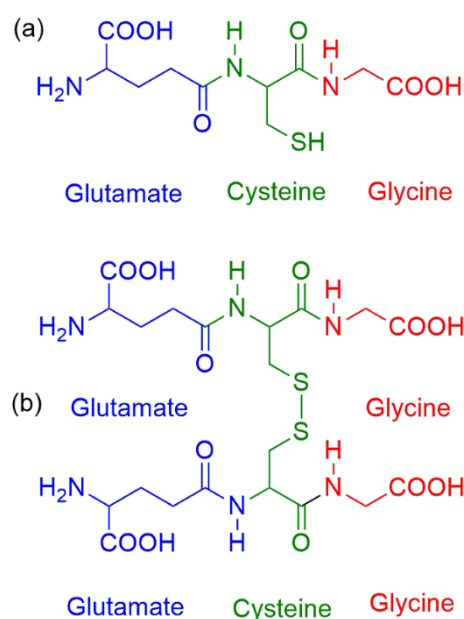
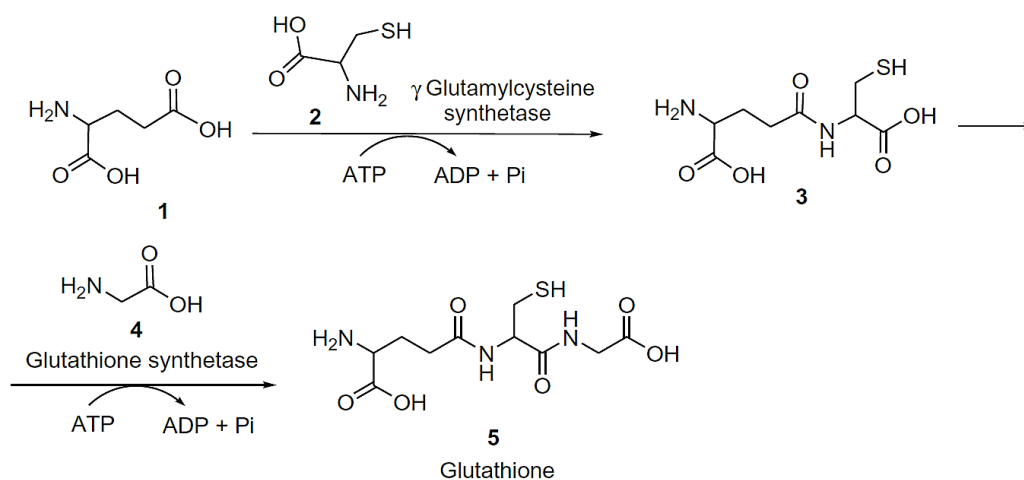


Fig. 1.4: Chemical structures of (a) glutathione reduced (GSH) and (b) glutathione oxidized (GSSG).

Noctor et al. [66] examined the biosynthesis, metabolism, and connection to stress tolerance in transformed plants. The glutathione biosynthesis pathway consists of two ATP-dependent processes that produce γ -glutamylcysteine **3** from L-glutamate **1** and L-cysteine **2**, followed by the creation of glutathione **5** by adding glycine **4** to the C-terminal end of the γ -glutamylcysteine **3** [67]. These reactions are catalyzed by γ -glutamylcysteine synthetase and glutathione synthetase (Scheme 1.1).



Scheme 1.1: Biosynthesis of glutathione.

Glutathione is involved in both xenobiotic and endogenous chemical detoxification. It helps with cellular excretion (Hg), bodily excretion such as persistent organic pollutants (POPs), Hg, and direct neutralisation (POPs, numerous oxidative chemicals). Glutathione supports the transport of toxins across plasma membranes by at least four processes, the most important of which is the production of glutathione S-conjugates. The total intracellular glutathione content comprises of more than 99.5 % GSH, while GSSG is present in modest amounts. Some key roles of glutathione are summarized in Table 1.6.

Table 1.6: The critical roles of Glutathione.

1. Direct chemical neutralization of singlet oxygen, hydroxyl radicals, and superoxide radicals
2. Cofactor for several antioxidant enzymes
3. Regeneration of vitamins C and E
4. Neutralization of free radicals produced by Phase I liver metabolism of chemical toxins
5. One of approximately 7 liver Phase II reactions, which conjugate the activated intermediates produced by Phase I to make them water soluble for excretion by the kidneys
6. Transportation of mercury out of cells and the brain
7. Regulation of cellular proliferation and apoptosis
8. Vital to mitochondrial function and maintenance of mitochondrial DNA (mtDNA)

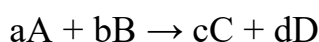
The use of cellular glutathione depletion as an experimental tool in studies of tripeptide mechanism and function has proved extremely useful.

- a) Glutathione depletion is caused by the usage of chemicals like diamide.
- b) Depletion by use of compounds that react with glutathione (diethyl maleate, 1-chloro-2,4-dinitrobenzene).
- c) Glutathione depletion caused by the use of oxidising agent.
- d) Glutathione depletion caused by inhibition of γ -glutamylcysteine synthetase.
- e) The administration of buthionine sulfoximine depletes glutathione, which has a significant effect on metabolic activity.
- f) The decreasing cellular level of glutathione by inhibiting glutathione synthetase level.

The level of glutathione in the liver and kidney is significantly reduced after administration of buthionine sulfoximine. Reversible glutathione disulphide conversion occurs in both mitochondria and cytoplasm, but glutathione synthesis occurs only in the cytoplasm. Because glutathione reduced is the predominant intracellular form, glutathione disulphide is most likely the major transport form. The transport of glutathione-disulphide, which can be formed in mitochondria under severe oxidative stress, acts as a protective mechanism. Rapid labelling of mitochondrial glutathione after administering isotopically labelled cysteine supports the theory that the mitochondrial membrane contains an exchange carrier that is accessible to both mitochondrial and cytoplasmic glutathione. Glutathione is vital for mitochondrial activity. Glutathione's net outflow from the mitochondria is extremely slow. This suggests that the transport pathway works to conserve mitochondrial glutathione during periods of cytoplasmic glutathione depletion, which can be caused by nutritive factors as well as oxidative stress and the presence of hazardous compounds.

1.4 Chemical Kinetics

Chemical kinetics is one of the oldest branches of physical chemistry. It is the study of reaction rates in order to infer kinetic mechanisms for the chemical conversion of reactants into products. The rate of a chemical reaction is expressed as the change in concentration of some species in specific time. The concentration of the reactants decreases as the reaction progresses, while the concentration of the products increases over time (Fig. 1.5). For the reaction,



$$\text{Rate of the reaction} = -\frac{1}{a} \frac{\Delta[A]}{\Delta t} = -\frac{1}{b} \frac{\Delta[B]}{\Delta t} = \frac{1}{c} \frac{\Delta[C]}{\Delta t} = \frac{1}{d} \frac{\Delta[D]}{\Delta t}$$

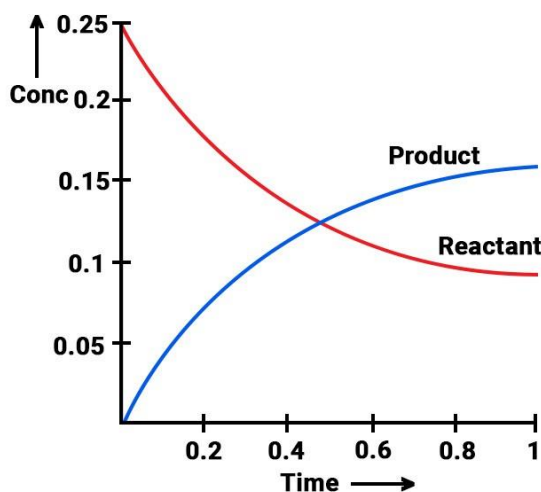


Fig. 1.5: Hypothetical reaction profile of the variation of concentration of reactants and products with time.

1.4.1 Factors that affect reaction rates

During chemical reactions, the rates at which reactants are consumed and products are formed vary greatly. The various factors that commonly influence the rates of chemical reactions:

- (a) Concentrations of reactants: Rate of a reaction is directly proportional to the concentration of reactants. Reaction rate increases with increase in concentration of the reactants.
- (b) Temperature at which reaction occurs: The rate of nearly all reactions increases as the temperature increases.
- (c) Presence of a catalyst: A catalyst increases the rate of reaction by providing a new path with lower activation energy for the reaction to follow.
- (d) Surface area: If a solid reactant is used, the rate of the reaction increases with increase in the surface area of the solid reactant.
- (e) The chemical nature of the reacting substances: The nature of bonding in the reactants determines the rate of a reaction. Ionic compounds usually react faster than covalent compounds. Reactions between ionic compound reactions in water are particularly quick because they only involve the exchange of ions that have already been separated in aqueous solutions during their dissolution.

1.4.2 Activation energy and the rate of the reaction

Depending upon the magnitude of the activation energy, the following three cases are possible:

- 1) The lower the activation energy (E_a), the faster the chemical reaction will be.
- 2) The higher the activation energy (E_a), the slower the chemical reaction will be.
- 3) If the activation energy (E_a) is zero (0), the reaction proceeds at a very fast rate or is instantaneous.

1.4.3 Arrhenius rate equation

The Arrhenius equation is an expression that provides a relationship between the rate constant (of a chemical reaction), the absolute temperature, and the A factor (also known

as the pre-exponential factor; can be visualized as the frequency of correctly oriented collisions between reactant particles). It provides insight into the dependence of reaction rates on the absolute temperature. The Arrhenius equation is

$$k = Ae^{-E_a / (RT)}$$

Where, k is the coefficient of the rate of reaction, A is the pre-exponential factor/frequency factor, R is the universal gas constant, T is the temperature in Kelvin and E_a is the Activation Energy. The fraction of molecules with energy equal to or greater than E_a is given by the exponential term $e^{-E_a / (RT)}$.

The Arrhenius equation can be written in a non-exponential form as

$$\ln k = \ln A - \frac{E_a}{RT}$$

$$\text{Or, } 2.303 \log k = 2.303 \log A - \frac{E_a}{RT}$$

$$\text{Or, } \log k = \log A - \frac{E_a}{2.303RT}$$

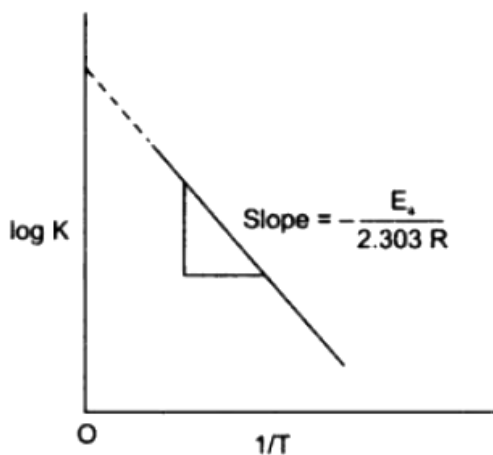


Fig. 1.6: A plot between $\log k$ and $1/T$.

Thus, a plot of $\log k$ against $1/T$ should give a straight line with negative slope, in which

$$\text{Slope} = -\frac{E_a}{2.303R} \text{ and Intercept} = \log A$$

1.5 Spectroscopic Features of Lanthanides

The [Xe]4fⁿ electronic configuration of Ln(III) ions produces a plethora of electronic levels [68]. Because the 4f electrons are shielded, these levels are well-defined, with sharp absorption and emission bands [69,70]. Moreover, interactions with the ligands are weak, resulting in the splitting of electronic levels of a few hundred cm⁻¹ only so that electronic properties may be adequately described within the frame of the ligand (crystal) field theory. The line width of the bands is smaller than the absorption spectra of the transition metals. The peak position of the spectral lines reveals the electronic structure (of a part) of the 4fⁿ configuration. The crystal field splitting is useful for the determination of site symmetry of the Ln ion either by absorption or emission spectroscopy. Absorption and luminescence spectroscopy are important techniques in the study of lanthanide systems because they allow for the determination of lanthanide's natural frequencies. In solution or in glasses, the absorption spectra of lanthanide doped single crystals of lanthanide compounds reveal a set of narrow lines that broaden to one absorption band; these bands must be attributed to an electronic to electronic transition inside the 4f shell. Each group or band corresponds to the transition between ^{2S+1}L_J free ion levels (or J-manifolds). These are intraconfigurational transitions because they are not accompanied by a change in configuration. Since the 4f electrons are effectively shielded by the filled 5s and 5p shells, which have a higher energy than the 4f shell, the 4f→4f transitions are sharp. The transitions have a low intensity. The intensity of these transitions is weak and can be interpreted by the three mechanisms [69] as detailed in the following sub-sections (a) Induced Electric Dipole Transitions (b) Magnetic-Dipole Transitions (c) Electric Quadrupole Transition.

(a) Induced Electric Dipole Transitions

Induced electric dipole transitions account for the vast majority of optical transitions seen in lanthanide ions. An electric dipole transition occurs when a spectroscopically active ion (the lanthanide ion) interacts with the electric field vector via an electric dipole. The formation of an electric dipole necessitates a charge movement that is linear. The parity of such a transition is odd. Hence, when the electric dipole operator is inverted with respect to an inversion centre, it has odd transformation properties. The Laporte selection rule prohibits intraconfigurational electric dipole transitions however, mixing of electronic states of opposite parity is allowed by non-centrosymmetrical interactions. The observed transitions are significantly weaker than ordinary electric dipole transitions and are often called induced electric dipole transitions. The selection rules for the induced electric-dipole transitions are

$$\Delta l = \pm 1, \Delta \tau = 0, \Delta S = 0, \Delta L \leq 6, \Delta J \leq 6, \Delta J = 2, 4, 6 \text{ if } J = 0 \text{ or } J' = 0.$$

(b) Magnetic Dipole Transitions

The interaction of the spectroscopic active ion (i.e., the lanthanide ion) with the magnetic field component of the electromagnetic radiation via a magnetic dipole causes a magnetic dipole transition. If a charge is displaced along a curved path during a transition, it will have magnetic transition dipole intensity. The curvature of the displacement will be only weakly visible in a region as small as the extent of an ion. Since the intensity is proportional to the square of the transition dipole moment, the intensity of the magnetic dipole transition is weak. Magnetic dipole radiation can also be thought of as a charge rotational displacement. A magnetic dipole transition has even parity because the sense of a rotation is not reversed when inverted through a point (or inversion centre). As a result, a magnetic dipole operator has even transformation properties when inverted and allows transition

between states of equal parity (i.e. intraconfigurational transitions). The intensity of the magnetic dipole transitions is weaker (of the order of 10^{-8}) than induced electronic dipole transitions. Selection rules are given by $\Delta\tau = \Delta S = \Delta L = 0$, $\Delta J = 0, \pm 1$ but $0 \leftrightarrow 0$ is forbidden.

(c) Electric Quadrupole Transitions

The electric quadrupole transition results from a quadrupolar charge displacement. An electric quadrupole is made up of four point charges with zero charge and dipole moment. It can be visualised as two dipoles arranged in such a way that their dipole moments cancel. Electric quadrupole has even parity. Electric-quadrupole transitions are much weaker than induced electric-dipole and magnetic-dipole transitions. The hypersensitive transitions are treated as pseudo-quadrupole transitions because they follow the selection rules of quadrupole transitions ($|\Delta S| = 0$, $|\Delta L| \leq 2$ and $|\Delta J| \leq 2$).

1.5.1 Hypersensitive Transitions

Generally, the 4f electrons are affected little by the surrounding environment because they are well shielded by closed-shell 5s and 5p electrons from outside. Therefore, the crystal or ligand field splittings are smaller than the spin-orbit (SO) splittings, and the electronic states of the lanthanide trivalent ion (Ln^{3+}) in crystal or ligand fields are usually similar to those of free Ln^{3+} . Although the electronic states are labelled by the Russell-Saunders scheme ($^{2S+1}L_J$), only the total angular momentum J is assumed to remain a good quantum number because of the large SO effect.

In spite of the shielding effect, there are some exceptional f-f transitions (electric dipole transitions) whose oscillator strengths are very sensitive to a small change in the surrounding environment. These transitions have been called “hypersensitive transitions” by Jørgensen and Judd [71] and have been extensively studied [72–80]. The hypersensitive transitions obey the selection rules of electric-quadrupole transitions $|\Delta S| = 0$, $|\Delta L| \leq 2$ and

$|\Delta J| \leq 2$, and their oscillator strengths are usually enhanced greatly compared with those of Ln(III) in aqueous solution. Studies indicate that their intensities have a quadrupole character, hence *hypersensitive transitions* are also known as *pseudo-quadrupolar transitions*. Gruen et al. observed that the oscillator strengths of hypersensitive transitions in gaseous lanthanide trihalide (LnX_3) molecules were much larger than those of Ln(III) in solutions or crystals [81,82]. Moeller et al. were the first to notice the high sensitivity of spectral intensities to ligand environment for β -diketonate and EDTA complexes of Nd(III), Ho(III) and Er(III) long before Judd-Ofelt Theory [83,84]. Hypersensitive transitions observed for Ln(III) ions are given in Table 1.7.

Karraker studied the hypersensitive transitions of Nd(III), Ho(III) and Er(III) in non-aqueous environments, looking at the absorption spectra of six, seven and eight coordinated β -diketonates to see how the coordination number affected the intensity and fine structure of the spectra [85]. The β -diketonates attach to Ln(III) ions in a bidentate way involving two oxygen donor atoms, resulting in a six-membered chelate ring. His work revealed that the hypersensitive transitions displayed differences that were characteristic of the lanthanide ion's coordination and symmetry. The following findings led to the conclusion:

- I. For hypersensitive transitions between six, seven eight and nine coordinated lanthanide ions, the appearance of the absorption bands differs.
- II. When a unidentate ligand is added to a solution of six or seven coordinated complexes, the spectra produced resemble those of seven or eight coordinated complexes.
- III. When water is removed from a hydrated complex, the spectra changes resembling those of a lower coordination lanthanide.

IV. The intensity of hypersensitive transitions and the lanthanide coordination number are correlated.

Table 1.7: Experimentally observed hypersensitive transitions of Ln(III) ions in optical spectra [86]. Energies/wavelengths are approximate

Ln	Transition	$\tilde{\nu}(\times 10^3 \text{cm}^{-1})$	λ/nm
Pr ³⁺ ($4f^2$)	$^3\text{H}_4 \rightarrow ^3\text{F}_2$	5.2	1920
Nd ³⁺ ($4f^3$)	$^4\text{I}_{9/2} \rightarrow ^4\text{G}_{5/2}$	17.3	578
Sm ³⁺ ($4f^5$)	$^6\text{H}_{5/2} \rightarrow ^4\text{F}_{3/2}, ^4\text{F}_{1/2}$	6.4	1560
Eu ³⁺ ($4f^6$)	$^7\text{F}_1 \rightarrow ^5\text{D}_1$	18.7	535
	$^7\text{F}_0 \rightarrow ^5\text{D}_2$	21.5	465
	$^7\text{F}_2 \rightarrow ^5\text{D}_0$	16.3	613
Gd ³⁺ ($4f^7$)	$^8\text{S}_{7/2} \rightarrow ^6\text{P}_{7/2}, ^6\text{P}_{5/2}$	32.5	308
Tb	^a	-	-
Dy ³⁺ ($4f^9$)	$^6\text{H}_{15/2} \rightarrow ^6\text{F}_{11/2}$	7.7	1300
	$^6\text{H}_{15/2} \rightarrow ^4\text{I}_{15/2}, ^4\text{G}_{11/2}$	23.4	427
Ho ³⁺ ($4f^{10}$)	$^5\text{I}_8 \rightarrow ^5\text{G}_6$	22.1	452
	$^5\text{I}_8 \rightarrow ^3\text{H}_6$	27.7	361
Er ³⁺ ($4f^{11}$)	$^4\text{I}_{15/2} \rightarrow ^2\text{H}_{11/2}$	19.2	521
	$^4\text{I}_{15/2} \rightarrow ^4\text{G}_{11/2}$	26.4	379
Tm ³⁺ ($4f^{12}$)	$^3\text{H}_6 \rightarrow ^3\text{F}_4$	5.9	1695
	$^3\text{H}_6 \rightarrow ^3\text{H}_4$	12.7	787
	$^3\text{H}_6 \rightarrow ^1\text{G}_4$	21.3	469

^aNone identified positively, but the $^5\text{D}_4 \rightarrow ^7\text{F}_5$ transition shows sometimes ligand-induced pseudo-hypersensitivity

For Praseodymium, Pr(III) and Neodymium, Nd(III), the $^3\text{H}_4 \rightarrow ^3\text{P}_2$ and $^4\text{I}_{9/2} \rightarrow ^4\text{G}_{5/2}$ transitions, which occurs around $5,200 \text{ cm}^{-1}$ and $17,300 \text{ cm}^{-1}$ respectively have been identified as hypersensitive transitions. Transitions such as $^3\text{H}_4 \rightarrow ^3\text{P}_2$, $^3\text{P}_1$ and $^1\text{D}_2$ for Pr³⁺ and $^4\text{I}_{9/2} \rightarrow ^4\text{G}_{7/1}$, $^4\text{F}_{7/2}$ and $^4\text{F}_{5/2}$ in case of Nd(III) which are not normally hypersensitive have also been found to exhibit hypersensitivity in the presence of ligands. A few transitions of Pr(III) such as the $^3\text{H}_4 \rightarrow ^3\text{P}_2$, $^3\text{P}_1$ and $^1\text{D}_2$ transitions and $^4\text{I}_{9/2} \rightarrow ^4\text{G}_{7/1}$, $^4\text{F}_{7/2}$,

$^4F_{5/2}$ transitions of Nd(III) are found to be very sensitive to the environment and in the complexed lanthanide ion [87,88]. These electronic transitions show enhanced sensitivity of intensity to their coordination environment respective to the normal $f-f$ transitions. In addition, previous studies have reported hypersensitivity in the $^4I_{9/2} \rightarrow ^4G_{5/2}$ and $^4G_{7/2} \rightarrow ^4K_{13/1}$ transitions of Nd(III) [89]. Studies on Nd(III) complexes by Misra et al. showed unusual sensitivities in $^4I_{9/2} \rightarrow ^4F_{7/2}$ and $^4F_{5/2}$ transitions with varying binding properties which respect to the ligand under study[90]. These transitions were termed as '*Ligand Mediated Pseudohypersensitive Transitions*' [88,91,92].

1.6 Purpose of the Research

Lanthanide chemistry is fascinating due to its wide range of applications. Optical spectroscopy is an important technique for the study of the coordination chemistry of Ln(III) ions in solution, as attested to by the many reviews of the application of either absorption or luminescence spectroscopy to its research [93–96]. In this view, the present thesis attempts to study the spectral properties of lanthanide(III) complexes in solution with the intention of exploring the potential of lanthanides as spectral and structural probes of chemical systems. The chemistry of lanthanide ions in solution, particularly in aqueous solution, has pushed us and others to move on from being enthralled. Studies of lanthanide complexes in solution provides valuable information pertaining to its reaction pathways and mechanism. Comparative absorption spectroscopic studies can help understand the structure, conformation and biological activities of biomolecules upon their coordination with the lanthanide.

Several important metal ions, such as calcium(II) and magnesium(II), which are complexed to biological macromolecules cannot be studied by either magnetic or spectroscopic methods as they are diamagnetic and have no useful spectral transitions.

Lanthanides have been used extensively in biochemistry as probes of calcium binding sites in proteins because of their similarities with Ca(II). The lanthanides can also substitute for other metals as well such as Mg(II), Fe(II) or Mn(II)) in proteins. Our choice of the metal, Mg(II), was based on its biological importance. Magnesium acts as a cofactor in regulating the functions of various enzymes which in turn are responsible for various chemical reactions. Magnesium typically occurs as Mg(II) ion. Mg(II) is diamagnetic and spectroscopically inactive. On the other hand, lanthanides being spectroscopically active can be used as substitutes for magnesium ions in studying biological systems through their isomorphous substitution. The isomorphous substitution of Mg(II) by Ln(III) can prove very useful in understanding the interaction of biomolecules with Mg(II). If magnesium plays a biochemical role, then Ln(III) substitution should lead to, at least, retention of activity. The replacement of Mg(II) by Ln(III) in the ligand system will help in studying the relationship between the metal ion and GSH. Lanthanide complexes, especially in solution, may be used as paramagnetic probes in biological studies to investigate the reaction systems of amino acids and proteins.

Solution spectral studies of f-f transitions provide comparatively less accurate information than that of crystal spectral analysis. It is because of the fact that processes like dissociation, association, isomerisation etc., are prevalent and thus more than one species might exist, resulting in an absorption spectrum, which is an average spectrum of all the species present in equilibrium. However, Absorption Band Gaussian Curve Analysis and Linear Curve Analyses greatly refine the reported spectrum data. Solution spectral analysis may not provide very distinct quantitative data but it is extremely useful for structural determination, mechanistic studies and the creation of optimal experimental conditions required for product formation of some desired pre-determined configurations with advanced technology employing much better resolution of solution spectral 4*f*-4*f* bands.

When studying human metabolism, only solution studies can provide relevant and valid information. For example, coagulated blood studied in the crystal/solid form will not be relevant in determining its specific role; it can only be studied in the solution/semi-solid form.

References

- [1] N.N. Greenwood, A. Earnshaw, Chemistry of the Elements, 2nd ed., Butterworth-Heinemann, Oxford, 2001.
- [2] K.B. P. Thyssen, Handbook on the Physics and Chemistry of Rare Earths, 41st ed., Elsevier Science B.V., Amsterdam, 2011.
- [3] R.L. Kohale, V.B. Pawade, S.J. Dhoble, A.H. Deshmukh, Introduction to phosphate phosphors, in: Opt. Prop. Phosphate Pyrophosphate Compd., 1st ed., Woodhead Publishing, Duxford, 2021: pp. 1–53. <https://doi.org/10.1016/B978-0-12-823044-2.00003-6>.
- [4] R.W. Hakala, Letters, *J. Chem. Educ.* **29** (1952) 581. <https://doi.org/10.1021/ed029p581.2>.
- [5] V.S. Sastri, J.C. Bünzli, V.R. Rao, G.V.S. Rayudu, J.R. Perumareddi, Modern Aspects of Rare Earths and Their Complexes, 1st ed., Elsevier Science, Amsterdam, 2003. <https://doi.org/10.1016/B978-0-444-51010-5.X5014-7>.
- [6] A. Dornemann, L. Johannsen, K.H. Neeb, L.J. Ottendorfer, Lanthanide, *Fresenius' Zeitschrift Für Anal. Chemie.* **206** (1964) 296–297. <https://doi.org/10.1007/BF00523234>.
- [7] R. Beatty, The Lanthanides, Marshall Cavendish Benchmark Books, New York, 2007.
- [8] C.J. Raub, Handbook on the physics and chemistry of rare earths, volume 21, *J. Alloys Compd.* **255** (1997) 266. [https://doi.org/10.1016/s0925-8388\(96\)02845-9](https://doi.org/10.1016/s0925-8388(96)02845-9).
- [9] R.E. Kirk, D.F. Othmer, C.A. Mann, Encyclopedia of Chemical Technology. Vol. II, *J. Phys. Colloid Chem.* **53** (2000) 591. <https://doi.org/10.1021/j150469a016>.
- [10] T. Behrsing, G.B. Deacon, P. Junk, The Chemistry of Rare-Earth Metals, in: S.T. Liddle, D.P. Mills, L.S. Natrajan (Eds.), Lanthanides Actinides Synth. React. Prop.

- Appl., World Scientific Publishing Europe Ltd., London, 2022: pp. 1–36.
- [11] K.L. Nash, A review of the basic chemistry and recent developments in trivalent f-elements separations, *Solvent Extr. Ion Exch.* **11** (1993) 729–768. <https://doi.org/10.1080/07366299308918184>.
- [12] H. Schmidbaur, Comprehensive Coordination Chemistry. The Synthesis, Reactions, Properties and Applications of Coordination Compounds, Pergamon Press, Oxford, 1989. <https://doi.org/10.1002/ange.19891010642>.
- [13] T. Moeller, D.F. Martin, L.C. Thompson, R. Ferrus, G.R. Feistel, W.J. Randall, The Coordination Chemistry of Yttrium and the Rare Earth Metal Ions, *Chem. Rev.* **65** (1965) 1–50. <https://doi.org/10.1021/cr60233a001>.
- [14] H.A. Höppe, Recent developments in the field of inorganic phosphors, *Angew. Chemie - Int. Ed.* **48** (2009) 3572–3582. <https://doi.org/10.1002/anie.200804005>.
- [15] Z. Xia, Z. Xu, M. Chen, Q. Liu, Recent developments in the new inorganic solid-state LED phosphors, *Dalt. Trans.* **45** (2016) 11214–11232. <https://doi.org/10.1039/c6dt01230b>.
- [16] X. Fan, Z. Liu, X. Yang, W. Chen, W. Zeng, S. Tian, X. Yu, J. Qiu, X. Xu, Recent developments and progress of inorganic photo-stimulated phosphors, *J. Rare Earths.* **37** (2019) 679–690. <https://doi.org/10.1016/j.jre.2018.12.003>.
- [17] I. Gupta, S. Singh, S. Bhagwan, D. Singh, Rare earth (RE) doped phosphors and their emerging applications: A review, *Ceram. Int.* **47** (2021) 19282–19303. <https://doi.org/10.1016/j.ceramint.2021.03.308>.
- [18] S. V. Eliseeva, J.C.G. Bünzli, Rare earths: Jewels for functional materials of the future, *New J. Chem.* **35** (2011) 1165–1176. <https://doi.org/10.1039/c0nj00969e>.
- [19] M. Zhang, J. Lu, Y. Chen, Y. Wei, Y. Shao, Z. Li, F. Ma, S. Huang, Z. Li, Z. Chen, R. Wang, Z. Li, Study on Er³⁺-Yb³⁺ co-doped La₂O₃-Al₂O₃ glasses for C-band

- optical waveguide amplifier with high luminous efficiency and low pump threshold, *Ceram. Int.* **48** (2022) 32236–32240. <https://doi.org/https://doi.org/10.1016/j.ceramint.2022.07.165>.
- [20] Q. Zhang, S. O'Brien, J. Grimm, Biomedical Applications of Lanthanide Nanomaterials, for Imaging, Sensing and Therapy, *Nanotheranostics*. **6** (2021) 184–194. <https://doi.org/10.7150/ntno.65530>.
- [21] X. Zhu, H. Zhang, F. Zhang, Ligand-Based Surface Engineering of Lanthanide Nanoparticles for Bioapplications, *ACS Mater. Lett.* **4** (2022) 1815–1830. <https://doi.org/10.1021/acsmaterialslett.2c00528>.
- [22] E. Cerrato, E. Gaggero, P. Calza, M.C. Paganini, The role of Cerium, Europium and Erbium doped TiO₂ photocatalysts in water treatment: A mini-review, *Chem. Eng. J. Adv.* **10** (2022) 100268. <https://doi.org/10.1016/j.cej.2022.100268>.
- [23] J.-C.G. Bünzli, S. V. Eliseeva, Basics of Lanthanide Photophysics, in: P. Hänninen, H. Härmä (Eds.), *Lanthan. Lumin.*, Springer Berlin, Heidelberg, 2010: pp. 1–45. https://doi.org/10.1007/4243_2010_3.
- [24] J.G. Bünzli, Lanthanide Photonics : Shaping the Nanoworld, *Trends Chem.* **1** (2019) 751–762. <https://doi.org/10.1016/j.trechm.2019.05.012>.
- [25] Y. Hasegawa, Y. Kitagawa, T. Nakanishi, Effective photosensitized, electrosensitized, and mechanosensitized luminescence of lanthanide complexes, *NPG Asia Mater.* **10** (2018) 52–70. <https://doi.org/10.1038/s41427-018-0012-y>.
- [26] S. Aime, M. Botta, M. Fasano, E. Terreno, Lanthanide(III) chelates for NMR biomedical applications, *Chem. Soc. Rev.* **27** (1998) 19–29. <https://doi.org/10.1039/A827019Z>.
- [27] O.Y. Selyutina, V.E. Koshman, M. V Zelikman, S.P. Babailov, Holmium complex with phospholipids as ¹H NMR temperature probe for membrane systems,

- BioMetals*. **35** (2022) 629–637. <https://doi.org/10.1007/s10534-022-00388-3>.
- [28] M.H. Khan, S.K. Mishra, A.B.M. Zakaria, J.M. Mihailović, D. Coman, F. Hyder, Comparison of Lanthanide Macrocyclic Complexes as ^{23}Na NMR Sensors, *Anal. Chem.* **94** (2022) 2536–2545. <https://doi.org/10.1021/acs.analchem.1c04432>.
- [29] M. Bottrill, L. Kwok, N.J. Long, Lanthanides in magnetic resonance imaging, *Chem. Soc. Rev.* **35** (2006) 557–571. <https://doi.org/10.1039/b516376p>.
- [30] S.P. Babailov, E.N. Zapolotsky, Dy-DTPA as supersensitive shifting and relaxational probe for NMR/MRI control of local temperature, *Polyhedron*. **194** (2021) 114908. <https://doi.org/10.1016/j.poly.2020.114908>.
- [31] A. Bianchi, L. Calabi, F. Corana, S. Fontana, P. Losi, A. Maiocchi, L. Paleari, B. Valtancoli, Thermodynamic and structural properties of Gd(III) complexes with polyamino-polycarboxylic ligands: Basic compounds for the development of MRI contrast agents, *Coord. Chem. Rev.* **204** (2000) 309–393. [https://doi.org/10.1016/s0010-8545\(99\)00237-4](https://doi.org/10.1016/s0010-8545(99)00237-4).
- [32] L. Lattuada, A. Barge, G. Cravotto, G.B. Giovenzana, L. Teid, The synthesis and application of polyamino polycarboxylic bifunctional chelating agents, *Chem. Soc. Rev.* **40** (2011) 3019–3049. <https://doi.org/10.1039/c0cs00199f>.
- [33] J.C.G. Bünzli, S. V. Eliseeva, Intriguing aspects of lanthanide luminescence, *Chem. Sci.* **4** (2013) 1939–1949. <https://doi.org/10.1039/c3sc22126a>.
- [34] C.M.R. Almeida, J.M.C.S. Magalhaes, F. Barroso, L. Durães, Latest advances in sensors for optical detection of relevant amines: Insight into lanthanide-based sensors, *J. Mater. Chem. C*. **10** (2022) 15263–15276. <https://doi.org/10.1039/D2TC03143D>.
- [35] P.R. Selvin, Principles and biophysical applications of lanthanide-based probes, *Annu. Rev. Biophys. Biomol. Struct.* **31** (2002) 275–302.

<https://doi.org/10.1146/annurev.biophys.31.101101.140927>.

- [36] J. Yan, B. Li, P. Yang, J. Lin, Y. Dai, Progress in Light-Responsive Lanthanide Nanoparticles toward Deep Tumor Theranostics, *Adv. Funct. Mater.* **31** (2021) 2104325. <https://doi.org/10.1002/adfm.202104325>.
- [37] J.A. Cotruvo, The Chemistry of Lanthanides in Biology: Recent Discoveries, Emerging Principles, and Technological Applications, *ACS Cent. Sci.* **5** (2019) 1496–1506. <https://doi.org/10.1021/acscentsci.9b00642>.
- [38] G.-Q. Jin, C. V Chau, J.F. Arambula, S. Gao, J.L. Sessler, J.-L. Zhang, Lanthanide porphyrinoids as molecular theranostics, *Chem. Soc. Rev.* **51** (2022) 6177–6209. <https://doi.org/10.1039/D2CS00275B>.
- [39] T. Jia, G. Chen, Lanthanide nanoparticles for near-infrared II theranostics, *Coord. Chem. Rev.* **471** (2022) 214724. <https://doi.org/https://doi.org/10.1016/j.ccr.2022.214724>.
- [40] K. Gkouvatsos, G. Papanikolaou, K. Pantopoulos, Regulation of iron transport and the role of transferrin, *Biochim. Biophys. Acta - Gen. Subj.* **1820** (2012) 188–202. <https://doi.org/10.1016/j.bbagen.2011.10.013>.
- [41] G.J.P. Deblonde, M. Sturzbecher-Hoehne, A.B. Mason, R.J. Abergel, Receptor recognition of transferrin bound to lanthanides and actinides: A discriminating step in cellular acquisition of f-block metals, *Metallomics.* **5** (2013) 619–626. <https://doi.org/10.1039/c3mt20237b>.
- [42] J.R. Duffield, D.M. Taylor, D.R. Williams, Chapter 129 The biochemistry of the f-elements, *Handb. Phys. Chem. Rare Earths.* (1994) 591–621. [https://doi.org/10.1016/S0168-1273\(05\)80052-2](https://doi.org/10.1016/S0168-1273(05)80052-2).
- [43] L. Zhang, A.F. Martins, Y. Mai, P. Zhao, A.M. Funk, M.V. Clavijo Jordan, S. Zhang, W. Chen, Y. Wu, A.D. Sherry, Imaging Extracellular Lactate In Vitro and In Vivo

- Using CEST MRI and a Paramagnetic Shift Reagent, *Chem. - A Eur. J.* **23** (2017) 1752–1756. <https://doi.org/10.1002/chem.201604558>.
- [44] D.M. Samhadaneh, G.A. Mandl, Z. Han, M. Mahjoob, S.C. Weber, M. Tuznik, D.A. Rudko, J.A. Capobianco, U. Stochaj, Evaluation of Lanthanide-Doped Upconverting Nanoparticles for in Vitro and in Vivo Applications, *ACS Appl. Bio Mater.* **3** (2020) 4358–4369. <https://doi.org/10.1021/acsabm.0c00381>.
- [45] O. Zak, P. Aisen, Spectroscopic and Thermodynamic Studies on the Binding of Gadolinium(III) to Human Serum Transferrin, *Biochemistry.* **27** (1988) 1075–1080. <https://doi.org/10.1021/bi00403a033>.
- [46] W.R. Harris, Binding Constants for Neodymium(III) and Samarium(III) with Human Serum Transferrin, *Inorg. Chem.* **25** (1986) 2041–2045. <https://doi.org/10.1021/ic00232a026>.
- [47] C.H. Evans, Biochemistry of the Lanthanides, 1st ed., Springer, New York, 1990. <https://doi.org/10.1007/978-1-4684-8748-0>.
- [48] F.N. Sayed, G.G. Mohamed, Newly synthesized lanthanides complexes of ferrocene-based Schiff base with high biological activities and improved molecular docking data, *J. Organomet. Chem.* **977** (2022) 122450. <https://doi.org/10.1016/j.jorganchem.2022.122450>.
- [49] R. G. Deghadi, G.G. Mohamed, Can New Series of Half-sandwich Lanthanum(III), Erbium(III), and Ytterbium(III) Complexes of Organometallic Ferrocenyl Schiff Base Ligands Display Biological Activities as Antibacterial and Anticancer Drugs?, *Comments Inorg. Chem.* **42** (2022) 368–401. <https://doi.org/10.1080/02603594.2022.2083608>.
- [50] R.G. Deghadi, G.G. Mohamed, N.F. Mahmoud, Bioactive La(III), Er(III), Yb(III), Ru(III), and Ta(V) complexes of new organometallic Schiff base: Preparation,

- structural characterization, antibacterial, anticancer activities, and MOE studies, *Appl. Organomet. Chem.* **36** (2022) e6675. <https://doi.org/https://doi.org/10.1002/aoc.6675>.
- [51] L. Lekha, K.K. Raja, G. Rajagopal, D. Easwaramoorthy, Synthesis, spectroscopic characterization and antibacterial studies of lanthanide(III) Schiff base complexes containing N, O donor atoms, *J. Mol. Struct.* **1056–1057** (2014) 307–313. <https://doi.org/10.1016/j.molstruc.2013.10.014>.
- [52] Y. Sui, R.H. Hu, D.S. Liu, Q. Wu, Adjustment of the structures and biological activities by the ratio of NiL to RE for two sets of Schiff Base complexes [(NiL)_nRE] (n = 1 or 2; RE = La or Ce), *Inorg. Chem. Commun.* **14** (2011) 396–398. <https://doi.org/10.1016/j.inoche.2010.12.010>.
- [53] S.P. Fricker, The therapeutic application of lanthanides, *Chem. Soc. Rev.* **35** (2006) 524–533. <https://doi.org/10.1039/b509608c>.
- [54] B. Marydasan, K. Suryaaletha, A.M. Lena, A. Sachin, T. Kawai, S. Thomas, J. Kumar, Chiral nanostructures derived from europium(III) complexes for enhanced circularly polarised luminescence and antibacterial activity, *J. Mater. Chem. C* **10** (2022) 13954–13963. <https://doi.org/10.1039/d2tc02193e>.
- [55] I. Cota, V. Marturano, B. Tylkowski, Ln complexes as double faced agents: Study of antibacterial and antifungal activity, *Coord. Chem. Rev.* **396** (2019) 49–71. <https://doi.org/10.1016/j.ccr.2019.05.019>.
- [56] A.A. Abu-Yamin, M.S. Abduh, S.A.M. Saghir, N. Al-Gabri, Synthesis, Characterization and Biological Activities of New Schiff Base Compound and Its Lanthanide Complexes, *Pharmaceuticals* **15** (2022) 1–15. <https://doi.org/10.3390/ph15040454>.
- [57] C. Soto, P.H. Rodríguez, O. Monasterio, Calcium and gadolinium ions stimulate the

- GTPase activity of purified chicken brain tubulin through a conformational change, *Biochemistry*. **35** (1996) 6337–6344. <https://doi.org/10.1021/bi952320e>.
- [58] A. Meister, On the discovery of glutathione, *Trends Biochem. Sci.* **13** (1988) 185–188. [https://doi.org/10.1016/0968-0004\(88\)90148-X](https://doi.org/10.1016/0968-0004(88)90148-X).
- [59] G. Hunter, B.A. Eagles, Non-Protein Sulfur Compounds of Blood, *J. Biol. Chem.* **72** (1927) 133–146.
- [60] R.D. Simoni, R.L. Hill, M. Vaughan, The Discovery of Glutathione by F. Gowland Hopkins and the Beginning of Biochemistry at Cambridge University, *J. Biol. Chem.* **277** (2005) 27–29.
- [61] S. Chakravarthi, C.E. Jessop, N.J. Bulleid, The role of glutathione in disulphide bond formation and endoplasmic-reticulum-generated oxidative stress, *EMBO Rep.* **7** (2006) 1–5. <https://doi.org/10.1038/sj.embor.7400645>.
- [62] D.A. Dickinson, H.J. Forman, Cellular glutathione and thiols metabolism, *Biochem. Pharmacol.* **64** (2002) 1019–1026. [https://doi.org/https://doi.org/10.1016/S0006-2952\(02\)01172-3](https://doi.org/https://doi.org/10.1016/S0006-2952(02)01172-3).
- [63] A. Meister, Glutathione Metabolism, *Methods Enzymol.* **113** (1995) 3–7. [https://doi.org/10.1016/0076-6879\(95\)51106-7](https://doi.org/10.1016/0076-6879(95)51106-7).
- [64] S. Kosower, E.M. Kosower, The Glutathione Status of Cells, *Int. Rev. Cytol.* **54** (1978) 109–160. [https://doi.org/10.1016/S0074-7696\(08\)60166-7](https://doi.org/10.1016/S0074-7696(08)60166-7).
- [65] H.J. Forman, H. Zhang, A. Rinna, Glutathione: Overview of its protective roles, measurement, and biosynthesis, *Mol. Aspects Med.* **30** (2009) 1–12. <https://doi.org/10.1016/j.mam.2008.08.006>.
- [66] G. Noctor, A.C.M. Arisi, L. Jouanin, K.J. Kunert, H. Rennenberg, C.H. Foyer, Glutathione: Biosynthesis, metabolism and relationship to stress tolerance explored in transformed plants, *J. Exp. Bot.* **49** (1998) 623–647.

<https://doi.org/10.1093/jxb/49.321.623>.

- [67] A. Meister, Glutathione metabolism and its selective modification, *J. Biol. Chem.* **263** (1988) 17205–17208. [https://doi.org/10.1016/s0021-9258\(19\)77815-6](https://doi.org/10.1016/s0021-9258(19)77815-6).
- [68] P. Hänninen, H. Härmä, Lanthanide Luminescence, Photophysical, Analytical and Biological Aspects, 1st ed., Springer, Berlin, 2011.
- [69] B.G. Wybourne, W.F. Meggers, Spectroscopic Properties of Rare Earths, First, John Wiley, New York, 1965. <https://doi.org/10.1063/1.3047727>.
- [70] W.T. Carnall, H. Crosswhite, H.M. Crosswhite, Energy level structure and transition probabilities in the spectra of the trivalent lanthanides in LaF₃, United States, 1978. <https://doi.org/10.2172/6417825>.
- [71] B.R. Judd, Hypersensitive transitions in rare-earth ions, *J. Chem. Phys.* **44** (1966) 839. <https://doi.org/10.1063/1.1726774>.
- [72] S.N. Misra, K. John, Difference and Comparative Absorption Spectra and Ligand Mediated Pseudohypersensitivity for 4f-4f Transitions of Pr(III) and Nd(III), *Appl. Spectrosc. Rev.* **28** (1993) 285–325. <https://doi.org/10.1080/05704929308018115>.
- [73] S.N. Misra, M. Indira Devi, C.M. Suveerkumar, K.M. Suma, Electric dipole intensity parameters for a series of structurally related praseodymium(III) and neodymium(III) complexes and unusual sensitivities of some 4f-4f transitions, *Rev. Inorg. Chem.* **14** (1994) 347–362. <https://doi.org/10.1515/REVIC.1994.14.5.347>.
- [74] T. Moaienla, N. Bendangsenla, T. David Singh, C. Sumitra, N. Rajmuhon Singh, M. Indira Devi, Comparative 4f–4f absorption spectral study for the interactions of Nd(III) with some amino acids: Preliminary thermodynamics and kinetic studies of interaction of Nd(III):glycine with Ca(II), *Spectrochim. Acta Part A Mol. Biomol. Spectrosc.* **87** (2012) 142–150. <https://doi.org/10.1016/J.SAA.2011.11.028>.
- [75] N. Bendangsenla, T. Moaienla, T. David Singh, C. Sumitra, N. Rajmuhon Singh, M.

- Indira Devi, Evaluation of intensity and energy interaction parameters for the complexation of Pr(III) with selected nucleoside and nucleotide through absorption spectral studies, *Spectrochim. Acta - Part A Mol. Biomol. Spectrosc.* **103** (2013) 160–166. <https://doi.org/10.1016/j.saa.2012.11.011>.
- [76] M. Hatanaka, S. Yabushita, Theoretical study on the f-f transition intensities of lanthanide trihalide systems, *J. Phys. Chem. A.* **113** (2009) 12615–12625. <https://doi.org/10.1021/jp9049507>.
- [77] D. Singh, S. Bhagwan, A. Dalal, K. Nehra, R.K. Saini, K. Singh, A.P. Simantilleke, S. Kumar, I. Singh, Oxide ancillary ligand-based europium β -diketonate complexes and their enhanced luminosity, *Rare Met.* **40** (2021) 2873–2881. <https://doi.org/10.1007/s12598-020-01543-w>.
- [78] S.A. Bhat, K. Iftikhar, NIR luminescence, hypersensitivity in the 4f – 4f absorption spectra and NMR of seven-, eight- and nine-coordinate ternary neodymium(III) complexes, *Opt. Mater. (Amst).* **122** (2021) 111660. <https://doi.org/10.1016/j.optmat.2021.111660>.
- [79] M.T. Candela, F. Aguado, J. González-Lavín, J.A. González, R. Valiente, Modification of the spectroscopic properties of Tb₂O₃ phosphor under the high-pressure phase transitions sequence, *J. Alloys Compd.* **859** (2021) 157899. <https://doi.org/10.1016/j.jallcom.2020.157899>.
- [80] K. Mariselvam, R.A. Kumar, The emission characteristics of Er³⁺: BBFB glasses for infra-red laser and gamma ray shielding applications, *Optik (Stuttg).* **226** (2021) 165910. <https://doi.org/10.1016/j.ijleo.2020.165910>.
- [81] D.M. Gruen, C.W. Dekock, Absorption spectra of gaseous NdBr₃ and NdI₃, *J. Chem. Phys.* **45** (1966) 455. <https://doi.org/10.1063/1.1727588>.
- [82] D.M. Gruen, C.W. DeKock, R.L. McBeth, Electronic Spectra of Lanthanide

- Compounds in the Vapor Phase, in: P.R. Fields, T. Moeller (Eds.), Lanthanide/Actinide Chem., 1st ed., American Chemical Society, Washington, 1967: pp. 102–121. <https://doi.org/10.1021/ba-1967-0071.ch008>.
- [83] T. Moeller, J.C. Brantley, Observations on the Rare Earths. LVIII. Reaction between Neodymium and Ethylenediaminetetraacetate Ions in Aqueous Solution, *J. Am. Chem. Soc.* **72** (1950) 5447–5451. <https://doi.org/10.1021/ja01168a022>.
- [84] T. Moeller, D.E. Jackson, Rare Earths. Separation Extraction of Certain Rare Earth Elements as 5,7-Dichloro-8-quinolinol Chelates, *Anal. Chem.* **22** (1950) 1393–1397. <https://doi.org/10.1021/ac60047a012>.
- [85] D.G. Karraker, Hypersensitive transitions of six-, seven-, and eight-coordinate neodymium, holmium, and erbium chelates, *Inorg. Chem.* **6** (1967) 1863–1868. <https://doi.org/10.1021/ic50056a022>.
- [86] C. Görller-Walrand, K. Binnemans, Chapter 167 Spectral intensities of f-f transitions, *Handb. Phys. Chem. Rare Earths.* **25** (1998) 101–264. [https://doi.org/10.1016/S0168-1273\(98\)25006-9](https://doi.org/10.1016/S0168-1273(98)25006-9).
- [87] M.T. Devlin, E.M. Stephens, F.S. Richardson, Comparison of Electric-Dipole Intensity Parameters for a Series of Structurally Related Neodymium, Holmium, and Erbium Complexes in Aqueous Solution. Theory and Experiment, *Inorg. Chem.* **27** (1988) 1517–1524. <https://doi.org/10.1021/ic00282a003>.
- [88] S.N. Misra, S.O. Sommerer, Absorption Spectra of Lanthanide Complexes in Solution, *Appl. Spectrosc. Rev.* **26** (1991) 151–202. <https://doi.org/https://doi.org/10.1080/05704929108050880>.
- [89] R.D. Peacock, The intensities of lanthanide f \leftrightarrow f transitions, in: E. Nieboer, C.K. Jørgensen, R.D. Peacock, R. Reisfeld (Eds.), Rare Earths, First, Springer Berlin Heidelberg, Berlin, 2007: pp. 83–122. <https://doi.org/10.1007/bfb0116556>.

- [90] S.N. Misra, S.B. Mehta, Ligand-Mediated Pseudohypersensitivity of Some 4f–4f Transitions in Neodymium(III) Interaction with Fluorinated Nucleic Acid Components, *Bull. Chem. Soc. Jpn.* **64** (1991) 3653–3658. <https://doi.org/10.1246/bcsj.64.3653>.
- [91] S.N. Misra, S.O. Sommerer, The ligand mediated pseudohypersensitivity of the $3H_4 \rightarrow 3P_2$, $3H_4 \rightarrow 3P_1$, $3H_4 \rightarrow 3P_0$, and $3H_4 \rightarrow 1D_2$ transitions of praseodymium(III) complexes in solution media, *Can. J. Chem.* **70** (1992) 46–54. <https://doi.org/10.1139/v92-009>.
- [92] C. Görller-Walrand, K. Binnemans, Chapter 167 Spectral intensities of f-f transitions, *Handb. Phys. Chem. Rare Earths.* **25** (1998) 101–264. [https://doi.org/10.1016/S0168-1273\(98\)25006-9](https://doi.org/10.1016/S0168-1273(98)25006-9).
- [93] K. Nehra, A. Dalal, A. Hooda, S. Bhagwan, R.K. Saini, B. Mari, S. Kumar, D. Singh, Lanthanides β -diketonate complexes as energy-efficient emissive materials: A review, *J. Mol. Struct.* **1249** (2022) 131531. <https://doi.org/10.1016/j.molstruc.2021.131531>.
- [94] Y. Luo, L. Li, Y. Feng, R. Li, J. Yang, W.J.G.M. Peijnenburg, C. Tu, Quantitative tracing of uptake and transport of submicrometre plastics in crop plants using lanthanide chelates as a dual-functional tracer, *Nat. Nanotechnol.* **17** (2022) 424–431. <https://doi.org/10.1038/s41565-021-01063-3>.
- [95] A.A. Ansari, A.K. Parchur, G. Chen, Surface modified lanthanide upconversion nanoparticles for drug delivery, cellular uptake mechanism, and current challenges in NIR-driven therapies, *Coord. Chem. Rev.* **457** (2022) 214423. <https://doi.org/10.1016/j.ccr.2022.214423>.
- [96] Z. Huang, Y. Wang, L. Huang, B. Li, X. Yan, Y. Wang, M.J. Kipper, J. Tang, A review of lanthanide-based fluorescent nanofiber membranes by electrospinning and

their applications, *J. Mater. Sci.* **57** (2022) 3892–3922.
<https://doi.org/10.1007/s10853-021-06758-5>.

CHAPTER 2

SPECTRAL ANALYSIS OF THE COMPLEXATION OF Pr(III) WITH GSH IN THE PRESENCE AND ABSENCE OF Mg(II) AT DIFFERENT pH

2.1 Introduction

The coordination chemistry of lanthanides is an intriguing and widely emerging field. A good number of studies on the coordination chemistry of lanthanide complexes in solution have been reported [1–5]. The increasing interest in lanthanides is largely because of their unique chemical, magnetic and optical properties. These properties are a result of their distinct 4f electrons which is a major feature of the lanthanides. The presence of the 4f electrons in easily accessible spectral regions yield spectral transitions of sharp and narrow bands with weak intensities. Kaczmarek and Lis studied the reaction systems of amino acids and protein using lanthanide-based probes [6]. Comparative absorption spectroscopic studies can help understand the possible structure, conformation and biological activities of biomolecules upon their coordination with the lanthanides [7].

For our study, we chose glutathione (reduced) as the ligand based on its biological relevance, easy availability, solubility and multidenticity. Glutathione is an endogenous peptide compound (γ -L-glutamyl-L-cysteinyl-glycine) synthesized exclusively in the cytosol component of the cell [8]. Glutathione has many metabolic functions but primarily acts as an

antioxidant in preventing oxidative stress by reducing cell-damage and is also known to pique the immune system. Over 90% of it abounds in the thiol form for which it is noteworthy as the most common non-protein thiol present in cells [9,10]. It is present in millimolar concentrations of up to 10Mm in cells and is found in high concentrations in the liver. Glutathione by nature exists in two states; predominantly reduced glutathione (GSH), and oxidized glutathione (GSSG) [11,12]. Its polydentate nature allows it to host probable binding sites of two carboxylates, a sulphhydryl group, one amino nitrogen, and two amide groups [13,14].

Magnesium is an essential macronutrient present in biological systems and typically occurs as Mg(II) ion. Due to the bonding behaviour of Mg(II) with biomolecules and its isomorphous character with Pr(III), its complexation can provide useful information in the study of biological systems. Several investigations have reported studies on the interaction of Ln(III) with Ca(II) based on the substitution of Ca(II) ion by Ln(III) due to their isomorphous character [3-8]. Similarly, the replacement of Mg(II) by Ln(III) can render valuable information about its interaction with glutathione since Mg(II) is diamagnetic and spectroscopically inactive while Ln(III) due to its paramagnetic nature is spectroscopically active.

The present chapter has theoretically discusses the spectral parameters of the interaction between Pr(III) ion and the ligand, glutathione in the presence and absence of Mg(II) in binary mixtures of MeCN:H₂O (50:50 vol. %) and DMF:H₂O (50:50 vol %) at pH 2, 4 and 6. We have computed and evaluated the values of the interaction energies through different energy parameters such as Slater-Condon (F_k), Racah (E^k), Lande (ξ_{4f}), nephelauxetic (β), bonding ($b^{1/2}$) and percent covalency (δ) parameters using 4f-4f transition

spectra to study the mode of complexation. The experimentally computed oscillator strengths of the different 4f transitions and the Judd-Ofelt, T_{λ} ($\lambda=2, 4, 6$) intensity parameters were used to compare and investigate the interaction between the lanthanide and the ligand. The computed intensity parameters suggest that the lanthanide complexes show greater sensitivity towards the ligand environment and exhibit intensified oscillator strengths when the ions are in complexation form than in its free ionic state. These changes indicate the correlation between the relative intensities, the behaviour of the ions towards the solvents, ligand sensitization and pH effect on the complexation of the lanthanide with the ligand (GSH) and Mg(II).

2.2 Experimental

Praseodymium nitrate hexahydrate (99.9%), obtained from Sigma-Aldrich, L-glutathione reduced (GSH, $\geq 98\%$) and magnesium nitrate hexahydrate from HiMedia were used for spectral analysis. The solvents used are acetonitrile (99.0%, Emplura), and dimethylformamide (99.5% Merck). GSH is kept at 2-8°C and fresh solutions were prepared for each experiment. UV-Vis spectra recordings were performed on a Perkin Elmer Lambda 365 UV/Vis spectrometer in the range of 400-620 nm. pH measurements were carried out on a Eutech pH 700 digital pH meter.

For absorption study, Pr(III), GSH and Mg(II) concentrations are kept at 0.003 M. Standard solutions are added and pH was adjusted by adding HCl or NaOH whenever needed. The pH measurement was made using a pH meter. For Pr(III):GSH complex study, the molar ratio was set to 1:1 while for multimetal complexation study of

Pr(III):GSH:Mg(II), the molar ratio was kept at 1:1:1. The solutions were prepared in aquated organic solvents of DMF:H₂O (50% v/v) and MeCN:H₂O (50% v/v).

2.3. Methods

The crystal field effect on the lanthanide ions results in the removal of the degeneracy of the $2J+1$ levels of the free ion. The crystal field effect is also responsible for shifting the baricenter of the $^{2S+1}L_J$ electronic level. This is known as the Nephelauxetic effect [15] caused by covalency, originating in the ionic bonds of the lanthanide and ligand [16]. This effect involves the transfer of electrons to the bonding molecular orbital leading to an increase in the electron's size, surrounding the lanthanide ion. This also causes a lowering in the interelectronic repulsion in comparison to the free ion of the lanthanide. Reisfeld and Jorgensen have written some great reviews on the chemistry of lanthanides [17]. Misra et al. reported studies on the structural properties based on the complexation interaction of the ligand and lanthanides[18].

Nephelauxetic ratio is considered a measure of covalency and can be interpreted in respect of Slater–Condon and Racah parameters as:

$$\beta = \frac{F_k^C}{F_k^f} \text{ or } \frac{E_C^k}{E_f^k} \quad \text{Eq. 1}$$

Here the Slater-Condon parameter, F_k ($k=2,4,6$) and the Racah parameter, E^k ($k=2, 4, 6$) correspond for complexes (C) and the free ions (f). The nephelauxetic ratio is directly linked up to the values of the bonding parameter ($b^{1/2}$) and consequently, the percentage covalency is given below,

$$b^{1/2} = \left[\frac{1-\beta}{2} \right]^{1/2} \quad \text{Eq. 2}$$

$$\delta = \left[\frac{1-\beta}{\beta} \right] \times 100 \quad \text{Eq. 3}$$

E_0 can be expressed in view of the Slater-Condon parameter (F_k) as

$$E_0 = \sum_{k=0}^{k=6} K^k F_k \quad \text{Eq. 4}$$

F_k can be represented using the relation,

$$F_1^k = \int_0^\infty \int_0^\infty \frac{r_i^k}{r_i^{k+1}} R_i^2(r_i) R_j^2(r_j) r_i^2 r_j^2 dr_i dr_j \quad \text{Eq. 5}$$

Where,

$R=4f$ -radial wave function

$r_<$ and $r_>$ =maximum and minimum radii of electrons

i and j = the electrons in question

The F_k integrals were reproduced by Condon and Shortley [19] with regard to reduced integral as:

$$F_k = \frac{F^k}{D_k} \quad \text{Eq. 6}$$

Eq. (5) and (6) are combined to reproduce the Slater-Condon integral as

$$F_k = \frac{1}{D_K} \int_0^\infty \int_0^\infty r_i^k r_j^{k+1} R_i^2(r_i) R_j^2(r_j) T_i^2 r_j^2 dr_i dr_j \quad \text{Eq. 7}$$

Here, D_k and F_k are the denominator and coefficient of linear combination, respectively.

A linear combination of F_k gives the Racah parameter E^{ki}

$$E^1 = (70 \times F_2 + 231F_4 + 20.02F_6)/9$$

$$E^2 = (F_2 - 3F_4 + 7F_6)/9 \quad \text{Eq. 8}$$

$$E^3 = (5F_2 + 6F_4 - 9F_6)/3$$

The spin-orbit interaction energy, E_{so} of 4f-4f transitions which originates from magnetic interactions, can be shown as,

$$E_{so} = A_{so} \zeta_{4f} \quad \text{Eq. 9}$$

Here, A_{so} represents the angular component of the spin-orbit coupling. ζ_{4f} is the Lande's parameter and denotes the radial integral. According to Wong [7], the energy E_j of the j^{th} level can be represented as

$$E_j(F_k, \zeta_{4f}) = E_{oj}(F_k^0, \zeta_{4f}) + \frac{\partial E_j}{\partial F_k} \Delta F_k + \frac{\partial E_j}{\partial \zeta_{4f}} \Delta \zeta_{4f} \quad \text{Eq. 10}$$

Where, E_{oj} represents the j^{th} level's zero order energy.

F_k and ζ_{4f} values can be found out from the equation given,

$$F_k = F_k^0 + \Delta F_k \text{ and } \zeta_{4f} = \zeta_{4f}^0 + \Delta \zeta_{4f} \quad \text{Eq. 11}$$

The zero order (ΔE_j) and observed (E_j) value energy differences can be evaluated by,

$$\Delta E_j = \sum_{k=2,4,6} \frac{\partial E_j}{\partial F_k} \Delta F_k + \frac{\partial E_j}{\partial \zeta_{4f}} \Delta \zeta_{4f} \quad \text{Eq. 12}$$

Using Wong's partial derivative and zero order energy,[20] we can solve Eq. (11) by using the least square technique to find out the values of ΔF_k and $\Delta \zeta_{4f}$. The values of F_2 , F_4 , F_6 and ζ_{4f} are also calculated using Eq. 11.

Table 2.1: The zero-order energies and partial derivatives with respect to F_k and ξ_{4f} parameters for Pr(III) [20].

Level	$E_{oj}^{(a)}$	$\frac{\delta E_j}{\delta F_2}$	$\frac{\delta E_j}{\delta F_4}$	$\frac{\delta E_j}{\delta F_6}$	$\frac{\delta E_j}{\delta \xi_{4f}}$
1D_2	16972	45.97	-37.63	510	2.906
3P_0	20412	70.17	81.17	-1253	1.905
3P_1	20990	70.07	80.66	-1278	3.974
3P_2	22220	67.56	68.42	-1077	5.029

$$(a) \quad F_2^0 = 305.000 \text{ cm}^{-1} \quad F_4^0 = 51.880 \text{ cm}^{-1}$$

$$F_6^0 = 5.321 \text{ cm}^{-1} \quad \xi_{4f}^0 = 730.50 \text{ cm}^{-1}$$

The band intensities are calculated based on the Judd-Ofelt theory [21,22]. According to Judd and Ofelt, the intensity of 4f-4f transition is a result of electric dipole mechanism. The oscillator strength (P_{cal}) of electric-dipole transition $\psi J \rightarrow \psi' J'$ with transition energy $\bar{\nu}$ is given by

$$P_{cal} = \sum_{\lambda=2,4,6} T_{\lambda} \sigma(f^n \psi J \| U^{\lambda} \| f^n \psi' J')^2 \quad Eq. 13$$

Where U^{λ} ($\lambda = 2, 4, 6$) are the matrix elements of Pr(III) given by Carnall [23] connecting $f^n \psi J$ to $f^n \psi' J'$. T_{λ} ($\lambda = 2, 4, 6$) are the empirical parameters which could provide the details of lanthanide-ligand field interaction. The matrix elements for Pr(III) are given in Table 2.2. T_2 , T_4 and T_6 parameters have strong sensitivity even with small changes in co-ordination around Ln(III) ion and symmetry of the complexes formed. The absorption band intensity can be measured experimentally from the determined oscillator strength (P_{obs}). The region beneath the absorption curve is equivalent to the oscillator strength (P_{obs}) which is achieved using Gaussian absorption curve analysis as

$$P_{obs} = 4.6 \times 10^{-9} \times \mathcal{E}_{max} \times \Delta \nu_{1/2} \quad Eq. 14$$

Where, \mathcal{E}_{max} = molar extinction coefficient,

$\Delta\nu_{1/2}$ = half bandwidth

From these, values of T_2 , T_4 and T_6 are calculated applying

$$\frac{P_{obs}}{\nu} = [U^2]^2 \cdot T_2 + [U^4]^2 \cdot T_4 + [U^6]^2 \cdot T_6 \quad Eq. 15$$

The values of T_2 , T_4 and T_6 are computed with a developed software.

Table 2.2: Matrix elements $U^{(\lambda)}$ for Pr(III) aquo [24].

Levels	$[U^{(2)}]^2$	$[U^{(4)}]^2$	$[U^{(6)}]^2$
1D_2	0.0026	0.0170	0.0520
3P_0	0	0.1728	0
3P_1	0	0.1707	0
3P_2	0	0.0362	0.1355

2.4 Results and Discussions

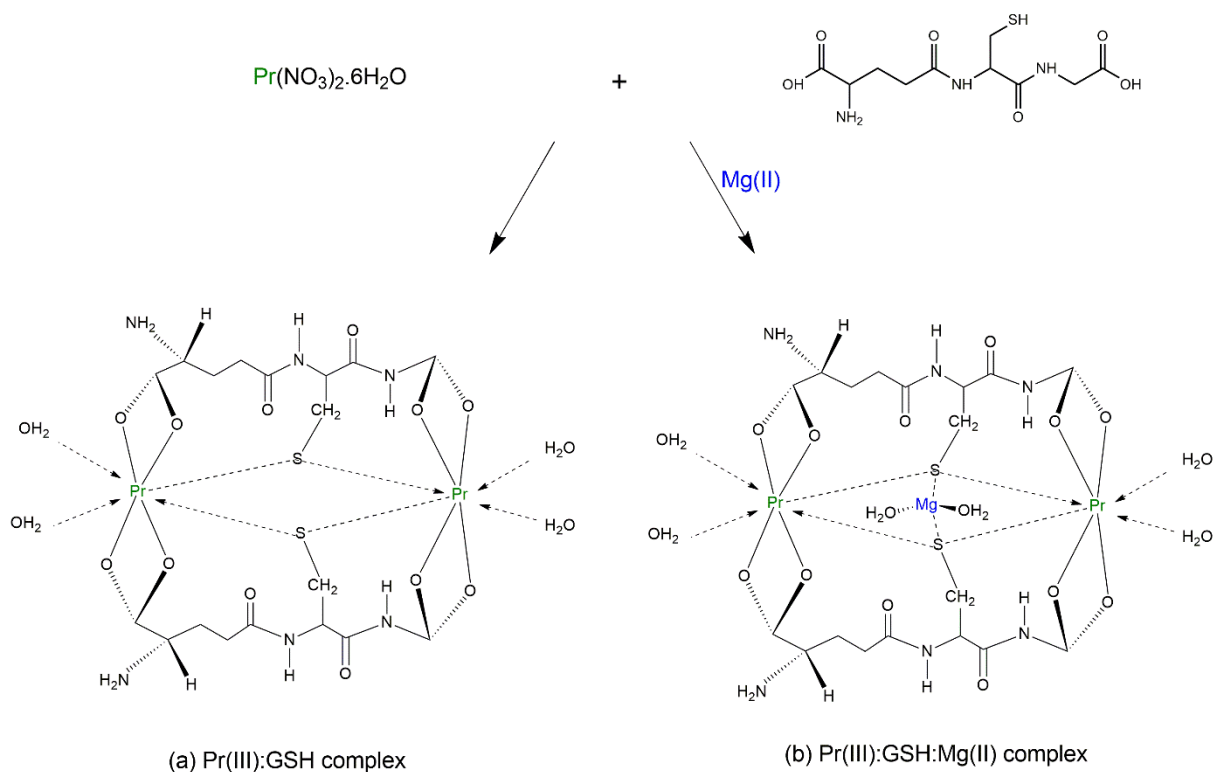
The spectra of lanthanides occur due to transitions involving a redistribution of electrons within the levels of $4f^n$ configurations. The 4f electrons of lanthanide ions are well shielded by the 5s and 5p electrons due to which the intensities of most of the 4f transitions in lanthanides are very poorly affected by their surrounding ions. However, in comparison with the normal f-f transitions, the oscillator strengths of some of these transitions have been found to show enhanced sensitivity to changes in their chemical environment. These transitions which obey the selection rules ($|\Delta S| = 0$, $|\Delta L| \leq 2$, $|\Delta J| \leq 2$) have been called hypersensitive transitions [25]. Hypersensitive transitions occur in almost all of the Ln(III) ions. In the case of Pr(III), the hypersensitive transition $^3H_4 \rightarrow ^3F_2$ is found beyond the UV region and has been excluded from the spectral studies. The 4f-4f electronic transitions of

Pr(III) ion exhibits four absorption bands in the range of 400-600 nm; they are $^3H_4 \rightarrow ^3P_2$, $^3H_4 \rightarrow ^3P_1$, $^3H_4 \rightarrow ^3P_0$ and $^3H_4 \rightarrow ^1D_2$ transitions. These four transitions do not obey the selection rules and are known as non-hypersensitive transitions. However, they show considerable sensitivity to subtle changes in their coordination environment which is reflected by variations in their evaluated energies and oscillator values. These changes are considered to be a result of non-hypersensitive transitions brought about by the ligand. These transitions are thus termed as Pseudohypersensitive transitions [26,27].

The comparative UV-Visible absorption spectra of Pr(III), Pr(III):GSH and Pr(III):GSH:Mg(II) in different solvent and pH levels are shown from Fig. 2.1 to 2.6. From the figure, it is clearly seen that there is a variation in the peak intensities, with the intensity increasing on the addition of glutathione to Pr(III). This is assumed as an indication of the interaction between Pr(III) and GSH. Again, the peaks are even further intensified by the addition of Mg(II) to Pr(III):GSH. This intensification of the peaks suggests the interaction of the lanthanide and ligand orbitals.

The evaluated values reported in Table 2.3 shows the variations in the magnitude of the spectral energy parameters viz. Slater-Condon (F_k), Lande (ζ_{4f}), Racah parameters (E^k), nephelauxetic ratio (β), bonding ($b^{1/2}$) and covalency parameter (δ) of the different systems. From the table, it is observed that the addition of GSH and Mg(II) to Pr(III) leads to change in the energies of the 4f-4f bands which leads to lowering of Slater-Condon (F_k) and Racah (E^k) values. This is due to the fact that when complexation occurs, the central metal ion orbital expands, thereby decreasing the inter-electronic repulsion between the ligand and the central metal ion causing the nephelauxetic effect [26,28]. Since F_k and E^k are interrelated, any changes in the values of E^k (k=2, 4, 6) directly correspond to the value of F_k . In all the

systems, the nephelauxetic value is found to be less than unity while the bonding parameter values are positive, indicating the occurrence of a metal-ligand interaction in solution. We observe a decrease in the nephelauxetic effect (β) as a result of the complexation of Pr(III) with the ligands. This means that the Pr(III) orbital has expanded slightly in solution. The value of β for the complex is found to be less than the free metal ion since the electron repulsion is typically found to be weaker in complexes than in free ions. The possible octa-coordinated structure of the lanthanide and GSH complexes is shown in scheme 2.1.



Scheme 2.1: Probable structure of (a) Pr(III):GSH and (b) Pr(III):GSH:Mg(II) complex.

The values for the computed and observed transition energies and their root mean square (RMS) deviation values are shown in Table 2.4. The RMS deviation value tells us about the accuracy of the energy parameters. In Table 2.5 we have the observed and the computed

oscillator strengths (P) and Judd-Ofelt (T_{λ}) parameter values of the transition bands for Pr(III), Pr(III):GSH and Pr(III):GSH:Mg(II) in different pH. The substantial change in the oscillator strength values and the enhancement of the Judd-Ofelt parameters suggests the binding of GSH with Pr(III). The intensification grows on adding Mg(II) to Pr(III):GSH, revealing the involvement of Mg(II) in complexation. A marked difference in intensification in the different solvents is observed which predicts the effect of the solvent in complex formation. This observation is supported by the computed energy and intensity parameter values (Tables 2.3 and 2.5). Maximum intensification was observed when DMF was involved rather than acetonitrile, implying that DMF has a greater capacity to intensify the 4f-4f transition. This is due to the fact that the oxygen donor site of DMF is preferred over the nitrogen donor of CH₃CN to the hard metal ion (Pr³⁺) coordination site. In general, the binding preference of various donor atoms for Ln(III) is O > N > S [29]. DMF typically binds to hard acids such as lanthanide ions through oxygen, while CH₃CN binds through nitrogen. This implies that, in comparison to acetonitrile, DMF solvent has a higher coordinating capacity with the metal ion (Pr³⁺). GSH ligand has three kinds of coordinating sites viz. hard donor sites such as carboxylic groups, soft donor sites such as the sulphydryl group and borderline donor sites such as the peptide and amino groups. This means that shifts in spectral absorption intensities in various solvents are not going to be very strong, but noticeable to be readily detected. For hard metal ions or soft metal ions, the borderline donor sites have a similar preference and thus make the complexes highly erratic in nature. As observed in previous studies, [4,27] we find DMF to be the better solvent quite capable of competing with H₂O for the lanthanide coordination site. Further, it may be mentioned that

the involvement of oxygen donor from both the 50% water mixed with the solvents DMF and CH₃CN may be neglected since its effect is counterbalanced.

The significant change in the T_{λ} ($\lambda=2,4,6$) values are influenced by the change in the coordination of the lanthanide as well as change in the symmetry of the complex. On analysis of T_4 and T_6 values, there are significant changes when Mg(II) is added to Pr(III):GSH complex which shows the possibility of inner sphere coordination of Mg(II) to Pr(III):GSH complex, whereas the values of T_4 and T_6 in the complexation of Pr(III) and GSH changes only slightly which may be due to the outer sphere coordination of GSH to Pr(III). The value of T_2 is found negative as a result, it is neglected. It may be because the hypersensitive transition of Pr(III), $^3H_4 \rightarrow ^3F_2$ is found beyond the UV-Vis range.

Glutathione's structure restricts the simultaneous coordination of its multiple binding sites to the same metal ion. The pH values greatly affect the bonding capacity of GSH as pH controls the degree of protonation/deprotonation in the binding sites of GSH. This effect is clearly observed from the change in the intensity parameters (T_{λ} , $\lambda=2,4,6$). As hard metal ions prefer hard donor sites, the bonding between Pr(III) and GSH primarily takes place through the interaction of lanthanide with the carboxylic group of GSH. The absorption data implies how glutamyl of GSH deprotonates at a lower pH allowing Pr(III) to bind through it. At a higher pH of 4.0, the carboxylic group of glycine deprotonates and at pH 6.0 sulphydryl group deprotonates. It is reflected in the values of Judd-Ofelt, $T_{\lambda}(\lambda=2, 4, 6)$ which are found to be greater at higher pH values (Table 2.5).

*The work presented in this chapter has been published in *Polyhedron*, 200, 115099, **2021**.

References

- [1] T. Moaienla, N. Bendangsenla, T. David, C. Sumitra, N.R. Singh, M.I. Devi, Spectrochimica Acta Part A : Molecular and Biomolecular Spectroscopy Comparative 4f – 4f absorption spectral study for the interactions of Nd (III) with some amino acids : Preliminary thermodynamics and kinetic studies of interaction of Nd (III): glycine , *Spectrochim. Acta Part A Mol. Biomol. Spectrosc.* **87** (2012) 142–150. <https://doi.org/10.1016/j.saa.2011.11.028>.
- [2] J.P. Mehta, P.N. Bhatt, S.N. Misra, An absorption spectral study of Nd (III) with glutathione (reduced), GSH in aqueous and aquated organic solvent in presence and absence of Zn (II), *J. Solid State Chem.* **171** (2003) 175–182. [https://doi.org/10.1016/S0022-4596\(02\)00205-0](https://doi.org/10.1016/S0022-4596(02)00205-0).
- [3] M.A. Gagnani, S.K. Hari, S.N. Misra, Comparative absorption spectroscopy involving 4f-4f transitions to complex & compositional dependence of intensity parameters, *J. Solid State Chem.* **4** (2003) 374–383.
- [4] N. Bendangsenla, M.I. Devi, T. Moaienla, T.D. Singh, Comarative 4f-4f Absorption Spectral Approach to Study the Complexation of Pr(III) with Guanosine and Guanosine Tri Phosphate (GTP) in the Presence and Absence of Ca(II), *Int. J. Basic Appl. Chem. Sci.* **3** (2013) 19–30.
- [5] R.S. Naorem, N.P. Singh, N.M. Singh, 4f–4f Spectral Analysis and Solvent Effect for the Interaction of Pr(III) with l-Tryptophan Using Different Aquated Solvents in the Presence and Absence of Zn(II), *Chem. Africa.* **3** (2020) 171–180. <https://doi.org/10.1007/s42250-019-00111-9>.

- [6] M. Kaczmarek, S. Lis, Influence of lanthanide(III) ions on the reaction system tryptophan - H₂O₂ -Fe(II), *Int. J. Photoenergy*. **2007** (2006) 042582. <https://doi.org/10.1155/2007/42582>.
- [7] S.N. Misra, M.A. Gagnani, I.D. M., R.S. Shukla, Biological and Clinical Aspects of Lanthanide Coordination Compounds, *Bioinorg. Chem. Appl.* **2** (2004) 155–193. <https://doi.org/10.1155/S1565363304000111>.
- [8] S. Chakravarthi, C.E. Jessop, N.J. Bulleid, The role of glutathione in disulphide bond formation and endoplasmic-reticulum-generated oxidative stress, *EMBO Rep.* **7** (2006) 1–5. <https://doi.org/10.1038/sj.embor.7400645>.
- [9] D.A. Dickinson, H.J. Forman, Cellular glutathione and thiols metabolism, *Biochem. Pharmacol.* **64** (2002) 1019–1026. [https://doi.org/https://doi.org/10.1016/S0006-2952\(02\)01172-3](https://doi.org/10.1016/S0006-2952(02)01172-3).
- [10] A. Meister, Glutathione Metabolism, *Methods Enzymol.* **113** (1995) 3–7. [https://doi.org/10.1016/0076-6879\(95\)51106-7](https://doi.org/10.1016/0076-6879(95)51106-7).
- [11] S. Kosower, E.M. Kosower, The Glutathione Status of Cells, *Int. Rev. Cytol.* **54** (1978) 109–160. [https://doi.org/10.1016/S0074-7696\(08\)60166-7](https://doi.org/10.1016/S0074-7696(08)60166-7).
- [12] H.J. Forman, H. Zhang, A. Rinna, Glutathione: Overview of its protective roles, measurement, and biosynthesis, *Mol. Aspects Med.* **30** (2009) 1–12. <https://doi.org/10.1016/j.mam.2008.08.006>.
- [13] P.A. Karplus, E.F. Pai, G.E. Schulz, A crystallographic study of the glutathione binding site of glutathione reductase at 0.3-nm resolution, *Eur. J. Biochem.* **703** (1989)

- 693–703. <https://doi.org/https://doi.org/10.1111/j.1432-1033.1989.tb14500.x>.
- [14] D.L. Rabenstein, R. Guevremont, C.A. Evans, *Metal Ions in Biological Systems*, Marcel Dekker, New York, 1979.
- [15] C.K. Jorgensen, Electron Transfer Spectra, *Progr. Inorg. Chem.* **12** (1970) 101. <https://doi.org/10.1002/9780470166130.ch2>.
- [16] R. Reisfeld, C.K. Jorgensen, *Lasers and Excited States of Rare Earths*, Springer-Verlag Berlin Heidelberg, 1977.
- [17] R. Reisfeld, C.K. Jorgensen, *Handbook on the Physics and Chemistry of Rare Earths*, Elsevier, 1987.
- [18] S.N. Misra, M. Indira Devi, C.M. Suveerkumar, K.M. Suma, Electric dipole intensity parameters for a series of structurally related praseodymium(III) and neodymium(III) complexes and unusual sensitivities of some 4f-4f transitions, *Rev. Inorg. Chem.* **14** (1994) 347–362. <https://doi.org/10.1515/REVIC.1994.14.5.347>.
- [19] E.U. Condon, G.H. Shortley, *The Theory of Atomic Spectra*, Cambridge: University Press, 1963.
- [20] E.Y. Wong, Configuration interaction of the Pr³⁺ ion, *J. Chem. Phys.* **38** (1963) 976–978. <https://doi.org/10.1063/1.1733794>.
- [21] G.S. Ofelt, Intensities of Crystal Spectra of RareEarth Ions, *J. Chem. Phys.* **37** (1962) 511–520. <https://doi.org/10.1063/1.1701366>.
- [22] B.R. Judd, Optical absorption intensities of rare-earth ions, *Phys. Rev.* **127** (1962)

- 750–761. <https://doi.org/10.1103/PhysRev.127.750>.
- [23] W.T. Carnall, P.R. Fields, B.G. Wybourne, Spectral intensities of the trivalent lanthanides and actinides in solution. I. Pr^{3+} , Nd^{3+} , Er^{3+} , Tm^{3+} , and Yb^{3+} , *J. Chem. Phys.* **42** (1965) 3797–3806. <https://doi.org/10.1063/1.1695840>.
- [24] W.T. Carnall, P.R. Fields, K. Rajnak, Electronic Energy Levels in the Trivalent Lanthanide Aquo Ions. I. Pr^{3+} , Nd^{3+} , Pm^{3+} , Sm^{3+} , Dy^{3+} , Ho^{3+} , Er^{3+} , and Tm^{3+} , *J. Chem. Phys.* **49** (1968) 4424. <https://doi.org/https://doi.org/10.1063/1.1669896>.
- [25] M. Hatanaka, S. Yabushita, Theoretical study on the f-f transition intensities of lanthanide trihalide systems, *J. Phys. Chem. A.* **113** (2009) 12615–12625. <https://doi.org/10.1021/jp9049507>.
- [26] S.N. Misra, S.O. Sommerer, Absorption Spectra of Lanthanide Complexes in Solution, *Appl. Spectrosc. Rev.* **26** (1991) 151–202. <https://doi.org/https://doi.org/10.1080/05704929108050880>.
- [27] N. Bendangsenla, T. Moaienla, T. David Singh, C. Sumitra, N. Rajmuhon Singh, M. Indira Devi, Evaluation of intensity and energy interaction parameters for the complexation of Pr(III) with selected nucleoside and nucleotide through absorption spectral studies, *Spectrochim. Acta - Part A Mol. Biomol. Spectrosc.* **103** (2013) 160–166. <https://doi.org/10.1016/j.saa.2012.11.011>.
- [28] S.N. Misra, G. Ramchandriah, M.A. Gagnani, R.S. Shukla, M.I. Devi, Absorption spectral studies involving 4f-4f transitions as structural probe in chemical and biochemical reactions and compositional dependence of intensity parameters, *Appl.*

Spectrosc. Rev. **38** (2003) 433–493. <https://doi.org/10.1081/ASR-120026330>.

- [29] S. Misra, Lanthanoid (III) ions as structural probe in biochemical reactions, *Proc. Indian Natn. Sci. Acad.* **60** (1994) 637–637.

Table 2.3: Computed values of various energy interaction parameters: Slater-Condon F_k (cm^{-1}), Lande ζ_{4f} (cm^{-1}), Racah E^k (cm^{-1}), nephelauxetic effect (β), bonding ($b^{1/2}$) and covalency (δ) for the different Pr(III) systems in aquated organic solvents (DMF:H₂O, MeCN:H₂O) at pH 2, 4 and 6.

System	pH	F ₂	F ₄	F ₆	ζ_{4f}	E ¹	E ²	E ³	β	$b^{1/2}$	δ
1. CH ₃ CN											
Pr(III)	2	309.4216	42.7157	4.6723	723.0818	3513.3743	23.7756	615.1508	0.9476	0.1619	5.5322
Pr(III):GSH		309.4079	42.7138	4.6721	723.0579	3513.2180	23.7746	615.1235	0.9475	0.1620	5.5363
Pr(III):GSH:Mg(II)		309.3856	42.7107	4.6717	723.0117	3512.9649	23.7728	615.0791	0.9475	0.1621	5.5434
Pr(III)	4	309.4034	42.7131	4.6720	722.9979	3513.1675	23.7742	615.1146	0.9475	0.1620	5.5416
Pr(III):GSH		309.3649	42.7078	4.6714	722.8690	3512.7301	23.7713	615.038	0.9473	0.1623	5.5577
Pr(III):GSH:Mg(II)		309.3803	42.7099	4.6716	722.6321	3512.9048	23.7724	615.0686	0.9472	0.1625	5.5732
Pr(III)	6	309.3834	42.7014	4.6717	723.0577	3512.9404	23.7727	615.0748	0.9475	0.1620	5.5403
Pr(III):GSH		309.3439	42.7049	4.6711	722.7856	3512.4922	23.7696	614.9964	0.9474	0.1624	5.5675
Pr(III):GSH:Mg(II)		309.3203	42.7017	4.6707	723.028	3512.2228	23.7678	614.9492	0.9473	0.1622	5.5528
2. DMF											
Pr(III)	2	308.9748	42.6540	4.6655	719.7136	3508.3008	23.7413	614.262	0.9446	0.1664	5.8628
Pr(III):GSH		308.9585	42.6517	4.6653	719.7277	3508.1153	23.7400	614.23	0.9446	0.1664	5.8644
Pr(III):GSH:Mg(II)		308.9438	42.6497	4.6651	719.6857	3507.9488	23.7389	614.20	0.9445	0.1665	5.8700
Pr(III)	4	309.9393	42.491	4.6650	719.6289	3507.8974	23.7386	614.1919	0.9447	0.1666	5.8751
Pr(III):GSH		308.9191	42.6463	4.6647	719.7688	3507.6683	23.7370	614.1518	0.9446	0.1665	5.8677
Pr(III):GSH:Mg(II)		308.8794	42.6408	4.6641	719.9671	3507.2177	23.7340	614.0729	0.9445	0.1664	5.8590
Pr(III)	6	308.9483	42.6503	4.6651	719.5982	3508.0004	23.7392	614.2099	0.9445	0.1666	5.8760
Pr(III):GSH		308.9506	42.6506	4.6652	719.3717	3508.0265	23.7394	614.2145	0.9443	0.1668	5.8930
Pr(III):GSH:Mg(II)		308.9109	42.6452	4.6646	719.5845	3507.5753	23.7364	614.1355	0.9444	0.1667	5.8832

Table 2.4: Observed and computed values of energies (cm^{-1}) and RMS values of the different Pr(III) complexation systems in different solvents (DMF:H₂O, MeCN:H₂O) at pH 2, 4 and 6.

System	pH	$^3\text{H}_4 \rightarrow \text{E}_{\text{obs}}$	$^3\text{P}_2\text{E}_{\text{cal}}$	$^3\text{H}_4 \rightarrow \text{E}_{\text{obs}}$	$^3\text{P}_1\text{E}_{\text{cal}}$	$^3\text{H}_4 \rightarrow \text{E}_{\text{obs}}$	$^3\text{P}_0\text{E}_{\text{cal}}$	$^3\text{H}_4 \rightarrow \text{E}_{\text{obs}}$	$^1\text{D}_2\text{E}_{\text{cal}}$	RMS
1. CH ₃ CN										
Pr(III)	2	22535.21	22481.42	21352.92	21270.34	20759.81	20708.13	16983.41	17153.70	101.72
Pr(III):GSH		22534.70	22480.37	21352.82	21269.28	20758.95	20707.12	16981.39	17153.00	102.57
Pr(III):GSH:Mg(II)		22533.18	22478.63	21350.64	21267.54	20757.65	20705.47	16979.95	17151.84	102.66
Pr(III)	4	22534.20	22479.77	21352.47	21268.73	20758.95	20706.70	16980.24	17152.62	102.98
Pr(III):GSH		22528.10	22476.52	21349.27	21265.52	20756.79	20703.75	16978.51	17150.48	102.55
Pr(III):GSH:Mg(II)		22524.55	22476.36	21349.73	21265.66	20758.36	20704.38	16977.93	17150.50	102.65
Pr(III)	6	22533.18	22478.72	21351.55	21267.57	20757.22	20705.41	16979.95	17151.88	102.79
Pr(III):GSH		22522.02	22474.68	21349.27	21263.72	20755.50	20702.12	16977.93	17149.27	102.19
Pr(III):GSH:Mg(II)		22528.10	22474.30	21347.00	21263.02	20752.92	20700.91	16977.06	17148.89	102.68
2. DMF										
Pr(III)	2	22502.25	22434.29	21301.52	21225.65	20746.89	20670.36	16911.89	17123.38	123.45
Pr(III):GSH		22499.72	22433.26	21300.26	21224.56	20745.60	20669.24	16912.18	17122.67	122.82
Pr(III):GSH:Mg(II)		22497.19	22432.06	21299.25	21223.37	20744.74	20668.14	16911.89	17121.87	122.43
Pr(III)	4	22497.19	22431.47	21298.80	21222.82	20744.74	20667.71	16910.46	17121.50	123.05
Pr(III):GSH		22497.19	22430.81	21298.80	21221.97	20742.58	20666.56	16910.46	17120.98	122.89
Pr(III):GSH:Mg(II)		22496.18	22429.12	21298.80	21219.97	20738.71	20664.15	16909.60	17119.73	122.90
Pr(III)	6	22498.20	22431.93	21298.35	21223.34	20745.60	20668.29	16910.75	17121.82	123.03
Pr(III):GSH		22494.15	22430.94	21295.63	21222.60	20746.89	20668.02	16911.03	17121.27	122.22
Pr(III):GSH:Mg(II)		22493.65	22429.33	21294.27	21220.66	20743.01	20665.63	16911.03	17120.06	121.69

Table 2.5: Observed and computed values of oscillator strength (P), and Judd-Ofelt (T_λ) parameters of the different Pr(III) systems in aquated organic solvents (DMF:H₂O, MeCN:H₂O) at pH 2, 4 and 6.

System	pH	$^3H_4 \rightarrow ^3P_2$		$^3H_4 \rightarrow ^3P_1$		$^3H_4 \rightarrow ^3P_0$		$^3H_4 \rightarrow ^1D_2$		T_2	T_4	T_6
		P_{obs}	P_{cal}	P_{obs}	P_{cal}	P_{obs}	P_{cal}	P_{obs}	P_{cal}			
1. DMF												
Pr(III)	2	12.268	12.268	4.5578	3.3365	2.086	3.2896	3.851	3.8507	60.083	9.1759	37.783
Pr(III):GSH		12.984	12.984	5.0033	3.7175	2.398	3.6652	4.192	4.1921	89.403	10.224	39.855
Pr(III):GSH:Mg(II)		14.529	14.529	6.5239	4.7376	2.910	4.6711	4.199	4.1998	-13.68	13.031	44.18
Pr(III)	4	12.268	12.268	4.9338	3.6006	2.236	3.5501	3.928	3.9276	76.596	9.9035	37.598
Pr(III):GSH		12.987	12.987	5.3718	3.8781	2.351	3.8233	4.009	4.0096	47.136	10.667	39.754
Pr(III):GSH:Mg(II)		13.811	13.811	5.7194	4.2331	2.708	4.1725	3.948	3.9457	-22.6	11.643	42.197
Pr(III)	6	12.973	12.973	5.3305	3.9699	2.573	3.9144	4.068	4.0683	61.66	10.919	39.636
Pr(III):GSH		13.995	13.995	5.9624	4.4592	2.915	4.3977	4.141	4.1412	8.8547	12.267	42.639
Pr(III):GSH:Mg(II)		14.382	14.382	6.5081	4.8173	3.083	4.7503	4.104	4.1043	-26.11	13.253	43.646

System	pH	$^3\text{H}_4 \rightarrow ^3\text{P}_2$		$^3\text{H}_4 \rightarrow ^3\text{P}_1$		$^3\text{H}_4 \rightarrow ^3\text{P}_0$		$^3\text{H}_4 \rightarrow ^1\text{D}_2$		T_2	T_4	T_6
		P_{obs}	P_{cal}	P_{obs}	P_{cal}	P_{obs}	P_{cal}	P_{obs}	P_{cal}			
2. CH_3CN												
Pr(III)	2	11.491	11.491	5.333	3.7222	2.078	3.0663	3.66	3.66	64.018	10.212	34.904
Pr(III):GSH		12.119	12.119	5.062	3.7077	2.316	3.6489	4.113	4.113	125.61	10.172	36.972
Pr(III):GSH:Mg(II)		12.8948	12.895	6.359	4.5537	2.705	4.4817	4.465	4.465	151.78	12.495	38.895
Pr(III)	4	11.564	11.564	4.242	2.9969	1.724	2.9494	3.5112	3.511	28.031	8.222	35.676
Pr(III):GSH		12.653	12.653	4.184	3.2534	2.286	3.202	3.7669	3.767	13.638	8.927	39.065
Pr(III):GSH:Mg(II)		12.9855	12.985	5.346	3.9595	2.533	3.8973	3.9539	3.954	31.802	10.865	39.644
Pr(III)	6	11.1090	11.109	4.305	3.1602	1.983	3.11	3.3829	3.383	28.224	8.6706	34.068
Pr(III):GSH		11.6443	11.644	4.473	4.3577	4.176	4.2887	2.2985	2.298	-256.7	11.958	34.962
Pr(III):GSH:Mg(II)		14.5290	14.529	6.524	4.7404	2.910	4.6651	4.1998	4.110	-16.01	13.009	44.121

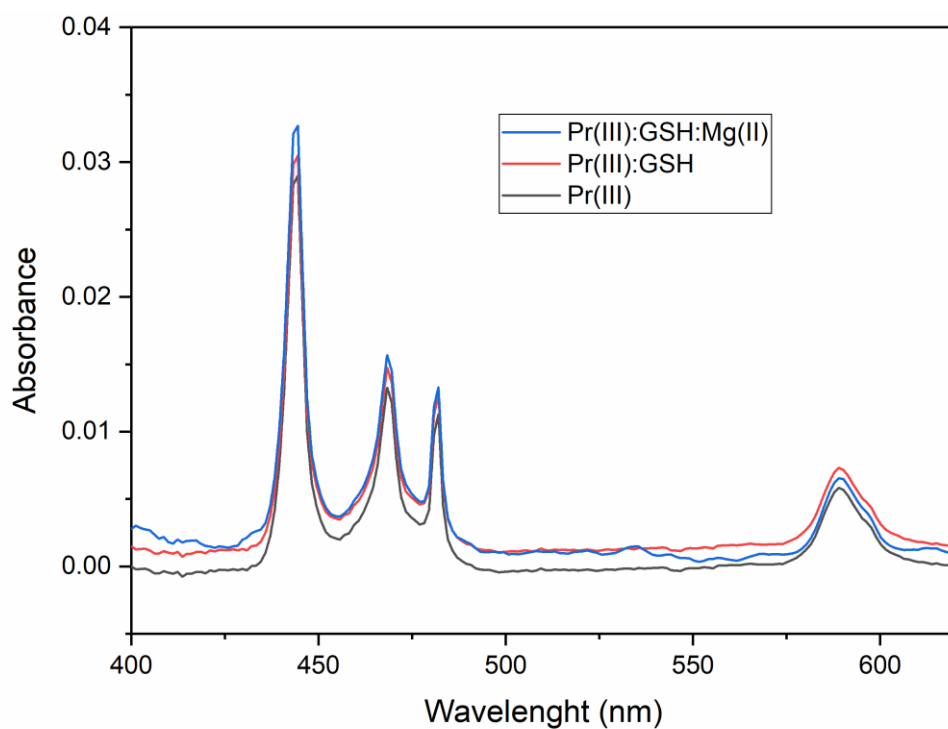


Fig. 2.1: Comparative absorption spectra of Pr(III), Pr(III):GSH and Pr(III):GSH:Mg(II) in DMF at pH 2.

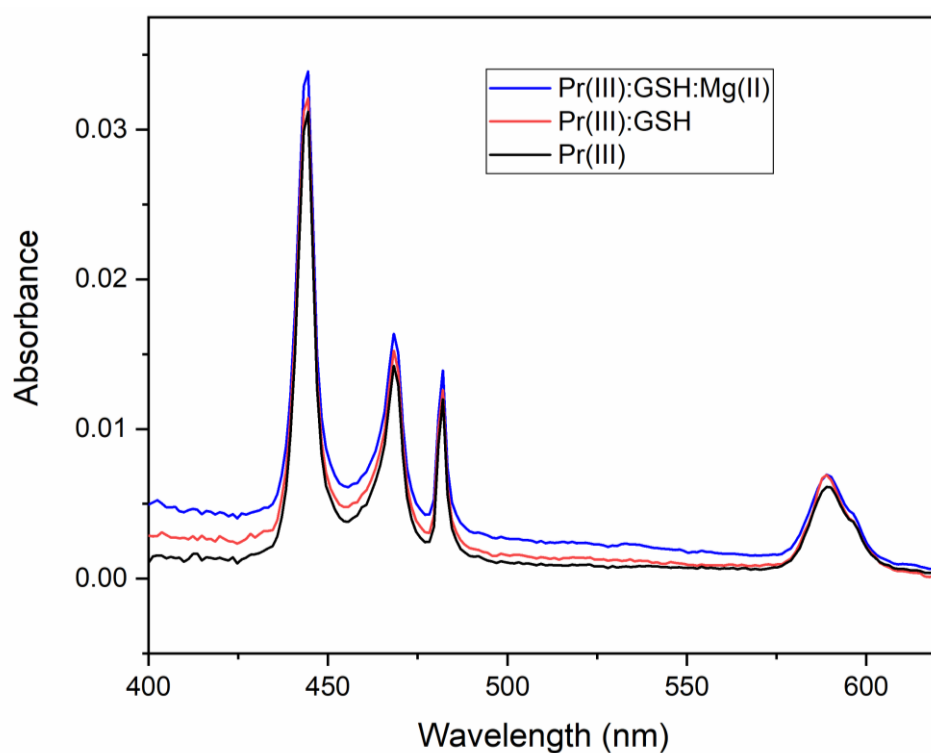


Fig. 2.2: Comparative absorption spectra of Pr(III), Pr(III):GSH and Pr(III):GSH:Mg(II) in DMF at pH 4.

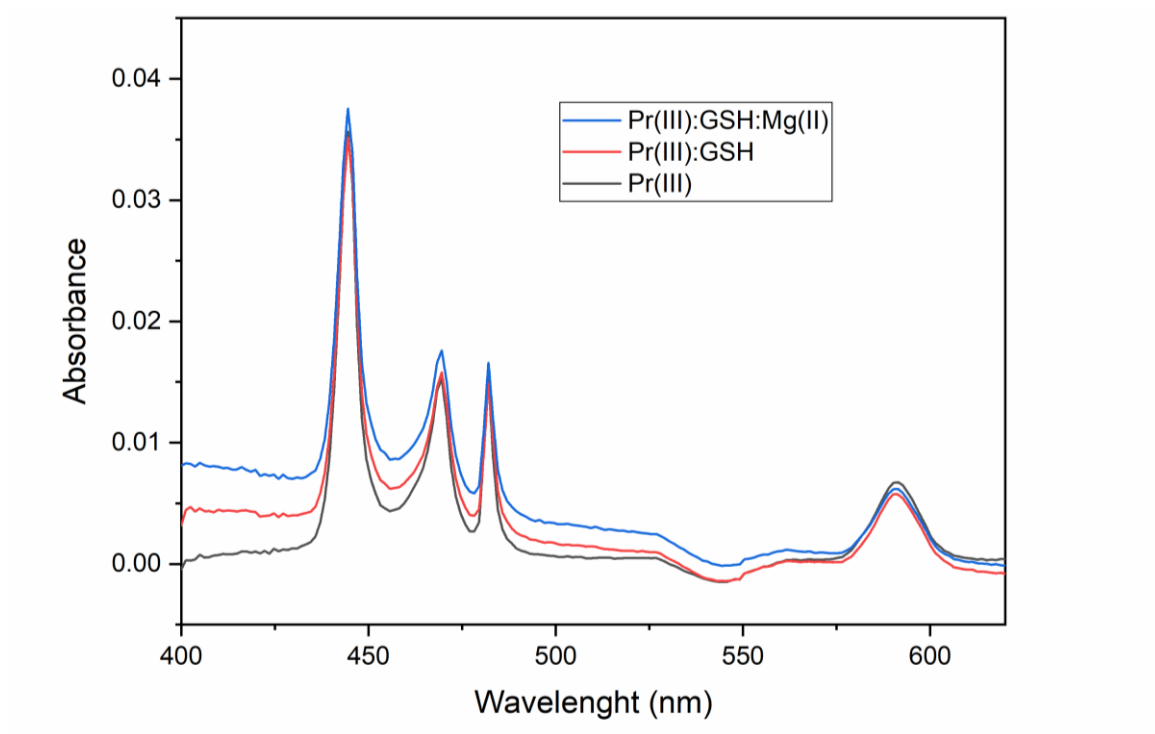


Fig. 2.3: Comparative absorption spectra of Pr(III), Pr(III):GSH and Pr(III):GSH:Mg(II) in DMF at pH 6.

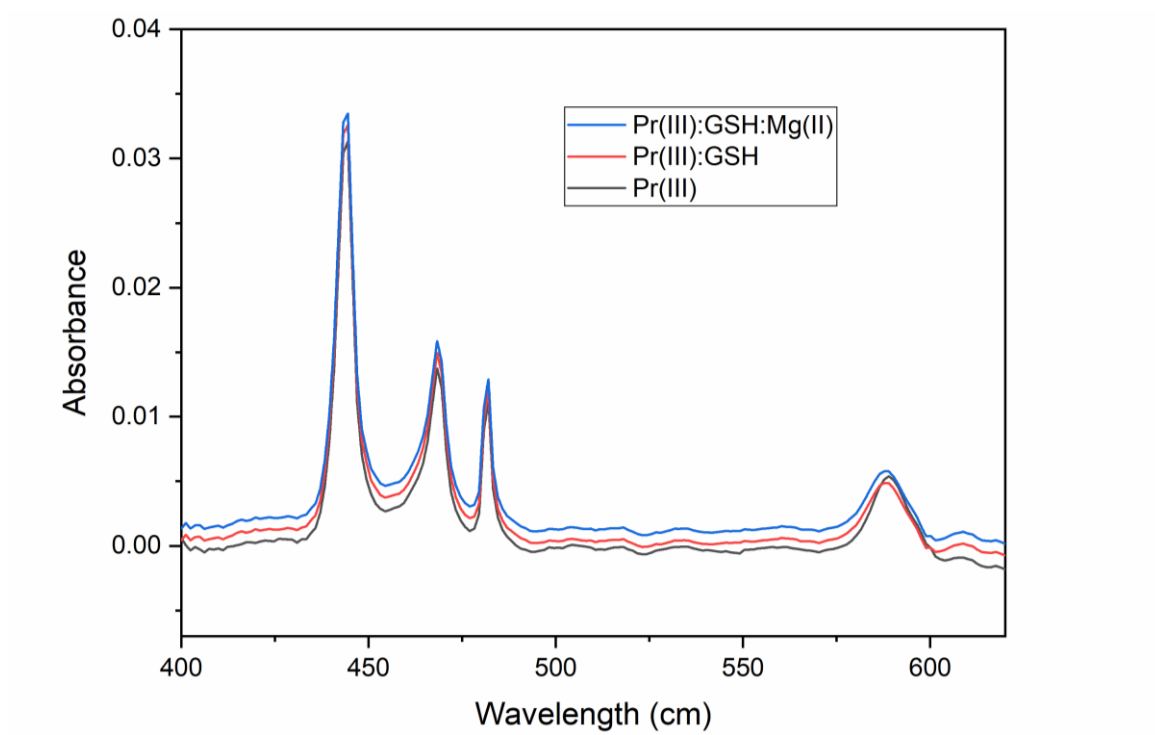


Fig. 2.4: Comparative absorption spectra of Pr(III), Pr(III):GSH and Pr(III):GSH:Mg(II) in CH₃CN at pH 2.

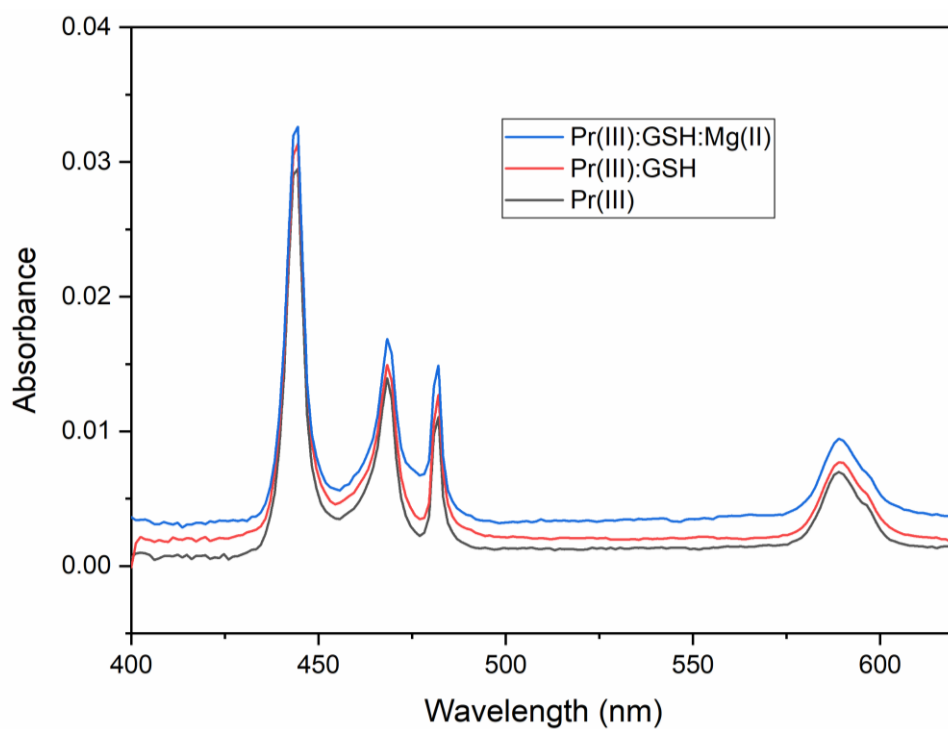


Fig. 2.5: Comparative absorption spectra of Pr(III), Pr(III):GSH and Pr(III):GSH:Mg(II) in CH₃CN at pH 4.

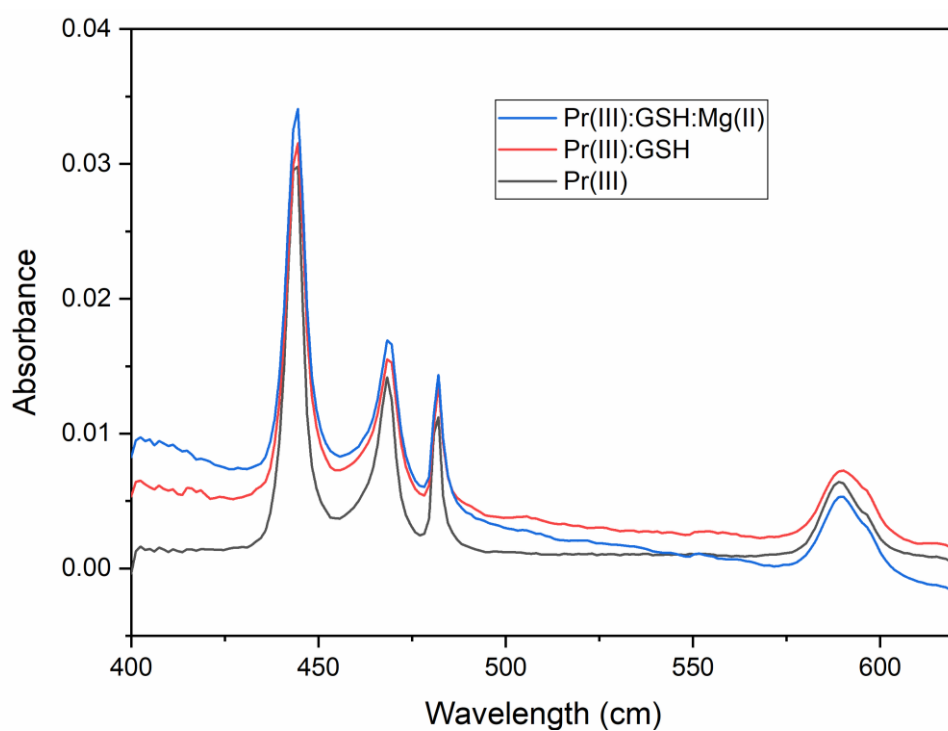


Fig. 2.6: Comparative absorption spectra of Pr(III), Pr(III):GSH and Pr(III):GSH:Mg(II) in CH₃CN at pH 6.

CHAPTER 3

SPECTRAL ANALYSIS OF THE COMPLEXATION OF Pr(III) WITH GSH IN THE PRESENCE AND ABSENCE OF Mg(II) IN DIFFERENT SOLVENTS AND KINETICS FOR THE COMPLEXATION OF Pr(III):GSH WITH Mg(II)

3.1 Introduction

In this chapter, we report a quantitative study on the absorption spectra of Pr(III) ion and its complexes with reduced glutathione (GSH) in the presence and absence of Mg(II) in four different aquated organic solvents (50% v/v) (Methanol:water, dioxane:water, acetonitrile:water and DMF:water). Using the spectral absorption data of the intra-4fⁿ electronic transitions, the spectral properties of pseudohypersensitive transitions ($^3\text{H}_4 \rightarrow ^3\text{P}_2$, $^3\text{H}_4 \rightarrow ^3\text{P}_1$, $^3\text{H}_4 \rightarrow ^3\text{P}_0$ and $^3\text{H}_4 \rightarrow ^1\text{D}_2$) of Pr(III) complexes with GSH and Mg(II) were investigated to understand the binding behaviour between Pr(III) and the ligand. We also investigated the effect of Mg(II) in the interaction of Ln(III) ion with GSH. The spectral (energy interaction and intensity) parameters in the formation of lanthanide complexes were measured by evaluating their values from the absorption spectra of the various 4f-4f transitions of Pr(III). The energy interaction parameters like Slater-Condon inter-electronic repulsion parameters (F_k , $k=2, 4, 6$), Racah coulombic interaction parameters (E^k , $k=2, 4, 6$), Lande spin-orbital interactions (ζ_{4f}), Nephelauxetic ratio (β), bonding parameter ($b^{1/2}$), per cent covalency (δ) and the intensity parameters like oscillator strength (P) and Judd-Ofelt intensity parameters T_λ ($\lambda=2, 4, 6$) were computed and analysed to examine the

coordination nature of the complexes formed by Pr(III) with glutathione and Mg(II). The oscillator strengths were calculated and compared to their experimental values. Furthermore, the reaction dynamics and thermodynamic properties for the complexation of Pr(III) with GSH and Mg(II) have been investigated using different computed parameters like rate constant (k), activation energy (E_a), A (pre-exponential factor) and thermodynamic parameters, ΔH^0 , ΔG^0 and ΔS^0 in different temperatures viz., 303K, 308K, 313K and 318K.

3.2 Experimental

All of the chemicals used in the experiments were of analytical grade. L-Glutathione reduced ($C_{10}H_{17}N_3O_6S$, $\geq 98.0\%$, Sigma-Aldrich), Praseodymium nitrate hexahydrate ($Pr(NO_3)_3 \cdot 6H_2O$, 99.99%, Sigma-Aldrich), Magnesium nitrate hexahydrate ($Mg(NO_3)_2 \cdot 6H_2O$, 97.0%, HiMedia). The solvents used are dioxane ($C_4H_8O_2$), methanol (CH_3OH), dimethylformamide (C_3H_7NO) and acetonitrile (CH_3CN). The solvents were purchased from HiMedia and have a purity of 99.0%.

3×10^{-3} M concentration of Pr(III), Pr(III):GSH, and Pr(III):GSH:Mg(II) were prepared in aqueous solutions of dioxane, methanol, DMF and acetonitrile. For all the cases, the ratio of organic solvent to water was 50:50 by volume. The UV-Visible solution study of Pr(III) and its complexes with GSH and Mg(II) were carried out at pH 4. All UV-Visible spectra of the prepared solutions were measured at ambient temperature using a Perkin Elmer Lambda 365 UV/Vis spectrometer within a range of 400-650 nm. For kinetics and thermodynamic investigations, the UV-VIS spectra of the Pr(III):GSH:Mg(II) complex are recorded in DMF-water solvent at four different temperatures of 298K, 303K, 308K, 313K and 318K.

3.3 Methods

(a) Energy interaction parameters: Nephelauxetic Ratio, Bonding parameter, Slater-Condon parameter, Lande's parameter, Racah parameter and Percent covalency

The Nephelauxetic ratio (β), is described as the ratio of inter-electronic repulsion of the free ion (f) and complex (c) and is linked with the Racah and Slater–Condon parameters [1,2].

$$\beta = \frac{F_k^c}{F_k^f} \text{ or } \frac{E_C^k}{E_f^k} \quad \text{Eq. 1}$$

E^k and F_k are the Racah and Slater-Condon parameters of the free ion and complex.

The bonding parameter ($b^{1/2}$) represents the degree of mixing of the ligand and 4f orbitals and is correlated to the nephelauxetic effect ($1 - \beta$) as

$$b^{1/2} = \left[\frac{1 - \beta}{2} \right]^{1/2} \quad \text{Eq. 2}$$

The electrostatic interaction energy term, E_0 , is calculated using the Slater radial integral, also called the Slater–Condon parameter, F_k ,

$$E_0 = \sum_{k=0}^{k=6} K^k F_k \quad \text{Eq. 3}$$

Where K^k is the angular coefficient

The Slater-Condon parameters (F_k) or also called direct-integrals are inversely related to K , as shown by the relationship.

$$F_1^k = \int_0^\infty \int_0^\infty \frac{r_i^k}{r_j^{k+1}} R_i^2(r_i) R_j^2(r_j) r_i^2 r_j^2 dr_i dr_j \quad \text{Eq. 4}$$

Here $r_<$ and $r_>$ denotes the smaller and greater radii of r_i and r_j respectively; the i th and j th electrons under examination are denoted i and j and R represent the 4f-radial wave function. F^k integrals as redefined by Condon and Shortley [3] in relation to the reduced integral F_k is

$$F_k = \frac{F^k}{D_k} \quad \text{Eq. 5}$$

Combining the previous two equations (Eq. 4 and 5) gives the reduced Slater-Condon integral:

$$F_k = \frac{1}{D_k} \int_0^\infty \int_0^\infty \frac{r_<^k}{r_>^{k+1}} R_i^2(r_i) R_j^2(r_j) r_i^2 r_j^2 dr_i dr_j \quad \text{Eq. 6}$$

Where D_k is the denominator and F_k is the coefficient of linear combination. F_k is the expected value of the scalar product ($C_1^k C_2^k$).

E^{ki} is a linear combination of F_k given by Racah's energy interaction parameter

$$\begin{aligned} E^1 &= \frac{70F_2 + 231F_4 + 20.02F_6}{9} \\ E^2 &= \frac{F_2 - 3F_4 + 7F_6}{9} \\ E^3 &= \frac{5F_2 + 6F_4 - 9F_6}{3} \end{aligned} \quad \text{Eq. 7}$$

The spin-orbital interaction is perhaps the most important of the magnetic interactions, and the energy associated with it E_{so} can be represented as

$$E_{so} = A_{so} \xi_{4f} \quad \text{Eq. 8}$$

A_{so} , denotes the angular component of spin-orbital interactions; ξ_{4f} denotes the radial integral or Lande spin-orbit coupling constant. The variations in the parameters F_k and 4f

under the impact of the solution matrix's electric field are minor. As a result, Wong [4], described E_j , the energy of the j th level as a first order approximation.

$$E_j(F_k, \xi_{4f}) = E_{0j}(F_k^0, \xi_{4f}^0) + \frac{\partial E_j}{\partial F_k} \Delta F_k + \frac{\partial E_j}{\partial \xi_{4f}} \Delta \xi_{4f} \quad \text{Eq. 9}$$

Here E_{0j} is the j th level's zero order energy. The values of Slater-Condon (F_k) and Lande spin-orbit interactions (ξ_{4f}) parameters are determined by Eq. 10 and 11.

$$F_k = F_k^0 + \Delta F_k \quad \text{Eq. 10}$$

$$\xi_{4f} = \xi_{4f}^0 + \Delta \xi_{4f} \quad \text{Eq. 11}$$

The difference between E_j value and the zero order, ΔE_j , value is calculated as

$$\Delta E_j = \sum_{k=2,4,6} \frac{\partial E_j}{\partial F_k} \Delta F_k + \frac{\partial E_j}{\partial \xi_{4f}} \Delta \xi_{4f} \quad \text{Eq. 12}$$

The values of ΔF_k and $\Delta \xi_{4f}$ can be obtained by using the least square technique to solve the above equation [4]. Using Eq. 10 and 11 the values of F_k ($k=2,4,6$) and ξ_{4f} are calculated.

The percent covalency (δ) is correlated to $(1 - \beta)$ (nephelauxetic effect) and is found out by

$$\delta = \left[\frac{1-\beta}{\beta} \right] \times 100 \quad \text{Eq. 13}$$

(b) Judd-Ofelt intensity parameters (T_λ , $\lambda=2,4,6$)

Theoretical calculations for the band intensities were done using Judd and Ofelt's theoretical technique. The 4f-4f transition absorption spectra of Ln(III) ions with a 4fⁿ shell structure are fundamentally electric dipole in nature and thus forbidden by principle. In light of this, Judd and Ofelt demonstrated that admixture of 4f configurations with reverse parity is possible due to crystal field potential, and that ground to excited multiplet transitions are allowed by induced electric dipole. By applying the Judd-Ofelt theory [5,6],

the oscillator strength, P_{cal} , of the induced-dipole transition between ψJ and $\psi' J'$ states is expressed as,

$$P_{cal} = \sum_{\lambda=2,4,6} T_{\lambda} \sigma(f^N \psi J \| U^{\lambda} \| f^N \psi' J')^2 \quad Eq. 14$$

where $U^{(\lambda)}$ ($\lambda=2,4,6$) are Carnall's reduced matrix elements for Pr^{III} [7]. The Judd-Ofelt intensity parameters, T_{λ} ($\lambda=2,4,6$) are phenomenological parameters that describe the intensity of the 4f electron transitions of lanthanides. The three quantities T_2 , T_4 and T_6 connects the ground and final states ($f^N \psi J$ and $f^N \psi' J'$) through the squared reduced matrix elements U^{λ} . The oscillator strength's accuracy and the type of transitions employed in their computation strongly influence the T_{λ} parameters. Even slight changes in the symmetry of the complexes and coordination surrounding the $\text{Ln}(\text{III})$ ion have a big impact on the T_2 , T_4 , and T_6 parameters.

The oscillatory strength is defined as the area under the absorption curve. This is given as

$$P = 4.6 \times 10^{-9} \left[\frac{9\eta}{(\eta^2 + \eta)^2} \right] \int \epsilon_{max} \bar{\nu} d\bar{\nu} \quad Eq. 15$$

Where $\bar{\nu}$, ϵ_{max} and η are wave number, molar extinction coefficient and refractive index respectively.

The probability (P) of radiant energy absorption is associated with the observed intensity of an absorption band. The oscillator strength (P) describes the strength of the electronic transitions and may be evaluated theoretically or experimentally from the absorption spectrum. Using the following expression, the experimental oscillator Strength (P_{obs}) values of the absorption bands are calculated

$$P_{obs} = 4.6 \times 10^{-9} \times \epsilon_{max} \bar{\nu}_{1/2} \quad Eq. 16$$

Where $\bar{\nu}_{1/2}$ is the half bandwidth

Using the value of P_{obs} and reduced matrix elements $U^{(\lambda)}$ [7], the Judd-Ofelt intensity parameters T_2 , T_4 and T_6 can be calculated from the following expression,

$$\frac{P_{obs}}{\nu} = [(U^2)^2.T_2 + [U^2]^2.T_4 + [U^2]^2.T_6 \quad Eq. 17$$

Where, ν = energy transition and U = matrix element

(c) Theory of reaction dynamics and thermodynamics

Using the Arrhenius reaction rate equation, the activation energy (E_a) for the complexation of Pr(III) with glutathione and Mg(II) in DMF:water was found out by plotting $\log k$ (k = rate constant) against $1/T$.

$$\log k = \log A - \frac{E_a}{2.303R} \frac{1}{T} \quad Eq. 18$$

Here the pre-exponential factor is represented by ' A ' which is related to the frequency of collisions and orientation probability of collisions for the reaction. The reaction rate (k) can be calculated from the Activation energy (E_a). The activation energy (E_a) is calculated using the slope as,

$$E_a = \text{slope} \times 2.303 \times R \quad Eq. 19$$

The thermodynamic parameters (ΔH^0 , ΔG^0 , ΔS^0) for the complexation are calculated using the Van't Hoff plot of $\log k$ vs $1/T \times 10^3$

$$\log k = - \frac{\Delta H^0}{R} \left[\frac{1}{T} \right] + \frac{\Delta S^0}{R} \quad Eq. 20$$

$$\text{Or } \log k = - \frac{\Delta G^0}{RT}$$

3.4 Results and Discussions

Fig. 3.1 to 3.4 represents the comparative absorption spectra of the different 4f-4f transitions for Pr(III), Pr(III):GSH and Pr(III):GSH:Mg(II) in different solvents in the UV-Vis region. From the figure, it is clearly visible that the band intensity varies in the presence of the ligands. It is found that the intensity of the 4f-4f transition bands enhances with a minor red shift when GSH is added to Pr(III) aqua ion, and further increases on adding Mg(II) to the Pr(III):GSH complex. This illustrates the possibility of the interaction between Pr(III), GSH and Mg(II) in solution. The enhancement in the intensities of the 4f-4f bands upon adding GSH to Pr(III) is possibly because of the interaction that takes place between Pr(III) and GSH due to the affinity of the hard metal ion, Pr(III) for the binding sites of GSH. It is likely that the stronger peaks in the presence of Mg(II) are because of their tendency to interact with the binding sites of GSH and its subsequent complexation resulting in the formation of a heterobimetallic Pr(III):GSH:Mg(II) complex in solution [8].

Table 3.1 presents the computed values of the energy interaction parameters, Slater-Condon factor (F_k), Lande spin-orbit interactions (ζ_{4f}), Racah (E^k), Nephelauxetic ratio (β), bonding ($b^{1/2}$), and percent covalency (δ) parameter of Pr(III), Pr(III):GSH and Pr(III):GSH:Mg(II) complex in 50% (v/v) aqueous solutions of CH₃OH, C₄H₈O₂, CH₃CN and DMF. The value of F_k ($k=2,4,6$), E^k ($k=2,4,6$) and Lande (ζ_{4f}) parameter decreases slightly as complexation continues with the addition of GSH and Mg(II) to Pr(III). Because F_k and E^k are inter-related, hence any change in the values of E^k corresponds proportionately to the variations in the values of F_k . The marginal decrease in F_k and ζ_{4f} values increases the bonding parameter ($b^{1/2}$) and percent covalency (δ) values indicating the shortening of distance in the metal-ligand bond. In all of the lanthanide systems in the different solvents, the values of nephelauxetic ratio are found to be less than 1 and the $b^{1/2}$ and δ values are both positive which suggests the possible involvement of the 4f orbitals of Pr(III) in

coordinate covalent bond between the metal ion and ligand when complexation takes place in solution [9,10]. The slight variation in the bonding parameter values also implies that the 4f orbitals are only partly involved in the Ln(III) complex bond formation. However, when compared to other solvents, the values of $b^{1/2}$ and δ are shown to be maximum in DMF:water, indicating that complexation between Pr(III) and the ligand is favoured more in this solvent. The RMS (root mean square deviation) value represents the accuracy of the computed energy parameters. The values of the energy parameters vary in different solvents, suggesting that the solvents also have their contribution to the values of energy parameters.

In Table 3.1 and 3.2 we see the computed spectral parameters of Pr(III), Pr(III):GSH and Pr(III):GSH:Mg(II) in aquated solvents of CH₃OH, C₄H₈O₂, CH₃CN and DMF. The effect of the solvent on the interaction between Pr(III) ion and GSH in the presence and the absence of Mg(II) is clear from the computed parameter values where the greatest enhancement is observed in aquated DMF solvent implying that it is the most favourable solvent for complexation. The values of oscillator strength are also found to be highest in DMF solvent. The intensity of the 4f bands is proportional to the degree of symmetry distortion in the solvated Pr(III) ion. DMF being a stronger oxygen donor than the other solvents is able to replace the nitrate ions from the solvated species more effectively, enhancing the 4f-4f transition intensity of the lanthanide [11]. DMF is also responsible for penetrating the hydration sphere and altering the field strength and symmetry around Pr(III), rendering transitions that were forbidden due to symmetry to be allowed resulting in a stronger 4f-4f band than that of other solvents [12]. For the organic solvents, the sensitivity order of 4f-4f band intensities is as follows DMF>CH₃CN>C₄H₈O₂>CH₃OH. This indicates that, of all the organic solvents, DMF has the greatest influence in the formation of complex in solution.

The comparative data of oscillator strengths (P) and Judd-Ofelt intensity parameters (T_2 , T_4 and T_6) of the 4f-4f transitions of Pr(III), Pr(III):GSH and Pr(III):GSH:Mg(II) systems in different solvents are reported in Table 3.2. The computed intensity parameters were used to analyse the various 4f transition peaks of the lanthanide systems in different solvents. The variations in the values of the evaluated oscillator strengths of the pseudohypersensitive transition and the corresponding values of Judd-Ofelt parameters T_λ ($\lambda=2, 4, 6$) could reveal the binding characteristics of Pr(III) with GSH. As the intensities of the absorption peaks for the pseudohypersensitive transitions of Pr(III) increases, their oscillator strength and T_λ values also increase. It is evident from the table that the values of P and T_2 , T_4 and T_6 increases when glutathione is added to Pr(III) and Mg(II) is added to the Pr(III):GSH complex. The increase in the values of these parameters suggests the possibility of binding between GSH and Pr(III) and the involvement of Mg(II) in the formation of the multimetal complex. The T_2 values are occasionally found to be negative and hence ignored which may be because of the fact that the hypersensitive transition, $^3H_4 \rightarrow ^3F_2$ is beyond the UV-Visible range [8]. T_4 and T_6 values on the other hand are greater than zero and thereby applicable in the Judd-Ofelt theory of 4f-4f transitions. Significant changes in the T_4 and T_6 values suggests a change in symmetry of the Pr(III) and its complex systems as well as changes in their immediate coordination environment. Judd [13] attributed the hypersensitivity of lanthanide ions to changes in the symmetry of its environment [14]. Based on the evaluated Judd-Ofelt intensity parameter values, T_6 value is found to be the most significant parameter, with the following order $T_6 > T_4 > T_2$. Higher values of oscillator strength (P) and their corresponding T_λ values indicate inner-sphere complexation while lower values of oscillator strength and T_λ indicate outer-sphere complexation. The changes in values of intensity parameters (Table 3.2) are regarded as strong evidence for the participation of GSH in inner-sphere coordination with Pr(III).

Solution absorption spectral analysis of the 4f transitions to probe the kinetics of Pr(III):GSH:Mg(II) complex formation were carried out in DMF:water (50% v/v) solvent at four different temperatures (303K, 308K, 313K and 318K) with a time interval of two hours. The absorption spectra of Pr(III):GSH:Mg(II) in DMF at 303K and 308K at different hours given in Fig. 3.5 and Fig. 3.6 shows that the intensity of its 4f transitions gradually increases over time. The values of oscillator strengths ($P \times 10^6$) and Judd-Ofelt parameters (T_λ) of the transitions for the formation of the complex at different temperatures (303K, 308K, 313K, 318K) are shown in Table 3.3, 3.4, 3.5 and 3.6. The intensity parameter (P and T_λ) values are found to increase with time and temperature suggesting an increase in the rate of complexation. The observed rate (k) values were evaluated on the basis of complex formation during the reaction process. The rate constant was calculated from the plots of P_{obs} value of $^3H_4 \rightarrow ^3P_2$ transition of Pr(III) complex with GSH and Mg(II) vs time (hr) for the different temperatures (Fig. 3.7). Tables 3.7 and 3.8 give the evaluated values of the rate constants (k), pre-exponential factor (A) activation energy (E_a) and the thermodynamic parameters, ΔH^0 , ΔG^0 and ΔS^0 for Pr(III):GSH:Mg(II) complexation in DMF:water at temperatures of 303K, 308K, 313K and 318K. The activation energy (E_a) and thermodynamic parameters (ΔH^0 , ΔG^0 and ΔS^0) were evaluated using the Van't Hoff plot ($\log k$ vs $1/T$) (Fig. 3.8). This method allows us to investigate the chemical dynamics and predict the thermodynamic nature of the complexation of Pr(III) with GSH and Mg(II) ligand by evaluating the different kinetic and thermodynamic parameters (Table 3.7 and 3.8). From the data obtained, it is evident that the rate of complexation increases with increasing temperature in the tune with Arrhenius prediction. The positive values of enthalpy (ΔH^0) reveal that the reaction system is endothermic in nature, the negative value of (ΔG^0) predicts the spontaneity of the reaction process as well as the favourable nature of the reaction in solution; the low value of entropy (ΔS^0) signifies the possibility of the

formation of complexes in solution. The positive value of 'A' substantiates the formation of complexes in solution.

*The work presented in this chapter has been published in *Journal of the Indian Chemical Society*, 98, 100232, **2021**.

References

- [1] D.E. Henrie, G.R. Choppin, Environmental effects on f-f transitions. II. “Hypersensitivity” in some complexes of trivalent neodymium, *J. Chem. Phys.* **49** (1968) 477–481. <https://doi.org/10.1063/1.1670099>.
- [2] C.K. Jørgensen, B.R. Judd, Hypersensitive pseudoquadrupole transitions in lanthanides, *Mol. Phys.* **8** (1964) 281–290. <https://doi.org/10.1080/00268976400100321>.
- [3] E.U. Condon, G.H. Shortley, C.W. Ufford, The Theory of Atomic Spectra, *Am. J. Phys.* **20** (1952) 383–383. <https://doi.org/10.1119/1.1933256>.
- [4] E.Y. Wong, Taylor series expansion of the intermediate coupling energy levels of Nd³⁺ and Er³⁺, *J. Chem. Phys.* **35** (1961) 544. <https://doi.org/10.1063/1.1731965>.
- [5] B.R. Judd, Optical absorption intensities of rare-earth ions, *Phys. Rev.* **127** (1962) 750–761. <https://doi.org/10.1103/PhysRev.127.750>.
- [6] G.S. Ofelt, Intensities of Crystal Spectra of RareEarth Ions, *J. Chem. Phys.* **37** (1962) 511–520. <https://doi.org/10.1063/1.1701366>.
- [7] W.T. Carnall, P.R. Fields, B.G. Wybourne, Spectral intensities of the trivalent lanthanides and actinides in solution. I. Pr³⁺, Nd³⁺, Er³⁺, Tm³⁺, and Yb³⁺, *J. Chem. Phys.* **42** (1965) 3797–3806. <https://doi.org/10.1063/1.1695840>.
- [8] S.N. Misra, M. Indira Devi, C.M. Suveerkumar, K.M. Suma, Electric dipole intensity parameters for a series of structurally related praseodymium(III) and neodymium(III) complexes and unusual sensitivities of some 4f-4f transitions, *Rev. Inorg. Chem.* **14** (1994) 347–362. <https://doi.org/10.1515/REVIC.1994.14.5.347>.

- [9] C.E. Schäffer, C. Klixbüll Jørgensen, The nephelauxetic series of ligands corresponding to increasing tendency of partly covalent bonding, *J. Inorg. Nucl. Chem.* **8** (1958) 143–148. [https://doi.org/10.1016/0022-1902\(58\)80176-1](https://doi.org/10.1016/0022-1902(58)80176-1).
- [10] S.P. Sinha, Spectroscopic investigations of some neodymium complexes, *Spectrochim. Acta.* **22** (1966) 57–62. [https://doi.org/10.1016/0371-1951\(66\)80008-5](https://doi.org/10.1016/0371-1951(66)80008-5).
- [11] A.A. Khan, H.A. Hussain, K. Iftikhar, 4f-4f absorption spectra of nine-coordinate Pr (III) and Nd (III) complexes in different environments, *Spectrochim. Acta - Part A Mol. Biomol. Spectrosc.* **59** (2003) 1051–1059. [https://doi.org/10.1016/S1386-1425\(02\)00277-9](https://doi.org/10.1016/S1386-1425(02)00277-9).
- [12] A.A. Khan, H.A. Hussain, K. Iftikhar, 4f-4f absorption spectra and hypersensitivity in nine-coordinate Ho(III) and Er(III) complexes in different environments, *Spectrochim. Acta - Part A Mol. Biomol. Spectrosc.* **60** (2004) 2087–2092. <https://doi.org/10.1016/j.saa.2003.10.042>.
- [13] B.R. Judd, Hypersensitive transitions in rare-earth ions, *J. Chem. Phys.* **44** (1966) 839. <https://doi.org/10.1063/1.1726774>.
- [14] D.G. Karraker, Hypersensitive Transitions of Six-, Seven-, and Eight-Coordinate Neodymium, Holmium, and Erbium Chelates, *Inorg. Chem.* **6** (1967) 1863–1868. <https://doi.org/10.1021/ic50056a022>.

Table 3.1: Computed values of the energy interaction parameters: Slater-Condon factor F_k (cm^{-1}), Lande spin-orbit interaction ξ_{4f} (cm^{-1}), Racah E^k , Nephelauxetic ratio (β), bonding ($b^{1/2}$) and percent covalency (δ) parameter of Pr(III) and its complexes in 50% (v/v) aquated solvents of CH_3OH , $\text{C}_4\text{H}_8\text{O}_2$, CH_3CN and DMF.

System	F_2	F_4	F_6	ξ_{4f}	E^1	E^2	E^3	β	$b^{1/2}$	δ	RMS
1. CH_3OH											
Pr(III)	309.3796	42.7099	4.6716	722.2858	3512.8971	23.7724	615.0673	0.9470	0.1628	5.5998	101.40
Pr(III):GSH	309.3703	42.7086	4.6715	722.2422	3512.7913	23.7717	615.0487	0.9469	0.1629	5.6046	101.74
Pr(III):GSH:Mg(II)	309.3617	42.7074	4.6714	722.1451	3512.6943	23.7710	615.0318	0.9468	0.1630	5.6134	101.41
2. Dioxane											
Pr(III)	309.3819	42.7102	4.6717	722.3167	3512.9230	23.7726	615.0718	0.9470	0.1628	5.5971	102.05
Pr(III):GSH	309.3615	42.7073	4.6714	722.1341	3512.6911	23.7710	615.0312	0.9468	0.1630	5.6143	102.29
Pr(III):GSH:Mg(II)	309.3509	42.7059	4.6712	721.9863	3512.5711	23.7702	615.0102	0.9467	0.1632	5.6273	102.05
3. CH_3CN											
Pr(III)	309.3819	42.7102	4.6717	722.3167	3512.9230	23.7726	615.0718	0.9470	0.1628	5.5971	102.05
Pr(III):GSH	309.3739	42.7091	4.6715	722.2760	3512.8328	23.7719	615.056	0.9470	0.1629	5.6015	102.10
Pr(III):GSH:Mg(II)	309.3087	42.7001	4.6706	722.2861	3512.0927	23.7669	614.9264	0.9469	0.1630	5.6113	101.90
4. DMF											
Pr(III)	309.3625	42.7075	4.6714	722.2902	3512.7032	23.7711	615.0333	0.9469	0.1629	5.6022	101.60
Pr(III):GSH	309.3224	42.7020	4.6708	721.5840	3512.2477	23.7680	614.9536	0.9464	0.1637	5.6627	98.89
Pr(III):GSH:Mg(II)	309.3013	42.6990	4.6704	721.7151	3512.0076	23.7664	614.9115	0.9465	0.1636	5.6562	98.66

Table 3.2: Observed and computed values of oscillator strengths ($P \times 10^6$) and Judd-Ofelt ($T_\lambda \times 10^{10}$) parameters of Pr(III) and its complexes in 50% (v/v) aquated solvents of CH₃OH, C₄H₈O₂, CH₃CN and DMF.

System	$^3\text{H}_4 \rightarrow ^3\text{P}_2$		$^3\text{H}_4 \rightarrow ^3\text{P}_1$		$^3\text{H}_4 \rightarrow ^3\text{P}_0$		$^3\text{H}_4 \rightarrow ^1\text{D}_2$		T ₂	T ₄	T ₆
	P _{obs}	P _{cal}	P _{obs}	P _{cal}	P _{obs}	P _{cal}	P _{obs}	P _{cal}			
1. CH ₃ OH											
Pr(III)	11.5837	11.5837	4.2559	3.1196	1.9531	3.0721	3.1227	3.1227	-61.76	8.5634	35.662
Pr(III):GSH	12.1616	12.1616	4.6909	3.3651	2.0083	3.3139	3.5806	3.5806	3.2421	9.2372	37.378
Pr(III):GSH:Mg(II)	12.2117	12.2117	4.9854	3.5617	2.1055	3.5075	3.7983	3.7983	48.634	9.7769	37.398
2. Dioxane											
Pr(III)	11.5647	11.5647	4.2428	2.9969	1.7245	2.9494	3.5112	3.5112	28.031	8.2222	35.676
Pr(III):GSH	11.9831	11.9831	4.3354	3.2952	2.2208	3.2451	3.6192	3.6192	23.928	9.0454	36.844
Pr(III):GSH:Mg(II)	12.9070	12.9070	4.6872	3.5168	2.3106	3.4632	3.6285	3.6285	-35.23	9.6535	39.709
3. CH ₃ CN											
Pr(III)	11.5647	11.5647	4.2428	2.9969	1.7245	2.9494	3.5112	3.5112	28.031	8.2222	35.676
Pr(III):GSH	12.5642	12.5642	4.1921	3.2253	2.1974	3.1202	3.6438	3.6438	13.572	8.8165	38.023
Pr(III):GSH:Mg(II)	12.9854	12.9854	5.3378	3.9275	2.5618	3.9132	3.9697	3.9697	31.821	10.872	39.673
4. DMF											
Pr(III)	12.2678	12.2678	4.9338	3.6006	2.2356	3.5501	3.9276	3.9276	76.596	9.9035	37.598
Pr(III):GSH	12.8892	12.8892	5.3685	3.8697	2.3495	3.8120	4.0089	4.0089	47.128	10.576	38.731
Pr(III):GSH:Mg(II)	13.7526	13.7526	5.6852	4.1783	2.6872	4.1543	3.8536	3.8536	-22.4	11.422	41.278

Table 3.3: Observed and calculated oscillator strengths ($P \times 10^6$) and Judd-Ofelt intensity parameters ($T_\lambda \times 10^{10}$) parameters for Pr(III):GSH:Mg(II) complex at 303K (30 °C) at different hours.

Time (in hr)	$^3H_4 \rightarrow ^3P_2$		$^3H_4 \rightarrow ^3P_1$		$^3H_4 \rightarrow ^3P_0$		$^3H_4 \rightarrow ^1D_2$		T_2	T_4	T_6
	P_{obs}	P_{cal}	P_{obs}	P_{cal}	P_{obs}	P_{cal}	P_{obs}	P_{cal}			
0	1.0505	1.0505	0.4108	0.3529	0.2905	0.3475	0.3173	0.3173	1.9273	0.9689	3.184
2	1.0551	1.0551	0.413	0.2987	0.1817	0.2942	0.423	0.423	25.759	0.8202	3.2389
4	1.0691	1.0691	0.4388	0.3241	0.2062	0.3192	0.4497	0.4497	30.818	0.8899	3.2662
6	1.0844	1.0844	0.5005	0.367	0.23	0.3614	0.4908	0.4908	38.996	1.0077	3.2846
8	1.0895	1.0895	0.4767	0.3521	0.2239	0.3467	0.5501	0.5501	52.166	0.9666	3.3125
10	1.0959	1.0959	0.4971	0.3658	0.2308	0.3602	0.5642	0.5642	54.896	1.0042	3.3233
12	1.1020	1.1020	0.4941	0.3649	0.232	0.3593	0.542	0.542	49.447	1.0018	3.344
14	1.1101	1.1101	0.4991	0.3682	0.2336	0.3626	0.5588	0.5588	52.722	1.0109	3.368
16	1.1141	1.1141	0.4957	0.3672	0.2349	0.3615	0.5309	0.5309	46.134	1.008	3.3821
18	1.1748	1.1748	0.4692	0.3595	0.246	0.354	0.581	0.581	53.545	0.987	3.5867
20	1.1349	1.1349	0.4692	0.3595	0.246	0.354	0.581	0.581	56.163	0.987	3.4558
22	1.1451	1.1451	0.4835	0.3612	0.2352	0.3557	0.5459	0.5459	47.528	0.9917	3.4881
24	1.1552	1.1552	0.4854	0.3678	0.2464	0.3622	0.5472	0.5472	47.149	1.0098	3.5163
26	1.1631	1.1631	0.4845	0.3686	0.2487	0.3629	0.5352	0.5352	43.907	1.0119	3.5414
28	1.1761	1.1761	0.5031	0.3816	0.2561	0.3758	0.5526	0.5526	46.951	1.0477	3.5747
30	1.1863	1.1863	0.5355	0.3994	0.2592	0.3933	0.5192	0.5192	38.657	1.0965	3.5951
32	1.2164	1.2164	0.5358	0.398	0.2561	0.3919	0.545	0.545	42.534	1.0926	3.6948
34	1.2344	1.2344	0.5435	0.4032	0.2589	0.397	0.5196	0.5196	35.589	1.107	3.7496

Table 3.4: Observed and calculated oscillator strengths ($P \times 10^6$) and Judd-Ofelt intensity parameter ($T_\lambda \times 10^{10}$) parameters for Pr(III):GSH:Mg(II) complex at 308K (35 °C) at different hours.

Time (in hr)	$^3H_4 \rightarrow ^3P_2$		$^3H_4 \rightarrow ^3P_1$		$^3H_4 \rightarrow ^3P_0$		$^3H_4 \rightarrow ^1D_2$		T ₂	T ₄	T ₆
	P _{obs}	P _{cal}	P _{obs}	P _{cal}	P _{obs}	P _{cal}	P _{obs}	P _{cal}			
0	1.0060	1.0060	0.3244	0.2373	0.1479	0.2336	0.2578	0.2578	-8.285	0.6513	3.122
2	1.0141	1.0141	0.346	0.2513	0.1543	0.2475	0.2689	0.2689	-6.352	0.6899	3.1382
4	1.0183	1.0183	0.346	0.2513	0.1543	0.2475	0.2689	0.2689	-6.627	0.6899	3.1519
6	1.0316	1.0316	0.346	0.2513	0.1543	0.2475	0.2689	0.2689	-7.504	0.6899	3.1958
8	1.0364	1.0364	0.3559	0.2631	0.1677	0.2591	0.2891	0.2891	-3.293	0.7222	3.2029
10	1.0476	1.0476	0.3659	0.2689	0.1692	0.2648	0.2996	0.2996	-1.649	0.738	3.2353
12	1.0524	1.0524	0.3559	0.2631	0.1677	0.2591	0.2891	0.2891	-4.34	0.7222	3.2552
14	1.0683	1.0683	0.3958	0.2912	0.1838	0.2868	0.3062	0.3062	-1.595	0.7994	3.2867
16	1.0731	1.0731	0.3759	0.2837	0.1886	0.2794	0.3112	0.3112	-0.743	0.7788	3.3079
18	1.0679	1.0679	0.4058	0.3011	0.1935	0.2965	0.3263	0.3263	4.2709	0.8266	3.2127
20	1.1550	1.1550	0.4025	0.2826	0.1603	0.2783	0.427	0.427	20.135	0.7758	3.5769
22	1.1785	1.1785	0.4324	0.3552	0.2737	0.3497	0.4119	0.4119	14.93	0.9749	3.601
24	1.2057	1.2057	0.4091	0.3517	0.2899	0.3464	0.4235	0.4235	15.786	0.9655	3.6925
26	1.2189	1.2189	0.4423	0.4095	0.3709	0.4032	0.5192	0.5192	36.407	1.124	3.6934
28	1.2385	1.2385	0.4387	0.3739	0.3045	0.3682	0.635	0.635	61.479	1.0264	3.7838
30	1.2403	1.2403	0.462	0.3856	0.3045	0.3797	0.6401	0.6401	62.466	1.0584	3.781
32	1.2544	1.2544	0.4819	0.3881	0.2899	0.3822	0.6562	0.6562	65.185	1.0654	3.8253
34	1.2585	1.2585	0.4885	0.3964	0.2996	0.3904	0.6864	0.6864	71.734	1.0881	3.8327

Table 3.5: Observed and calculated oscillator strengths ($P \times 10^6$) and Judd-Ofelt intensity parameter ($T_\lambda \times 10^{10}$) parameters for Pr(III):GSH:Mg(II) complex at 313K (40°C) at different hours.

Time (in hr)	$^3H_4 \rightarrow ^3P_2$		$^3H_4 \rightarrow ^3P_1$		$^3H_4 \rightarrow ^3P_0$		$^3H_4 \rightarrow ^1D_2$		T_2	T_4	T_6
	P_{obs}	P_{cal}	P_{obs}	P_{cal}	P_{obs}	P_{cal}	P_{obs}	P_{cal}			
0	0.9307	0.9307	0.3775	0.2787	0.1771	0.2744	0.4034	0.4034	29.483	0.765	2.845
2	1.0032	1.0032	0.403	0.293	0.1802	0.2885	0.4176	0.4176	27.902	0.8042	3.0721
4	1.0743	1.0743	0.4694	0.3359	0.1994	0.3308	0.4688	0.4688	34.714	0.9222	3.2736
6	1.0923	1.0923	0.518	0.3679	0.2145	0.3623	0.4863	0.4863	37.38	1.01	3.309
8	1.1072	1.1072	0.5299	0.3795	0.2257	0.3738	0.5149	0.5149	42.847	1.0418	3.3492
10	1.1350	1.1350	0.5038	0.3648	0.2224	0.3592	0.4836	0.4836	33.998	1.0014	3.4513
12	1.1579	1.1579	0.5406	0.3889	0.2336	0.383	0.5485	0.5485	47.111	1.0675	3.5087
14	1.1596	1.1596	0.549	0.3951	0.2376	0.3891	0.557	0.557	48.9	1.0846	3.5095
16	1.1724	1.1724	0.5589	0.4015	0.2403	0.3954	0.5701	0.5701	51.014	1.102	3.547
18	1.1868	1.1868	0.5639	0.4056	0.2435	0.3994	0.5879	0.5879	54.1	1.1134	3.5909
20	1.1946	1.1946	0.5832	0.4209	0.2547	0.4145	0.6466	0.6466	66.831	1.1554	3.6055
22	1.1981	1.1981	0.6	0.4333	0.2626	0.4267	0.6829	0.6829	74.771	1.1895	3.6078
24	1.2025	1.2025	0.6246	0.4517	0.2746	0.4448	0.7193	0.7193	82.685	1.24	3.6085
26	1.2193	1.2193	0.636	0.453	0.2658	0.4461	0.7468	0.7468	87.809	1.2435	3.6627
28	1.2344	1.2344	0.6351	0.4508	0.2625	0.444	0.7358	0.7358	84.329	1.2376	3.7137
30	1.2327	1.2327	0.6621	0.4722	0.2779	0.465	0.7666	0.7666	91.35	1.2961	3.6926
32	1.2536	1.2536	0.6914	0.4936	0.2913	0.4861	0.8254	0.8254	103.22	1.3548	3.7454
34	1.2626	1.2626	0.7441	0.531	0.3129	0.5229	0.9028	0.9028	120.04	1.4575	3.7476

Table 3.6: Observed and calculated oscillator strengths ($P \times 10^6$) and Judd-Ofelt intensity parameter ($T_\lambda \times 10^{10}$) parameters for Pr(III):GSH:Mg(II) complex at 318K (45°C) at different hours.

Time (in hr)	$^3H_4 \rightarrow ^3P_2$		$^3H_4 \rightarrow ^3P_1$		$^3H_4 \rightarrow ^3P_0$		$^3H_4 \rightarrow ^1D_2$		T_2	T_4	T_6
	P_{obs}	P_{cal}	P_{obs}	P_{cal}	P_{obs}	P_{cal}	P_{obs}	P_{cal}			
0	0.9706	0.9706	0.4008	0.2903	0.1771	0.2859	0.2669	0.2669	-4.09	0.7969	2.9673
2	1.0431	1.0431	0.403	0.2937	0.1817	0.2893	0.3726	0.3726	15.096	0.8063	3.2024
4	1.0611	1.0611	0.4056	0.3017	0.1949	0.2971	0.4003	0.4003	20.174	0.8283	3.2555
6	1.0644	1.0644	0.4008	0.2925	0.1815	0.2881	0.3397	0.3397	6.2549	0.8029	3.2729
8	1.0791	1.0791	0.4103	0.3048	0.1964	0.3002	0.3487	0.3487	7.291	0.8368	3.312
10	1.0959	1.0959	0.4306	0.3202	0.2065	0.3153	0.3628	0.3628	9.3301	0.8789	3.3558
12	1.1340	1.1340	0.4509	0.3441	0.2336	0.3388	0.3657	0.3657	7.4146	0.9445	3.463
14	1.1540	1.1540	0.4758	0.3574	0.2353	0.3519	0.4077	0.4077	15.573	0.981	3.5189
16	1.1565	1.1565	0.4957	0.3589	0.2187	0.3534	0.4302	0.4302	20.496	0.9852	3.5259
18	1.1644	1.1644	0.5024	0.3777	0.2492	0.372	0.4148	0.4148	16.439	1.0369	3.5381
20	1.1869	1.1869	0.515	0.3851	0.2514	0.3793	0.4233	0.4233	16.852	1.0572	3.6063
22	1.2054	1.2054	0.5339	0.3953	0.2528	0.3893	0.4465	0.4465	20.877	1.0852	3.6595
24	1.2110	1.2110	0.5581	0.407	0.2519	0.4008	0.4675	0.4675	25.229	1.1171	3.6693
26	1.2201	1.2201	0.5629	0.4145	0.2621	0.4082	0.4904	0.4904	29.789	1.1379	3.6935
28	1.2315	1.2315	0.5653	0.4191	0.2687	0.4127	0.5036	0.5036	32.018	1.1504	3.7275
30	1.2524	1.2524	0.587	0.4318	0.2724	0.4252	0.5656	0.5656	44.659	1.1853	3.7867
32	1.2665	1.2665	0.6165	0.4553	0.2897	0.4484	0.6304	0.6304	58.343	1.2499	3.8156
34	1.2863	1.2863	0.6311	0.4726	0.3093	0.4654	0.66	0.66	63.695	1.2974	3.8679

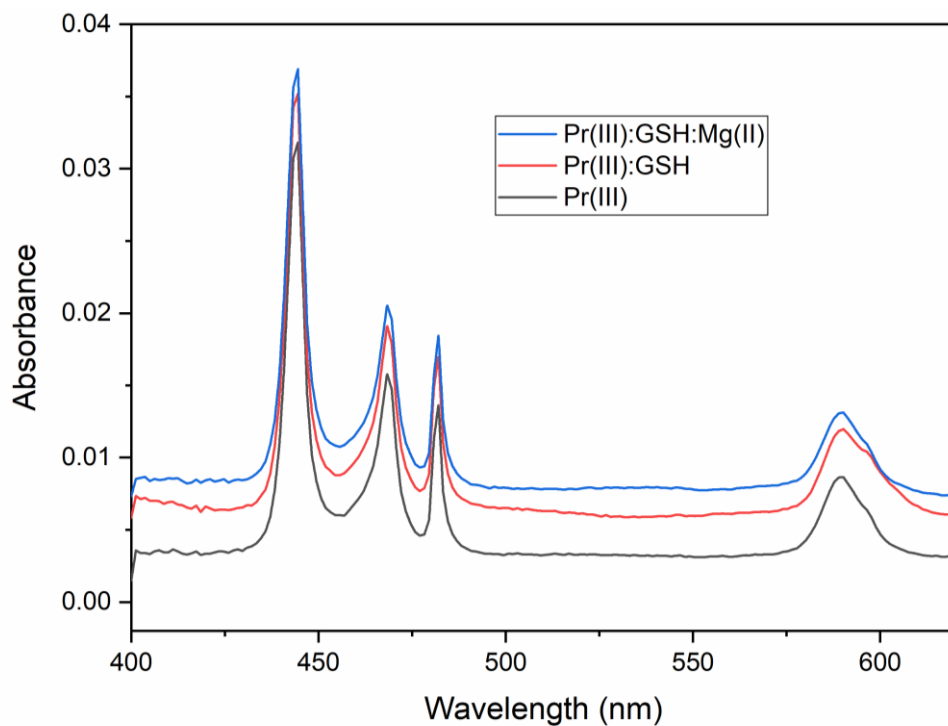


Fig. 3.1: Comparative absorption spectra of Pr(III), Pr(III):GSH and Pr(III):GSH:Mg(II) in DMF.

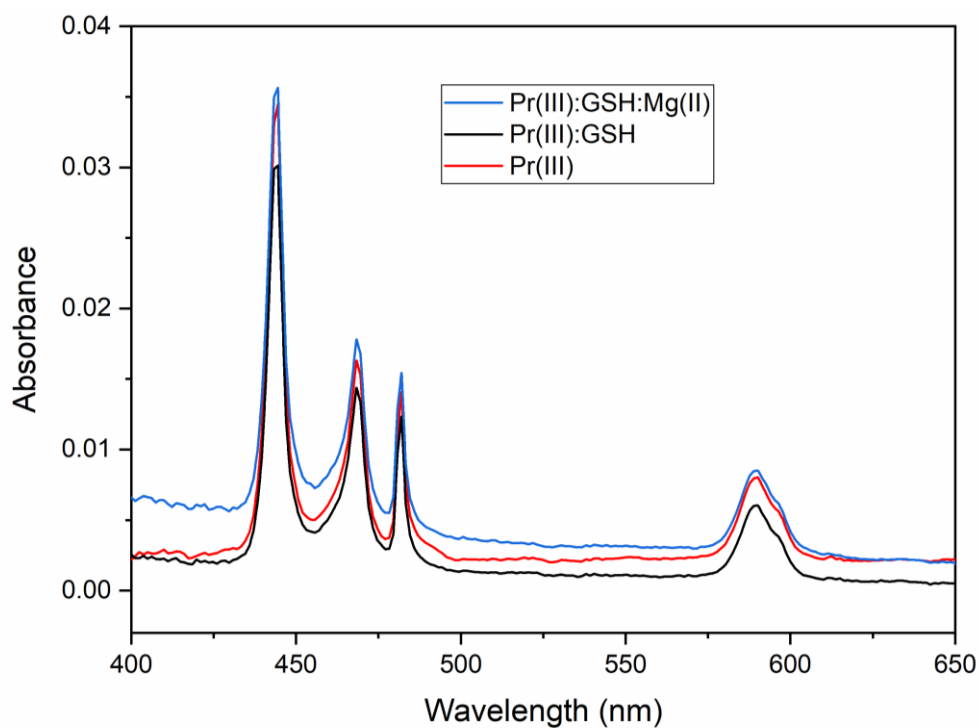


Fig. 3.2: Comparative absorption spectra of Pr(III), Pr(III):GSH and Pr(III):GSH:Mg(II) in CH₃CN.

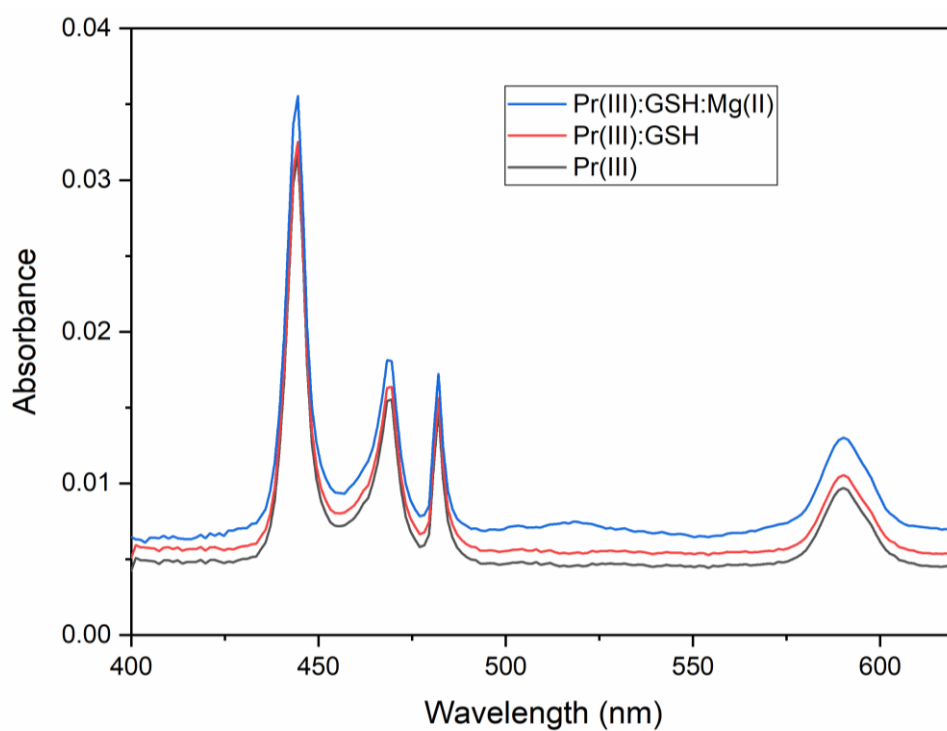


Fig. 3.3: Comparative absorption spectra of Pr(III), Pr(III):GSH and Pr(III):GSH:Mg(II) in dioxane.

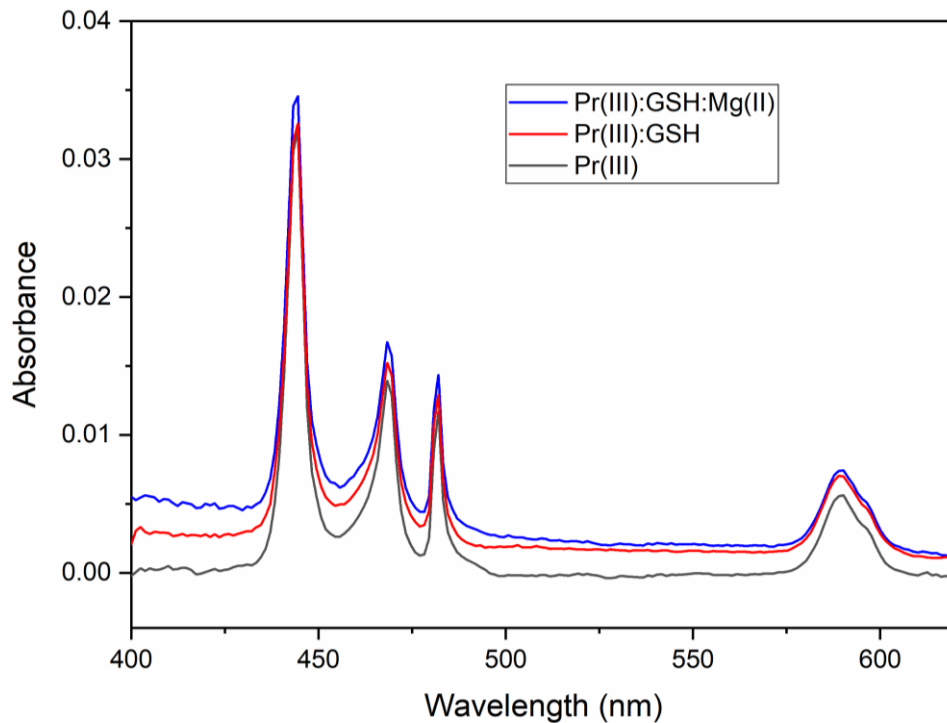


Fig. 3.4: Comparative absorption spectra of Pr(III), Pr(III):GSH and Pr(III):GSH:Mg(II) in methanol.

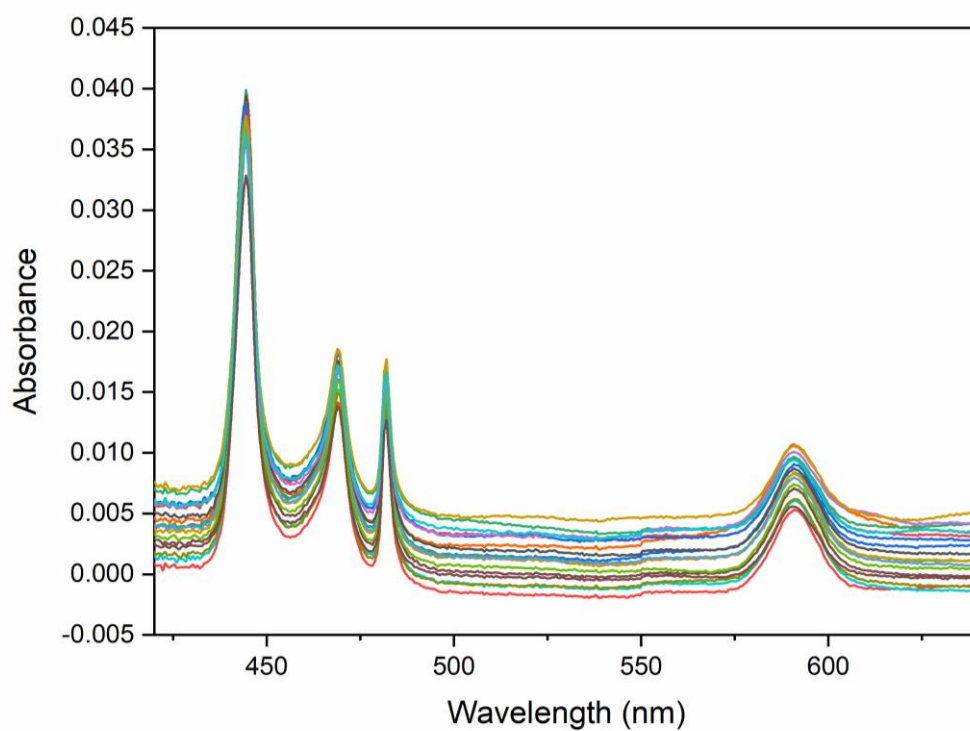


Fig. 3.5: Comparative UV-Vis absorption spectra of Pr(III):GSH:Mg(II) complex in DMF at 303K at different hours.

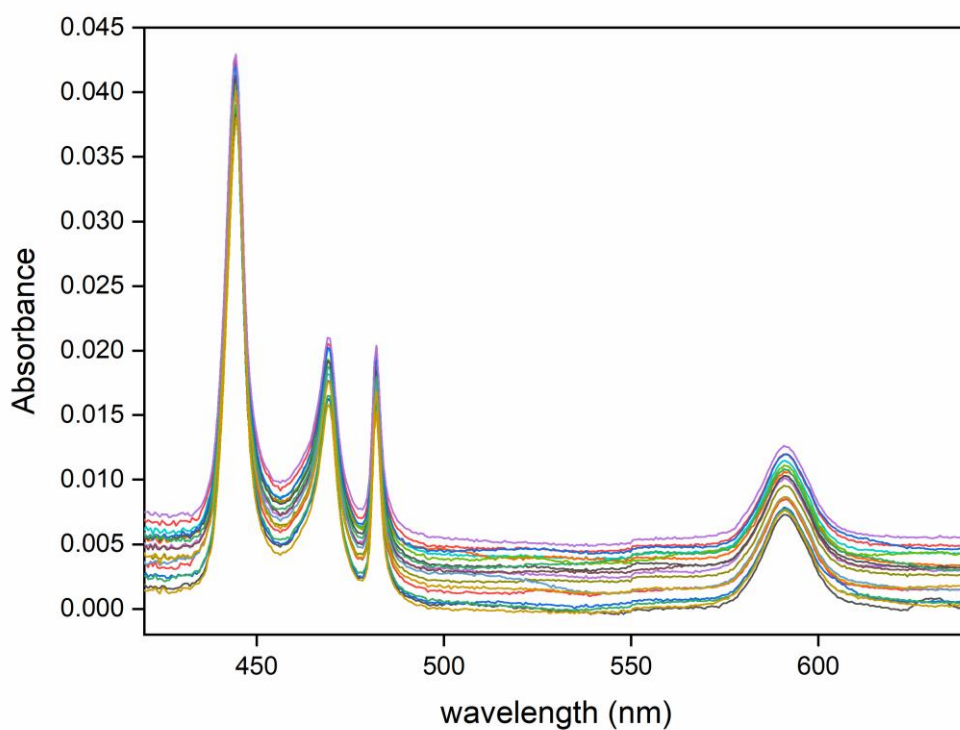


Fig. 3.6: Comparative UV-Vis absorption spectra of Pr(III):GSH:Mg(II) complex in DMF at 308K at different hours.

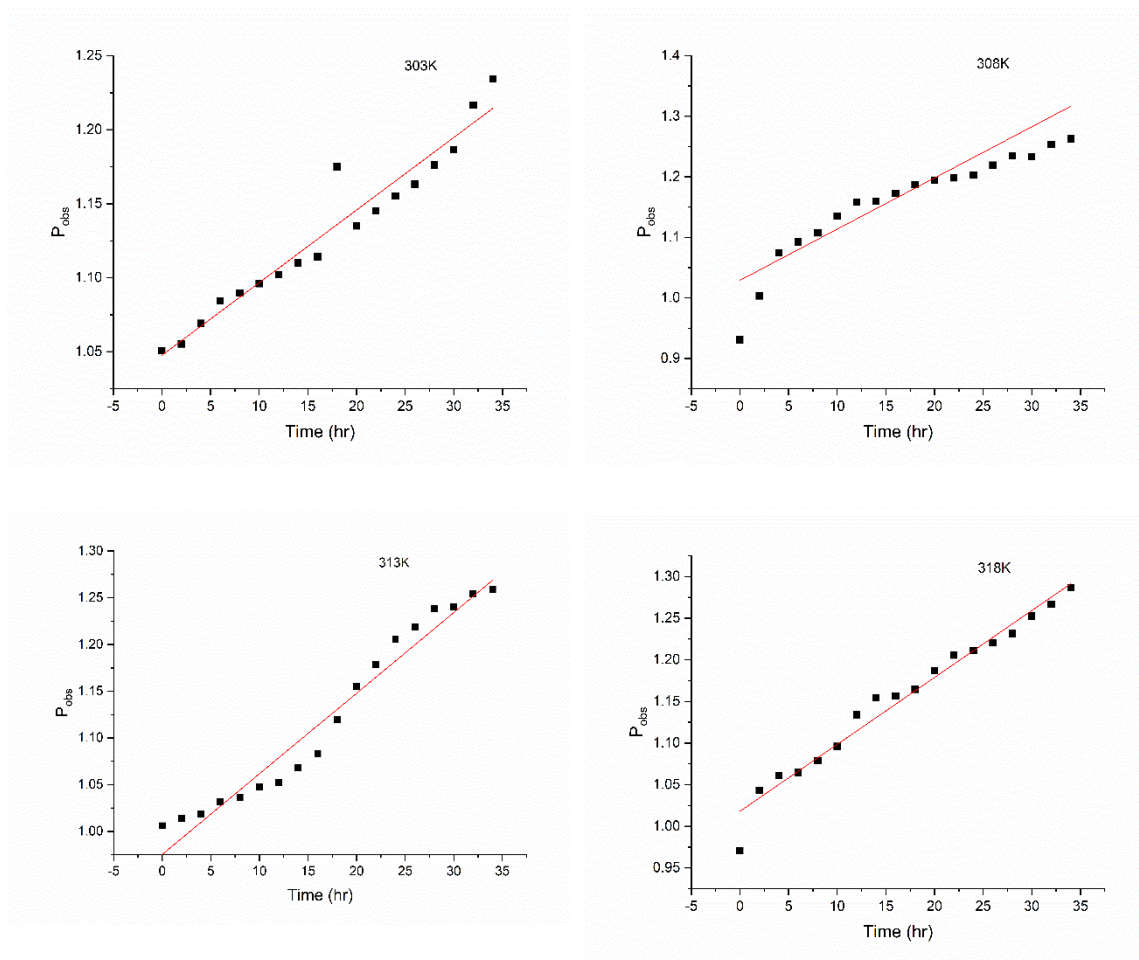


Fig. 3.7: Plot of P_{obs} vs time (hr) of the $^3H_4 \rightarrow ^3P_2$ transition of Pr(III):GSH:Mg(II) at 303K, 308K, 313K and 318K.

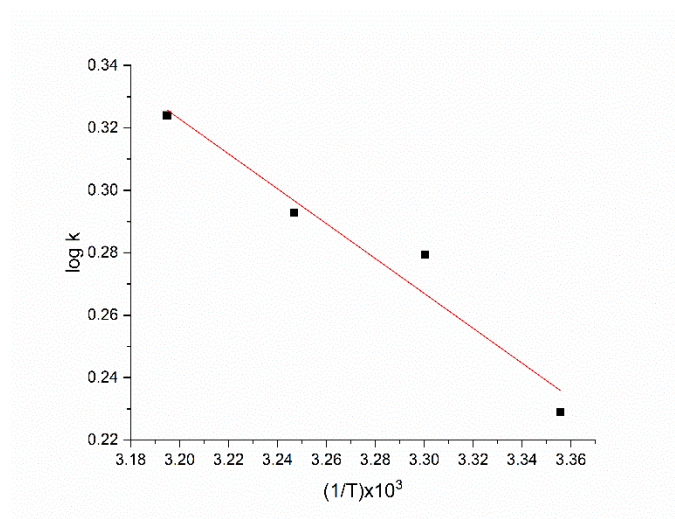


Fig. 3.8: Plot of $\log k$ vs $(1/T) \times 10^3$ of Pr(III):GSH:Mg(II) complex in DMF-water solvent.

Table 3.7: Rate constants at different temperatures (303K, 308K, 313K, 318K) and activation energy (E_a) of Pr(III):GSH:Mg(II).

Temperature (K)	$1/T \text{ K}^{-1} \times 10^3$	Rate Constant (k) $\text{mol L}^{-1} \text{ hr}^{-1}$	Rate Constant (k) $\text{mol L}^{-1} \text{ S}^{-1}$	Pre- exponential factor (A)	Activation Energy E_a (kJ mol^{-1})
303	3.3557	0.0061	1.6940	1.0476	0.0107
308	3.3003	0.0069	1.9030	1.0291	
313	3.2468	0.0071	1.9630	0.9753	
318	3.1949	0.0076	2.1090	1.0180	

Table 3.8: Thermodynamic parameters (ΔH^0 , ΔG^0 and ΔS^0) of Pr(III):GSH:Mg(II) complexation at different temperatures.

Temperature (K)	ΔH^0 (kJ mol^{-1})	ΔG^0 (kJ mol^{-1})	ΔS^0 ($\text{J K}^{-1} \text{ mol}^{-1}$)
303	0.0107	-1.3270	0.0044
308		-1.6470	0.0054
313		-1.7550	0.0056
318		-1.9710	0.0062

CHAPTER 4

SPECTRAL ANALYSIS OF THE COMPLEXATION OF Nd(III) WITH GSH IN THE PRESENCE AND ABSENCE OF Mg(II) AT DIFFERENT pH

4.1 Introduction

Lanthanides are actively used as probes in biochemical investigations, and as such, lanthanide coordination chemistry in solution is instrumental for understanding the basis of lanthanide application in biological systems [1–3]. One of the primary reasons for this is the ability of lanthanide ions to replace metal ions like Ca(II) due to their isomorphous character [4]. Such isomorphous substitution is greatly useful as it allows the Ln(III) ion to mimic Ca(II) thereby enabling us to study the role of Ca(II) in biomolecular interactions through spectroscopic analysis of the lanthanide. A good number of research in this area has been carried out. Moaienla et al. studied the binding interactions of neodymium with selected amino acids and Ca(II) through comparative 4f-4f transition spectra by employing intensity and energy parameters [5]. Similarly, Bendangsenla et al. have used the spectral intensity and energy parameters for analysing the binding behaviour of praseodymium ion with adenosine and Adenosinetriphosphate (ATP) through 4f-4f absorption spectrophotometry [6]. The hypersensitive transitions of lanthanides have been used in such studies of lanthanide systems. The Laporte selection rule forbids electric-dipole (ED) transitions (such as f-f transitions) with electronic states of the same parity. However, under the influence of a ligand field, lanthanide ions generate non-centrosymmetrical interactions which allow electronic states of the opposite parity ($4f^{n-1}5d^1$ configuration) to mix with $4f^n$

configuration. This relaxes the selection rules and allows the transitions to take place. Such transitions bearing odd parity are called induced ED transitions. Although the 4f-4f transitions of lanthanides are little affected by their environment because of the shielding effect, some of the induced ED transitions are extremely sensitive to even small changes in the Ln(III) ion's environment. These transitions are denoted "hypersensitive" transitions and they obey the electric quadrupole selection rules ($\Delta S = 0$, $|\Delta J| \leq 2$ and $|\Delta L| \leq 2$). However, in contrast to the quadrupole transitions, the intensity of hypersensitive transitions is found to show significant variations with change in the ligand environment. Hence, they are also called "pseudo-quadrupolar" transitions. The energies and intensities of hypersensitive transitions are greatly enhanced by the local environment in comparison to normal 4f-4f transitions and is more intense in complexed Ln(III) ion than in free Ln(III) ionic state. Although the phenomenon of hypersensitivity has been explained through a number of studies, no widely accepted theory exists [7]. Some of the prominent proposed mechanisms include molecular vibrations [8], covalency between lanthanide and ligand [9], ligand polarization [10] and ligand to metal charge transfer (LMCT) [11]. It is fair to assume that a variety of factors influence hypersensitivity and it cannot be correlated to a single parameter.

Comparative 4f→4f absorption spectroscopic analysis is a highly effective technique for studying the interactions of lanthanide ions with biomolecules. This chapter discusses the computed energy interaction parameters for Nd(III) and its complexes with GSH and Mg(II) in various aqueous organic solvents (50% v/v). We have also investigated the binding interactions of Nd(III) with GSH and Mg(II) at pH 2, 4 and 6 in DMF:Water solvent. This chapter focuses on the sensitivity of the hypersensitive and Pseudohypersensitive transitions ($^4I_{9/2} \rightarrow ^4G_{5/2}$ and $^4I_{9/2} \rightarrow ^4G_{7/2}$, $^4I_{9/2} \rightarrow ^4F_{7/2}$, $^4I_{9/2} \rightarrow ^4F_{5/2}$, and $^4I_{9/2} \rightarrow ^4F_{3/2}$) of Nd(III) ion in solution form. The energy interaction parameters like Slater-

Condon (F_k , $k = 2, 4, 6$), Lande spin-orbit interaction (ζ_{4f}), Racah (E^k), nephelauxetic ratio (β), bonding parameter ($b^{1/2}$) and percent covalency (δ) have been computed and evaluated to analyse the binding interaction of Nd(III) with GSH and Mg(II).

4.2 Experimental

L-Glutathione reduced ($C_{10}H_{17}N_3O_6S$, $\geq 98.0\%$) and Praseodymium trinitrate hexahydrate ($Pr(NO_3)_3 \cdot 6H_2O$, 99.99%) were obtained from Sigma-Aldrich. Dioxane ($C_4H_8O_2$), methanol (CH_3OH), dimethylformamide (C_3H_7NO) and acetonitrile (CH_3CN) were purchased from HiMedia.

Aqueous organic solutions (50% v/v) of Nd(III), Nd(III):GSH, and Nd(III):GSH:Mg(II) were prepared in different solvents (methanol, dioxane, acetonitrile and DMF) at a concentration of 3 mmol. The pH of the solution was maintained at 2, 4 and 6 and the UV-Vis spectra of the test solutions were recorded at 298K temperature using a Shimadzu UV-2600i spectrophotometer in the range of 400-900 nm.

4.3 Methods

Energy interaction parameters

The nephelauxetic effect refers to electron cloud expansion and is also considered the measure of covalent character of the metal-ligand interaction. The Nephelauxetic ratio (β) is associated with the electrostatic interactions between the electrons and its value can be obtained by dividing the Racah (E^k) and Slater-Condon (F_k) parameters of the free ion (f) and complex (c) [9,12].

$$\beta = \frac{F_k^c}{F_k^f} \text{ or } \frac{E_c^k}{E_f^k} \quad \text{Eq. 1}$$

The 4f orbitals of the lanthanides are known to take part in chemical bonding. The bonding parameter ($b^{1/2}$) expresses the degree to which the 4f and the ligand orbitals are mixed. The bonding parameter and nephelauxetic effect are correlated and is represented by the following equation

$$b^{1/2} = \left[\frac{1 - \beta}{2} \right]^{1/2} \quad \text{Eq. 2}$$

The tripositive lanthanide ions have an electronic configuration of $[\text{Xe}]4f^N$. The $4f^N$ configuration of Ln(III) and their corresponding energy levels vary distinctly. The energies of these states can be attributed to magnetic and electrostatic interactions that occur between electrons of the 4f orbital. The Slater radial integral, also known as the Slater-Condon parameter, F_k , is used to calculate the electrostatic interaction which is in energy term, E_0 as,

$$E_0 = \sum_{k=0}^{k=6} K^k F_k \quad \text{Eq. 3}$$

Where K^k denotes the angular coefficient

The Slater-Condon parameters F_k ($k=2,4,6$) represents the interelectronic repulsion interactions and are a decreasing function of K , as defined by the following relation

$$F_1^k = \int_0^\infty \int_0^\infty \frac{r_{<}^k}{r_{>}^{k+1}} R_i^2(r_i) R_j^2(r_j) r_i^2 r_j^2 dr_i dr_j \quad \text{Eq. 4}$$

Where $r_{<}$ and $r_{>}$ represents the lesser and greater radii of r_i and r_j for the f-electrons respectively; R is the 4f-radial wave function and i and j are the i th and j th electrons under evaluation. The F^k integrals were revised by Condon and Shortley in terms of the reduced F_k integrals [13]. These integrals are correlated and is given as

$$F_k = \frac{F^k}{D_k} \quad \text{Eq. 5}$$

The reduced Slater-Condon integral is obtained by combining Eqs. 4 and 5:

$$F_k = \frac{1}{D_k} \int_0^\infty \int_0^\infty \frac{r_i^k}{r_j^{k=1}} R_i^2(r_i) R_j^2(r_j) r_i^2 r_j^2 dr_i dr_j \quad \text{Eq. 6}$$

Where D_k and F_k are the denominator and coefficient of linear combination respectively.

The expected value of the scalar product ($C_1^k C_2^k$) is denoted by F_k .

E^k , the Racah energy interaction parameter, is a linear combination of F^k as given by

$$\begin{aligned} E^1 &= \frac{70F_2 + 231F_4 + 20.02F_6}{9} \\ E^2 &= \frac{F_2 - 3F_4 + 7F_6}{9} \\ E^3 &= \frac{5F_2 + 6F_4 - 9F_6}{3} \end{aligned} \quad \text{Eq. 7}$$

There are two major components to the energies of the 4f interelectronic transitions: electrostatic interaction and the spin-orbit interaction between 4f-electrons. The spin-orbital interaction energy denoted as E_{so} is given by

$$E_{so} = A_{so} \xi_{4f} \quad \text{Eq. 8}$$

In this case A_{so} constitutes the angular part of spin-orbit interaction, while ξ_{4f} is the Lande parameter and is a representation of the interaction of electron spin and orbital angular momenta. Since only very small variations in the F_k parameter and 4f are influenced by the electric field of the solution matrix, Wong [14] gives the energy of the j th level i.e. E_j by a first order approximation as

$$E_j(F_k, \xi_{4f}) = E_{0j}(F_k^0, \xi_{4f}^0) + \frac{\partial E_j}{\partial F_k} \Delta F_k + \frac{\partial E_j}{\partial \xi_{4f}} \Delta \xi_{4f} \quad \text{Eq. 9}$$

E_{0j} denotes the zero order energy of the j th level. The values of F_k and ξ_{4f} can be calculated by using Eq. 10 and 11.

Here E_{0j} is the j th level's zero order energy. Using Eqs. 10 and 11 the Slater-Condon (F_k) and Lande (ξ_{4f}) parameters can be calculated.

$$F_k = F_k^0 + \Delta F_k \quad \text{Eq. 10}$$

$$\xi_{4f} = \xi_{4f}^0 + \Delta \xi_{4f} \quad \text{Eq. 11}$$

ΔE_j which denotes the difference in values of the observed energy E_j and the zero order energy can be evaluated using the following relation

$$\Delta E_j = \sum_{k=2,4,6} \frac{\partial E_j}{\partial F_k} \Delta F_k + \frac{\partial E_j}{\partial \xi_{4f}} \Delta \xi_{4f} \quad \text{Eq. 12}$$

We can solve Eq. 12 by using the least squares method and the values of ΔF_k and $\Delta \xi_{4f}$ can be found out using Wong's zero order energy and partial derivatives of the Nd(III) ion (Table 4.1) [14]. The values of Slater-Condon ($F_k, k=2,4,6$) and Lande (ξ_{4f}) parameter values can be calculated using Eq. 10 and 11.

Table 4.1: The zero-order energies and partial derivatives with respect to F_k and ζ_{4f} parameters for Nd(III) [14].

Level	$E_{oj}^{(a)}$	$\frac{\delta E_j}{\delta F_2}$	$\frac{\delta E_j}{\delta F_4}$	$\frac{\delta E_j}{\delta F_6}$	$\frac{\delta E_j}{\delta \zeta_{4f}}$
$^4F_{3/2}$	11523.34	35.27	39.50	-588.9	1.02
$^4F_{5/2}$	12606.77	34.93	39.36	-631.4	2.58
$^4F_{7/2}$	13453.73	35.02	41.04	-602.5	3.24
$^4G_{5/2}$	17357.56	54.98	63.01	-991.2	1.29
$^4G_{7/2}$	19288.93	41.95	101.66	-620.8	4.13

$$(a) F_2^0 = 331.567 \text{ cm}^{-1}$$

$$F_4^0 = 49.057 \text{ cm}^{-1}$$

$$F_6^0 = 5.170 \text{ cm}^{-1}$$

$$\zeta_{4f}^0 = 906.00 \text{ cm}^{-1}$$

The covalency of metal-ligand bond in Nd(III) complex may be expressed by the parameter of covalency (δ) in percent as

$$\delta = \left[\frac{1-\beta}{\beta} \right] \times 100 \quad \text{Eq. 13}$$

4.4 Results and Discussions

The absorption spectra of lanthanide ions are caused by the interelectronic transitions within the levels of $4f^N$ configuration (4f-4f transition) of lanthanide ions. Such internal electron redistribution is orbitally forbidden by the quantum mechanical selection rules. In contrast to transition metal complexes, the crystal field effect on the 4f orbitals of lanthanide are negligible (around 200-300 cm^{-1}) and the energy levels of lanthanide ions are largely influenced by spin-orbit interaction. This is due to the shielding effect of 4f electrons by the 5s and 5p orbitals. As a result, the f-f transition bands are sharp, and the optical spectra are almost completely independent of the environment. The forbidden transitions within the 4f orbitals of Nd(III) causes absorption in the UV-Vis and near-infrared regions, which involves 13 energy levels. We have taken into account five transition bands ranging from 400-900 nm which are associated with $^4I_{9/2} \rightarrow ^4G_{7/2}$, $^4I_{9/2} \rightarrow ^4G_{5/2}$, $^4I_{9/2} \rightarrow ^4F_{7/2}$, $^4I_{9/2} \rightarrow ^4F_{5/2}$, and

$^4I_{9/2} \rightarrow ^4F_{3/2}$ transitions. Except in a few cases, adding GSH to Nd(III) ion in the absence or presence of Mg(II) has no effect on the structure of the bands. Furthermore, due to the weak crystal field splitting, these bands are sharp and narrow, and are very similar to those of the free ions.

From Fig. 4.1 to 4.4 which compares the UV-Vis spectra of Nd(III), Nd(III):GSH and Nd(III):GSH:Mg(II) in different solvents, it is evident that the absorption intensity of the various transition bands increases along with the occurrence of a marginal red shift upon addition of GSH to Nd(III) which is further enhanced when Mg(II) is introduced to the complex system. This may be a possible indication of the ligand's interaction with the Nd(III) ion. The red shift can be attributed to expansion of the metal ion orbital during complexation, which causes a decrease in inter-electron repulsion, thereby shortening the atomic radii of the central metal ion and the ligand resulting in the nephelauxetic effect. According to Karraker, the energy, intensity and shape of hypersensitive or pseudo-hypersensitive transitions are associated with coordination number and can be used to diagnose the surrounding environment of lanthanide [15].

The variations in the transition bands of Nd(III) on complexation have been investigated by evaluating its energy interaction parameters. These are the Slater-Condon (F_k), Racah (E^k), Lande (ξ_{4f}), nephelauxetic ratio (β), bonding ($b^{1/2}$) and covalency(δ) parameters. Table 4.2 lists the energy interaction parameter values for Nd(III) ion and its complexes with GSH and Mg(II) in different solvent systems. From Table 4.2 it can be observed that the nature of the solvent and the complex system has a considerable effect on the f-f transitions of Nd(III). The binding of GSH with Nd(III) causes alterations in the energies of the 4f-4f absorption bands which subsequently lowers the inter-electronic repulsion (Slater-Condon parameter) and brings about the nephelauxetic effect. This also intensifies the 4f-4f transitions. The inter-electronic repulsion parameters Racah (E^k) and

Slater-Condon (F_k) which represents the coulombic interactions are included and these two parameters are related to each other. In addition, the Lande (ζ_{4f}) parameter representing the spin-orbit interaction is also included in the energy parameter. This is due to the fact that the energies of the 4f-4f transitions are made up of two major aspects i.e. spin-orbit and coulombic interactions, which can be expressed as

$$E_{\text{obs}} = f^k F_k + A_{SO} \zeta_{4f}$$

f^k and A_{SO} denotes the angular counterpart of coulombic and spin-orbit interaction, respectively.

From the Table 4.2, we can see that the values of the interelectronic repulsion parameters; Slater-Condon (F_k), spin-orbit interaction Racah (E^k), Lande (ζ_{4f}) and Nephelauxetic ratio (β) decreases when GSH and Mg(II) are added to Nd(III). This is because of the enlargement of the metal orbital caused by the coordination of GSH and Mg(II) to Nd(III) during its complexation. The values of these parameters decrease when the free lanthanide ion forms a complex with the ligands. The declining values of the inter-electronic interaction parameters suggest that in the Nd(III) complexes there is relatively lesser repulsion between the two electrons of its doubly occupied metal orbital than there is in its free ion counterpart, implying that the orbital size is larger after complexation. There are two possible explanations for the effect of the electron cloud expansion: the first is that any negative charge on the ligands reduces the effective positive charge on the lanthanide metal, allowing the f-orbitals to slightly expand; the other is that the overlapping of metal orbital with the ligand orbital and the formation of covalent bonds increases the size of the orbital. Such changes suggest the binding interaction of Nd(III) ion with glutathione and Mg(II) in solution. The subsequent increase of bonding ($b^{1/2}$) and covalency (δ) parameter values on going from Nd(III) to Nd(III):GSH and Nd(III):GSH:Mg(II) indicates shortening of the Ln(III)-ligand bond distance due to stronger binding of Nd(III)

with GSH and Mg(II) as well as the covalent bonding nature of the Nd(III) complexes. The values for the Nephelauxetic effect(β) are less than one and the bonding parameters are found to be positive in all the systems suggesting a metal-ligand interaction in solution. The observed and calculated energy values for the various transitions of Nd(III) and its root mean square deviation (RMS) are presented in Table 4.3. The RMS value shows the accuracy of the evaluated energy parameters. The values of $b^{1/2}$ and δ (Table 4.2) of Nd(III) ion and its complexes are highest in aquated DMF (50:50 vol. %) which suggests that DMF is the better solvent for complexation and induces a stronger coordination potential than acetonitrile, dioxane and methanol. From the values of the energy parameters of the Nd(III) complex systems in different solvents, it is seen that the interaction energy undergoes the greatest change in DMF solvent meaning that DMF has in comparison the greater influence on the complexation of Nd(III) ion with the ligands. This is probably due to the stronger oxygen donating capacity of DMF, which allows it to enter the coordination sphere of Nd(III) by replacing one of the water groups [16,17]. The trend for the degree of interaction between Nd(III) and the ligands for the different solvents is DMF > acetonitrile > dioxane > methanol.

Fig. 4.5 to 4.7 compares the UV-Vis spectra of Nd(III) complexes with GSH and Mg(II) at pH 2,4,6 in DMF solvent. It is observed that the absorption peaks of the f-f transitions of Nd(III) intensify along with the occurrence of a marginal red shift as the pH increase from 2 to 4 and 4 to 6 indicating a stronger interaction at higher pH 6. In Table 4.4 we have the energy interaction parameters for Nd(III), Nd(III):GSH and Nd(III):GSH:Mg(II) in aquated DMF solvent at pH 2, 4 and 6. F_k , E^k and ζ_{4f} values decrease with increasing pH suggesting the expansion of the lanthanide metal orbital and decrease of interelectronic repulsion. Similarly, bonding and percent covalency values increases from pH 2 to 6 which suggests a stronger bond interaction at higher pH for the Nd(III)

complex systems. The influence of pH is prominent and is responsible for the deprotonation and protonation of the various binding sites of glutathione. Since GSH offers a number of binding sites in the form of carboxylates, thiol, amine and amide groups, the deprotonation of these sites at varying pH medium presents greater binding opportunities for the metal which is reflected in its energy parameters. The UV-Vis absorption spectral study could suggest that at pH 2 the carboxylate group of the glutamyl moiety of glutathione is deprotonated allowing Nd(III) to bind through its -COOH site. Nd(III), is a hard metal ion that preferentially coordinates with hard donor sites like -COOH group. Likewise, at pH 4, another -COOH group of the glycine moiety is deprotonated and further -SH group of cysteinyl is deprotonated at pH 6. Such deprotonation at different pH opens up binding possibilities for the lanthanide ion and Mg(II) with GSH at multiple coordination sites leading to stronger binding interactions. Table 4.5 presents the computed as well as the observed values of energies (cm^{-1}) of the different f-f transition bands of Nd(III), Nd(III):GSH, Nd(III):GSH:Mg(II) and their RMS values at pH 2, 4 and 6. The observed values could signify the validity of the evaluated data. The data obtained suggests that due to the availability of more coordination sites at a higher pH, the optimal pH for greater complexation of Nd(III) ion with GSH and Mg(II) is at pH 6.

*The work presented in this chapter has been published in *Chemical Physics Impact*, 5, 100090, **2022**.

References

- [1] Y. Ning, G.Q. Jin, M.X. Wang, S. Gao, J.L. Zhang, Recent progress in metal-based molecular probes for optical bioimaging and biosensing, *Curr. Opin. Chem. Biol.* **66** (2022) 102097. <https://doi.org/10.1016/j.cbpa.2021.102097>.
- [2] G. Sun, Y. Xie, L. Sun, H. Zhang, Lanthanide upconversion and downshifting luminescence for biomolecules detection, *Nanoscale Horizons.* **6** (2021) 766–780. <https://doi.org/10.1039/d1nh00299f>.
- [3] S. Dasari, S. Singh, Z. Abbas, S. Sivakumar, A.K. Patra, Luminescent lanthanide(III) complexes of DTPA-bis(amido-phenyl-terpyridine) for bioimaging and phototherapeutic applications, *Spectrochim. Acta - Part A Mol. Biomol. Spectrosc.* **256** (2021) 119709. <https://doi.org/10.1016/j.saa.2021.119709>.
- [4] S.N. Misra, G. Ramchandriah, M.A. Gagnani, R.S. Shukla, M.I. Devi, Absorption spectral studies involving 4f-4f transitions as structural probe in chemical and biochemical reactions and compositional dependence of intensity parameters, *Appl. Spectrosc. Rev.* **38** (2003) 433–493. <https://doi.org/10.1081/ASR-120026330>.
- [5] T. Moaienla, N. Bendangsenla, T. David, C. Sumitra, N.R. Singh, M.I. Devi, Spectrochimica Acta Part A: Molecular and Biomolecular Spectroscopy Comparative 4f – 4f absorption spectral study for the interactions of Nd (III) with some amino acids: Preliminary thermodynamics and kinetic studies of interaction of Nd (III): glycine, *Spectrochim. Acta Part A Mol. Biomol. Spectrosc.* **87** (2012) 142–150. <https://doi.org/10.1016/j.saa.2011.11.028>.
- [6] N. Bendangsenla, T. Moaienla, T. David Singh, C. Sumitra, N. Rajmuhon Singh, M. Indira Devi, Evaluation of intensity and energy interaction parameters for the complexation of Pr(III) with selected nucleoside and nucleotide through absorption spectral studies, *Spectrochim. Acta - Part A Mol. Biomol. Spectrosc.* **103** (2013)

- 160–166. <https://doi.org/10.1016/j.saa.2012.11.011>.
- [7] K. Binnemans, Interpretation of europium(III) spectra, *Coord. Chem. Rev.* **295** (2015) 1–45. <https://doi.org/10.1016/j.ccr.2015.02.015>.
- [8] D.M. Gruen, C.W. DeKock, R.L. McBeth, Electronic Spectra of Lanthanide Compounds in the Vapor Phase, in: P.R. Fields, T. Moeller (Eds.), *Lanthanide/Actinide Chem.*, 1st ed., American Chemical Society, Washington, 1967: pp. 102–121. <https://doi.org/10.1021/ba-1967-0071.ch008>.
- [9] D.E. Henrie, G.R. Choppin, Environmental effects on f-f transitions. II. “Hypersensitivity” in some complexes of trivalent neodymium, *J. Chem. Phys.* **49** (1968) 477–481. <https://doi.org/10.1063/1.1670099>.
- [10] S.F. Mason, R.D. Peacock, B. Stewart, Ligand-polarization contributions to the intensity of hypersensitive trivalent lanthanide transitions, *Mol. Phys.* **30** (1975) 1829–1841. <https://doi.org/10.1080/00268977500103321>.
- [11] D.E. Henrie, R.L. Fellows, G.R. Choppin, Hypersensitivity in the electronic transitions of lanthanide and actinide complexes, *Coord. Chem. Rev.* **18** (1976) 199–224. [https://doi.org/10.1016/S0010-8545\(00\)82044-5](https://doi.org/10.1016/S0010-8545(00)82044-5).
- [12] C.K. Jørgensen, B.R. Judd, Hypersensitive pseudoquadrupole transitions in lanthanides, *Mol. Phys.* **8** (1964) 281–290. <https://doi.org/10.1080/00268976400100321>.
- [13] E.U. Condon, G.H. Shortley, C.W. Ufford, The Theory of Atomic Spectra, *Am. J. Phys.* **20** (1952) 383–383. <https://doi.org/10.1119/1.1933256>.
- [14] E.Y. Wong, Taylor series expansion of the intermediate coupling energy levels of Nd³⁺ and Er³⁺, *J. Chem. Phys.* **35** (1961) 544. <https://doi.org/10.1063/1.1731965>.
- [15] D.G. Karraker, Hypersensitive Transitions of Six-, Seven-, and Eight-Coordinate Neodymium, Holmium, and Erbium Chelates, *Inorg. Chem.* **6** (1967) 1863–1868.

<https://doi.org/10.1021/ic50056a022>.

- [16] S. Misra, Lanthanoid (III) ions as structural probe in biochemical reactions, *Proc. Indian Natn. Sci. Acad.* **60** (1994) 637–637.
- [17] A.A. Khan, H.A. Hussain, K. Iftikhar, 4f-4f absorption spectra and hypersensitivity in nine-coordinate Ho(III) and Er(III) complexes in different environments, *Spectrochim. Acta - Part A Mol. Biomol. Spectrosc.* **60** (2004) 2087–2092.
<https://doi.org/10.1016/j.saa.2003.10.042>.

Table 4.2: Computed values of energy interaction parameters: Slater-Condon F_k (cm^{-1}), Lande ζ_{4f} (cm^{-1}), Racah (E^k), Nephelauxetic ratio (β), bonding ($b_{1/2}$) and percent covalency (δ) parameters of Nd(III) and its complexes with GSH and Mg(II) in 50% (v/v) aquated solvents of CH_3OH , $\text{C}_4\text{H}_8\text{O}_2$, CH_3CN and DMF.

System	F_2	F_4	F_6	ζ_{4f}	E^1	E^2	E^3	β	$b^{1/2}$	δ
1. CH_3OH										
Nd(III)	332.0554	45.8402	5.0140	900.2732	3770.3729	25.5148	660.1482749	0.9811	0.0971	1.9234
Nd(III):GSH	331.8344	45.8097	5.0107	900.6595	3767.8633	25.4978	659.7088589	0.9810	0.0974	1.9348
Nd(III):GSH:Mg(II)	331.8413	45.8107	5.0108	900.4497	3767.9414	25.4983	659.7225356	0.9809	0.0977	1.9458
2. Dioxane										
Nd(III)	331.9508	45.8258	5.0125	900.7311	3769.1849	25.5067	659.9402572	0.9812	0.0969	1.9130
Nd(III):GSH	331.7907	45.8037	5.0100	900.2140	3767.3679	25.4944	659.6221303	0.9807	0.0982	1.9670
Nd(III):GSH:Mg(II)	331.9403	45.8244	5.0123	899.5952	3769.0657	25.5059	659.9194004	0.9806	0.0985	1.9798
3. CH_3CN										
Nd(III)	331.9074	45.8198	5.0118	900.5944	3768.6925	25.5034	659.8540527	0.9811	0.0972	1.9274
Nd(III):GSH	331.5302	45.7678	5.0061	901.3726	3764.4100	25.4744	659.1042384	0.9810	0.0975	1.9400
Nd(III):GSH:Mg(II)	331.4155	45.7519	5.0044	900.5537	3763.1066	25.4656	658.8760164	0.9804	0.0991	2.0044
4. DMF										
Nd(III)	331.9528	45.8261	5.0125	900.7375	3769.2079	25.5069	659.9442993	0.9812	0.0969	1.9124
Nd(III):GSH	331.3882	45.7481	5.0040	898.2132	3762.7968	25.4635	658.8217766	0.9790	0.1024	2.1431
Nd(III):GSH:Mg(II)	330.9122	45.6824	4.9968	898.5570	3757.3919	25.4269	657.8754523	0.9785	0.1036	2.1958

Table 4.3: Computed and observed values of energies (cm^{-1}) and RMS values of Nd(III), Nd(III):GSH, Nd(III):GSH:Mg(II) in different solvents.

System	$^4\text{I}_{9/2}\rightarrow^4\text{F}_{3/2}$		$^4\text{I}_{9/2}\rightarrow^4\text{F}_{5/2}$		$^4\text{I}_{9/2}\rightarrow^4\text{F}_{7/2}$		$^4\text{I}_{9/2}\rightarrow^4\text{G}_{5/2}$		$^4\text{I}_{9/2}\rightarrow^4\text{G}_{7/2}$		RMS
	E _{obs}	E _{cal}	E _{obs}	E _{cal}	E _{obs}	E _{cal}	E _{obs}	E _{cal}	E _{obs}	E _{cal}	
1. CH ₃ OH											
Nd(III)	19165.90	19283.27	17367.14	17371.86	13502.57	13450.10	12589.70	12606.58	11554.42	11583.62	59.48
Nd(III):GSH	19165.90	19274.42	17351.77	17362.40	13494.91	13442.82	12586.53	12599.66	11549.34	11577.95	55.85
Nd(III):GSH:Mg(II)	19163.33	19278.14	17365.63	17369.82	13493.64	13446.05	12598.27	12603.28	11548.68	11583.25	57.76
2. Dioxane											
Nd(III)	19163.33	19280.89	17362.92	17369.30	13501.11	13448.14	12590.02	12604.71	11553.08	11582.08	59.54
Nd(III):GSH	19158.92	19268.28	17325.02	17349.57	13494.37	13437.45	12589.70	12593.55	11547.34	11568.73	57.05
Nd(III):GSH:Mg(II)	19157.09	19260.08	17313.62	17342.20	13494.73	13430.78	12586.53	12587.43	11540.68	11564.66	56.73
3. CH ₃ CN											
Nd(III)	19166.63	19285.77	17377.40	17377.02	13507.13	13452.28	12589.70	12609.05	11554.28	11587.32	61.10
Nd(III):GSH	19165.17	19278.09	17356.29	17365.37	13498.56	13445.79	12584.95	12602.33	11552.68	11579.50	57.69
Nd(III):GSH:Mg(II)	19162.96	19277.51	17356.89	17365.48	13496.01	13445.35	12588.12	12602.03	11552.01	11579.74	57.83
4. DMF											
Nd(III)	19166.27	19283.38	17367.14	17371.98	13504.39	13450.19	12589.70	12606.67	11554.02	11583.69	59.74
Nd(III):GSH	19162.59	19249.27	17322.02	17337.68	13495.28	13422.24	12510.95	12580.43	11547.34	11563.70	60.31
Nd(III):GSH:Mg(II)	19138.76	19230.72	17277.13	17311.96	13484.36	13406.68	12501.56	12564.69	11543.35	11546.84	62.77

Table 4.4: Computed values of energy interaction parameters: Slater-Condon F_k (cm^{-1}), Lande ζ_{4f} (cm^{-1}), Racah (E^k), Nephelauxetic ratio (β), bonding ($b_{1/2}$) and percent covalency (δ) parameters of Nd(III) and its complexes in 50% (v/v) aquated DMF at pH 2, 4 and 6.

System	pH	F_2	F_4	F_6	ζ_{4f}	E^1	E^2	E^3	β	$b^{1/2}$	δ
Nd(III)	2	331.4074	45.7508	5.0043	902.0185	3763.0146	25.4650	658.8599242	0.9811	0.0971	1.9216
Nd(III):GSH		330.8633	45.6757	4.9960	899.5023	3756.8375	25.4232	657.7783754	0.9790	0.1026	2.1487
Nd(III):GSH:Mg(II)		330.8797	45.6779	4.9963	899.2168	3757.0231	25.4244	657.8108814	0.9788	0.1029	2.1627
Nd(III)	4	331.9528	45.8261	5.0125	900.7375	3769.2079	25.5069	659.9442993	0.9812	0.0969	1.9124
Nd(III):GSH		331.3882	45.7481	5.0040	898.2132	3762.7968	25.4635	658.8217766	0.9790	0.1024	2.1431
Nd(III):GSH:Mg(II)		330.9122	45.6824	4.9968	898.5570	3757.3919	25.4269	657.8754523	0.9785	0.1036	2.1958
Nd(III)	6	331.1428	45.7143	5.0003	902.8024	3760.0106	25.4446	658.3339478	0.9812	0.0970	1.9167
Nd(III):GSH		330.8292	45.6710	4.9955	899.2879	3756.4499	25.4205	657.710521	0.9788	0.1030	2.1663
Nd(III):GSH:Mg(II)		330.8047	45.6676	4.9952	898.7275	3756.1716	25.4187	657.6617782	0.9785	0.1038	2.2023

Table 4.5: Computed and observed values of energies (cm^{-1}) and RMS values of Nd(III), Nd(III):GSH, Nd(III):GSH:Mg(II) in DMF solvent at pH 2, 4 and 6.

System	pH	$^4\text{I}_{9/2} \rightarrow ^4\text{F}_{3/2}$		$^4\text{I}_{9/2} \rightarrow ^4\text{F}_{5/2}$		$^4\text{I}_{9/2} \rightarrow ^4\text{F}_{7/2}$		$^4\text{I}_{9/2} \rightarrow ^4\text{G}_{5/2}$		$^4\text{I}_{9/2} \rightarrow ^4\text{G}_{7/2}$		RMS
		E _{obs}	E _{cal}	E _{obs}	E _{cal}	E _{obs}	E _{cal}	E _{obs}	E _{cal}	E _{obs}	E _{cal}	
Nd(III)	2	19157.09	19265.79	17316.02	17343.65	13477.09	13435.24	12578.62	12590.92	11554.02	11564.38	54.02
Nd(III):GSH		19140.59	19232.58	17271.16	17310.49	13483.45	13408.04	12507.82	12565.43	11544.68	11545.11	61.67
Nd(III):GSH:Mg		19142.42	19232.08	17271.16	17311.02	13486.18	13407.68	12515.64	12565.26	11540.68	11545.69	60.46
Nd(III)	4	19166.63	19285.77	17377.40	17377.02	13507.13	13452.28	12589.70	12609.05	11554.28	11587.32	61.10
Nd(III):GSH		19165.17	19278.09	17356.29	17365.37	13498.56	13445.79	12584.95	12602.33	11552.68	11579.50	57.69
Nd(III):GSH:Mg		19162.96	19277.51	17356.89	17365.48	13496.01	13445.35	12588.12	12602.03	11552.01	11579.74	57.83
Nd(III)	6	19164.43	19257.93	17286.08	17330.11	13495.28	13428.51	12580.20	12583.70	11543.35	11555.01	55.29
Nd(III):GSH		19142.42	19230.26	17266.68	17308.34	13486.18	13406.15	12510.95	12563.68	11540.68	11543.90	61.07
Nd(III):GSH:Mg		19140.59	19226.92	17265.19	17306.27	13482.54	13403.47	12507.04	12561.38	11539.35	11543.03	60.59

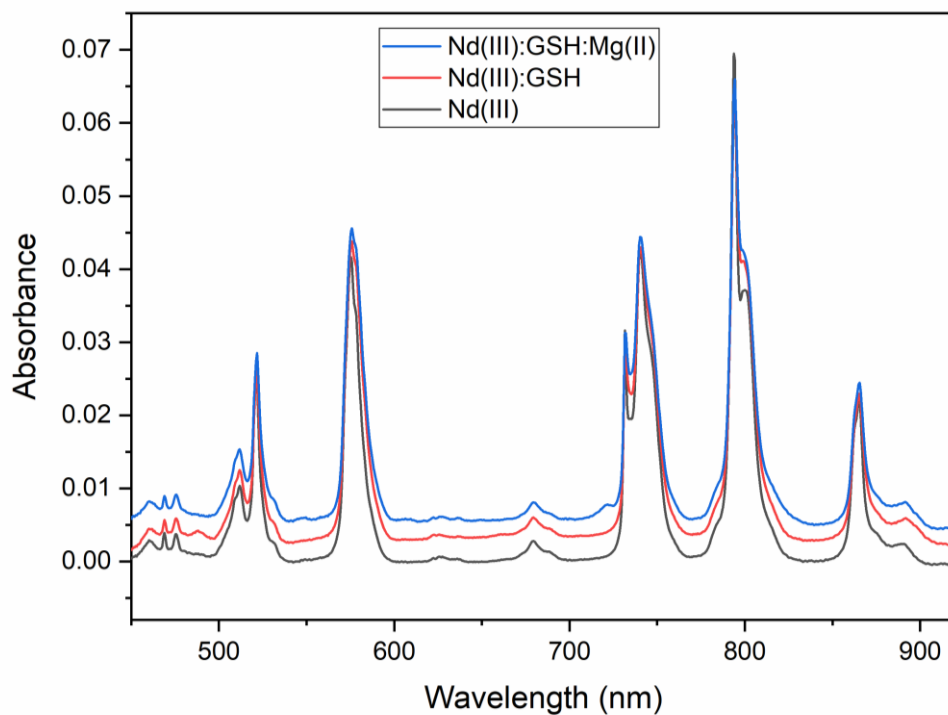


Fig. 4.1: Comparative absorption spectra of Pr(III), Pr(III):GSH and Pr(III):GSH:Mg(II) in CH_3CN .

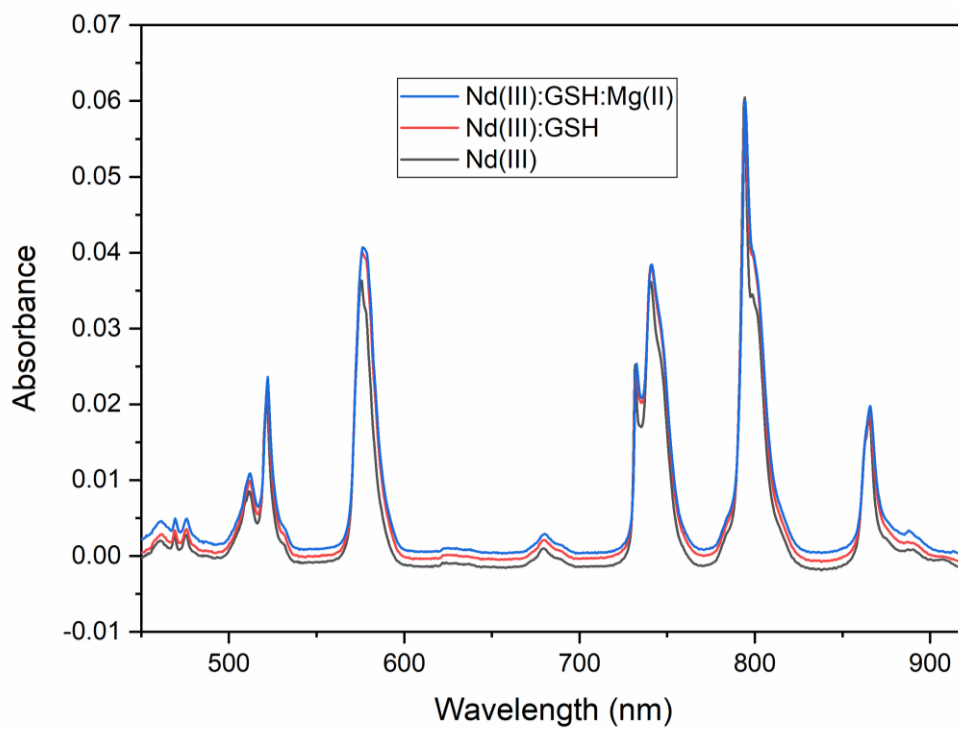


Fig. 4.2: Comparative absorption spectra of Pr(III), Pr(III):GSH and Pr(III):GSH:Mg(II) in CH_3OH .

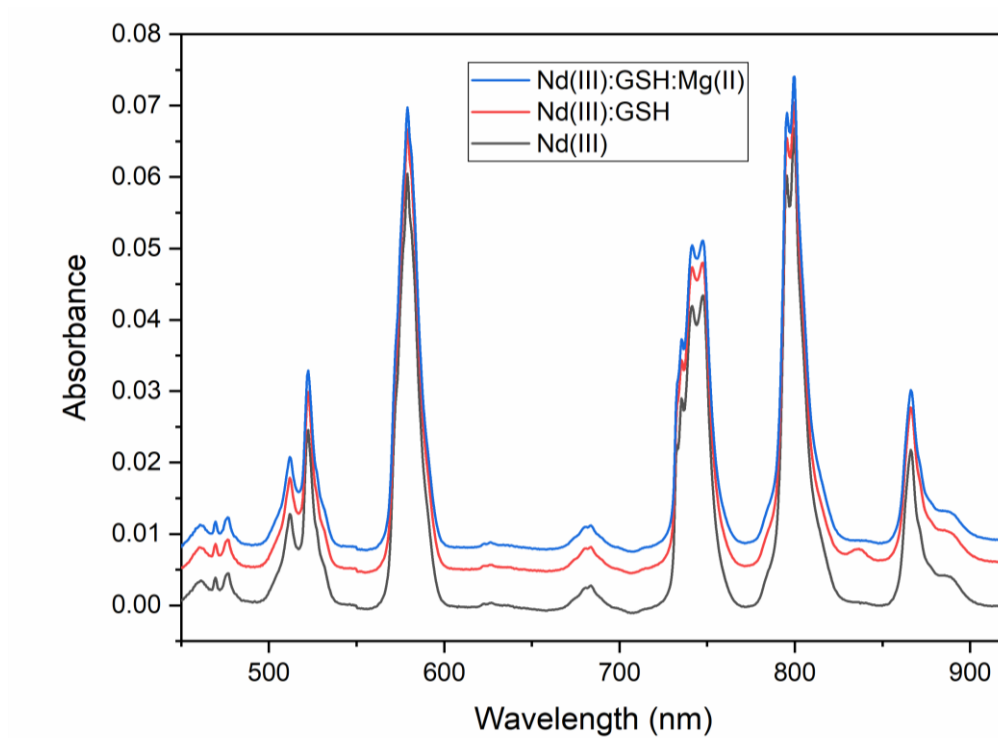


Fig. 4.3: Comparative absorption spectra of Pr(III), Pr(III):GSH and Pr(III):GSH:Mg(II) in DMF.

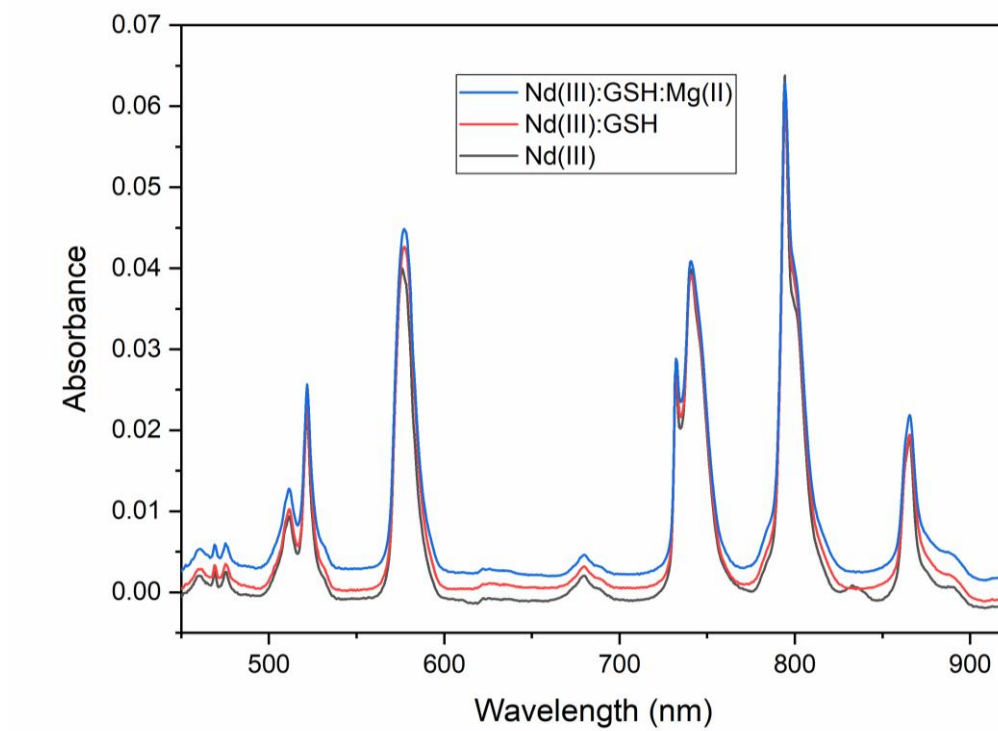


Fig. 4.4: Comparative absorption spectra of Pr(III), Pr(III):GSH and Pr(III):GSH:Mg(II) in dioxane.

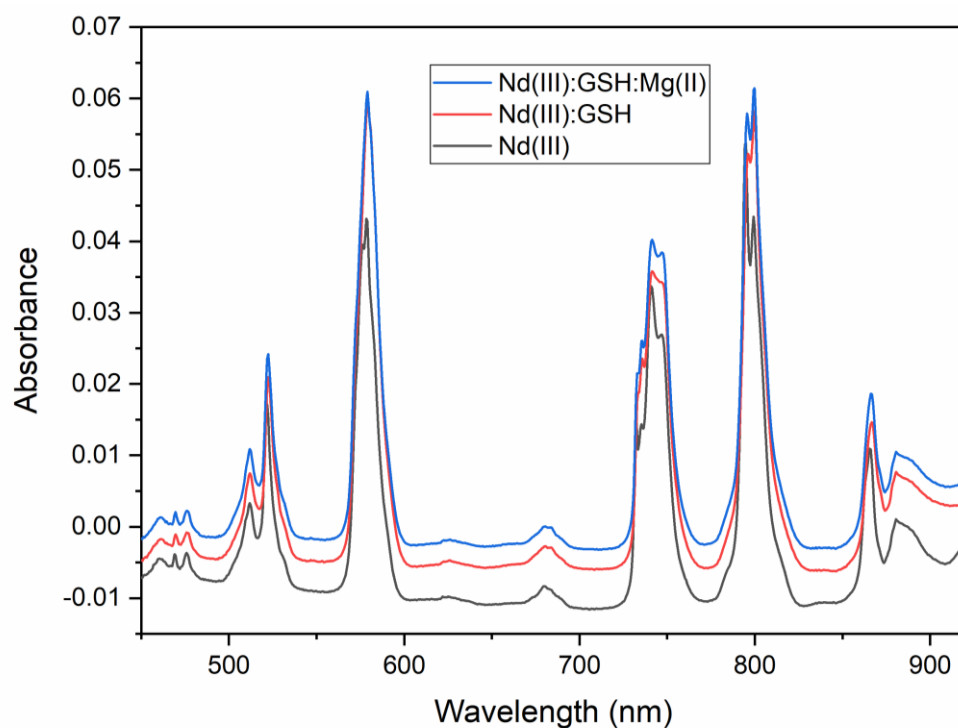


Fig. 4.5: Comparative absorption spectra of Pr(III), Pr(III):GSH and Pr(III):GSH:Mg(II) in DMF at pH 2.

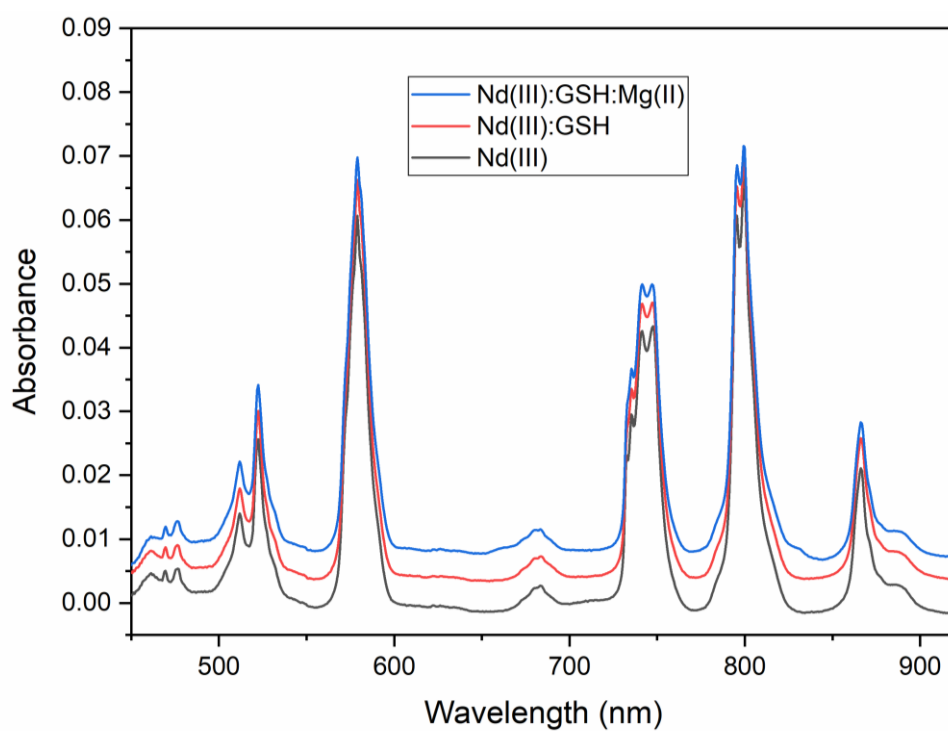


Fig. 4.6: Comparative absorption spectra of Pr(III), Pr(III):GSH and Pr(III):GSH:Mg(II) in DMF at pH 4.

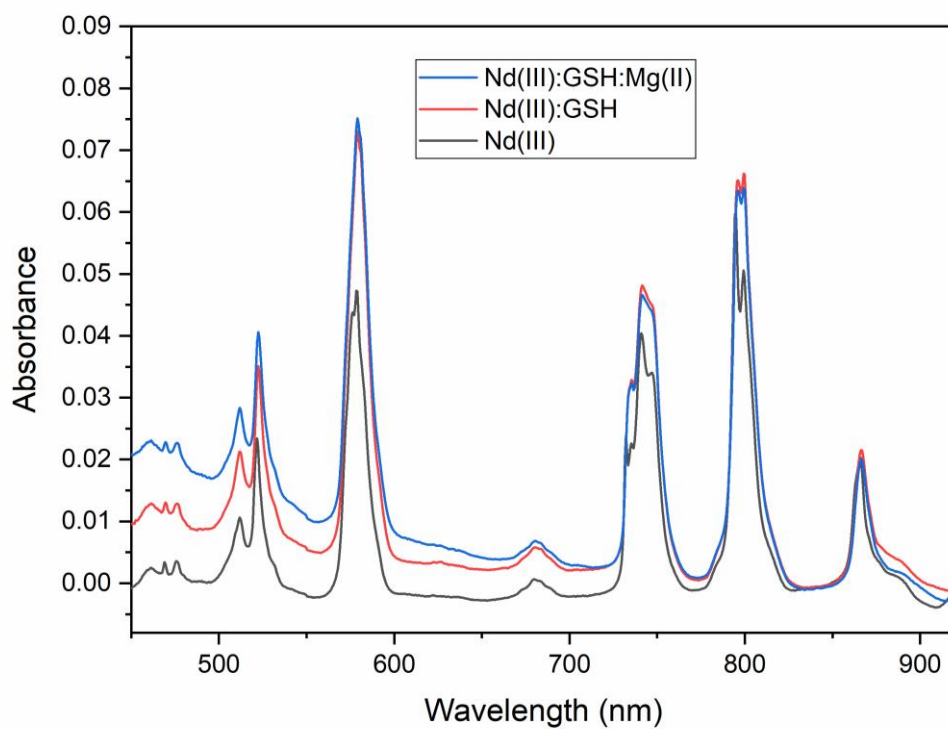


Fig. 4.7: Comparative absorption spectra of Pr(III), Pr(III):GSH and Pr(III):GSH:Mg(II) in DMF at pH 6.

CHAPTER 5

SYNTHESIS, CHARACTERIZATION, ANTIOXIDANT AND ANTIBACTERIAL STUDIES OF PRASEODYMIUM COMPLEX WITH GLUTATHIONE

5.1 Introduction

The field of lanthanide chemistry has seen a resurgence in interest as well as increased study over the last few decades [1,2]. A significant portion of these endeavours revolves around the development of complexes with novel structural features for the generation of advanced materials and utilisation of their special spectroscopic properties in the creation of biological probes and sensors in the areas of molecular biology and clinical chemistry [3]. Because of the wide range of uses of lanthanide complexes in biology and medicine, lanthanide coordination chemistry has become increasingly important and has been playing an increasingly important role in modern chemistry [4,5]. Lanthanide complexes are also known to show important pharmacological properties such as anticancer, antiallergic, anti-inflammatory and antibacterial properties [6]. Lanthanide research on polydentate ligands has been the subject of interest for researchers due to their potent biological properties. In this context, Ln(III) ion complexes can be exploited as bioactive compounds because of their high possible coordination numbers and good flexibility of metal ion coordination sphere which accounts for easy ligand changes [7].

In this chapter, we report the synthesis and characterization of Pr(III) complex with glutathione. Glutathione is a sulfur compound made up of three amino acids that occurs in two different forms viz; the active form, reduced glutathione (GSH) and the inactive form, oxidized glutathione (GSSG) [8,9]. GSH is well-known for its key role in oxidative stress management. The *in vitro* antibacterial activities of the synthesized compound against pathogenic bacteria (*Staphylococcus aureus*, *Klebsiella pneumoniae*, *Escherichia coli* and *Bacillus subtilis*) has been examined. We have also evaluated the *in vitro* antioxidant activities of the complex using DPPH and FRAP assays.

5.2 Experimental

5.2.1 Materials and Methods

L-Glutathione reduced ($C_{10}H_{17}N_3O_6S$, $\geq 98.0\%$) and Praseodymium trinitrate hexahydrate ($Pr(NO_3)_3 \cdot 6H_2O$, 99.99%) were procured from Sigma-Aldrich and used as received. Nutrient agar, streptomycin, DPPH, Trolox were purchased from HiMedia and Merck respectively. Distilled water was used to make the aqueous solutions.

Infrared spectra of the sample was obtained using a Perkin Elmer FT-IR spectrometer (Spectrum-Two) in the 400 to 4000 cm^{-1} range. The morphology of the sample was examined using a Sigma, Carl Zeiss (UK), Field emission scanning electron microscopy (FE-SEM). The X-ray powder diffraction (XRD) analysis was documented on a Rigaku Ultima IV X-ray diffractometer with Cu K_{α} radiation ($\lambda = 1.540 \text{ \AA}$) from 10° to 80° (2θ) at room temperature. Thermal analysis was carried out on SDT Q600 V20.9 Build 20 thermal analyzer with a heating rate of 20 $^\circ C/min$ using nitrogen atmosphere.

5.2.2 Preparation of the Complex

To an aqueous solution of $Pr(NO_3)_3 \cdot 6H_2O$ (0.01 mol), an aqueous solution of GSH (0.05 mol) was added dropwise with continuous stirring. The solution was stirred thoroughly and refluxed for about 4 hours. The resulting solution was concentrated and kept overnight. The

obtained solid product was collected by filtration and washed with acetone and distilled water before being dried in a vacuum oven.

5.2.3 *In vitro* Antioxidant assays

The antioxidant activity of the sample was evaluated utilising two separate assays: 2,2-diphenyl-1-picrylhydrazyl (DPPH) and ferric reducing antioxidant power (FRAP) assay [10]. The antioxidant activity of the sample was tested using the two assay and compared with the standard Trolox. The experiments were carried out in triplicates and the results were averaged. IC₅₀ values for standard and sample were derived for the DPPH assay. The DPPH free radical scavenging percentage was calculated using the measured absorbance by the following equation:

$$\text{DPPH scavenging activity (\%)} = \frac{A_{\text{control}} - A_{\text{sample}}}{A_{\text{control}}} \times 100$$

where A_{control} is the absorbance of the control (DPPH + methanol) and A_{sample} is the absorbance of the sample. The IC₅₀ value was used to assess the antioxidant activity. For the FRAP assay the absorbance of the reaction mixture was measured at 700nm on a UV/Vis spectrophotometer. Greater absorbance indicated greater reducing power.

5.2.4 *In vitro* Antibacterial activity

The *in vitro* bactericidal activity of Pr(III):glutathione complex was performed against four different strains of bacterial microorganisms like gram-negative bacteria (*Escherichia coli* and *Klebsiella pneumoniae*) and gram-positive bacteria (*Staphylococcus aureus* and *Bacillus subtilis*) by well diffusion method [11]. The antimicrobial property of the synthesised compound was evaluated by determining the zone of inhibition (mm) and compared with the inhibition diameter of positive control streptomycin. The minimum inhibitory concentration (MIC) of the sample was further was determined by two-fold serial broth dilution technique and compared with the standard drug streptomycin. All tests were carried out in triplicates.

5.3 Results and discussion

5.3.1 Fourier transform infrared spectroscopy (FTIR)

IR analysis was used to investigate the mode of complexation between praseodymium and GSH. FTIR analysis was useful in elucidating the chemical composition and environment of the complex formed. The IR spectra of free glutathione and the praseodymium complex are shown in Fig. 5.1. The IR spectra of GSH and Pr(III):GSH complex exhibits several vibrations. The appearance and disappearance of certain bands in the lanthanide complex as well as the free GSH provides information on the bonding mechanism of the complex. Such appearance and disappearance of bands as observed in the IR spectra of GSH and praseodymium complex were helpful in determining the binding mode in the complex formed. The presence of water molecules can be attributed to the broad band around 3000 to 3300 cm^{-1} . From the FTIR spectra of free glutathione in Fig. 5.1 the notable vibrations observed are at 2525 cm^{-1} , 1713 cm^{-1} and 1599 cm^{-1} which corresponds to the vibrations of sulphydryl (-SH) group and carbonyl group (C=O) of carboxylic and amide group respectively. The bands from N-H vibrations can be seen at 3348 cm^{-1} and 3251 cm^{-1} [12,13]. These bands are characteristic of the functional moieties of GSH.

Several important changes are observed in the IR spectrum of the praseodymium complex which indicates the coordination of Pr(III) with GSH. The formation of complex is supported by the disappearance of the -SH band in the IR spectra of the praseodymium complex. The disappearance of the thiol band of glutathione from the praseodymium complex can be attributed to the interaction of GSH with the lanthanide ion through the sulfur atom of the thiol group from the cysteine moiety of GSH. This could suggest the deprotonation of -SH and its subsequent participation in coordinating with the lanthanide ion. Additionally, the C=O band at 1713 cm^{-1} observed in the free GSH is found to appear at a lower frequency in the lanthanide complex. This is also an indication of the

involvement of the -COOH group of glycine in the coordination of glutathione with praseodymium. The shift of the N-H band to a lower frequency indicates that nitrogen is involved in bonding. Apart from these, the IR spectrum of the praseodymium complex also exhibits a new peak at 417 cm^{-1} which can be attributed to the stretch vibration of M-O bond [13]. This also could clearly demonstrate the formation of bond between the GSH and praseodymium in the formation of complex complex. Fig. 5.2 presents the possible structure of the complex.

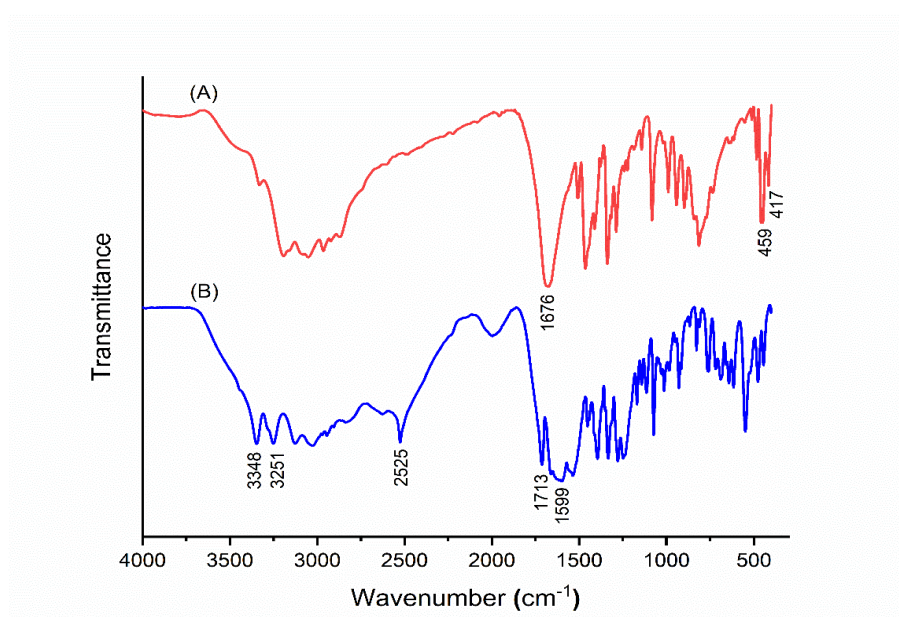


Fig. 5.1: FTIR spectra of (A) Pr(III):GSH complex and (B) Glutathione.

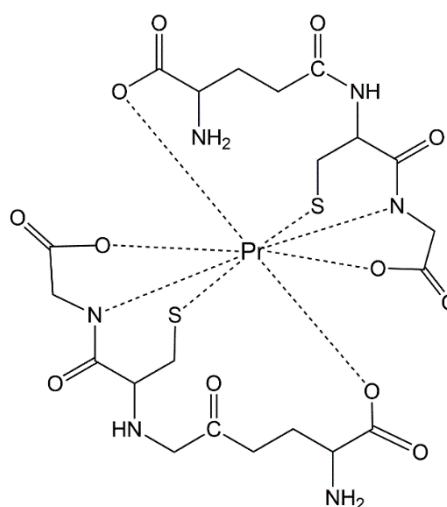


Fig. 5.2: Probable structure of Pr(III):GSH complex.

5.3.2 X-ray diffraction (XRD)

The X-ray diffraction (XRD) analysis of Praseodymium(III):GSH complex (Fig. 5.3) was scanned in the range of 5-80° at 2 θ angles at a wavelength of 1.54 Å. The XRD pattern of the praseodymium(III) complex is given in Fig. 5.3. Table 5.1 shows the resulting interplanar spacing (d) values for various 2 θ , as well as the associated (h k l) indices. GSAS II software was used to index the XRD pattern of the praseodymium(III) and glutathione complex in terms of major peaks with relative intensities greater than 10%. The lattice parameters calculated for the unit cell value of Pr(III):GSH are; $a=20.20867$ Å, $b=5.51476$ Å, $c=10.69533$ Å and unit cell volume $V=1191.95$ (Å)³. As a result, an orthorhombic crystal system has been formed for the praseodymium(III) complex with GSH. The crystallite size was calculated using Scherrer's equation where the full width at half maximum (FWHM) of the most intense peak was considered.

$$d = \frac{k\lambda}{\beta \cos \theta}$$

where k is the Scherer constant (~0.9), λ is the X-ray wavelength of Cu k_{α} radiation, β is the FWHM of the diffraction peak, and θ is the Bragg angle. The average crystallite size of the praseodymium(III):GSH complex was found to be 39.66 nm, suggesting the nanocrystalline phase of the system.

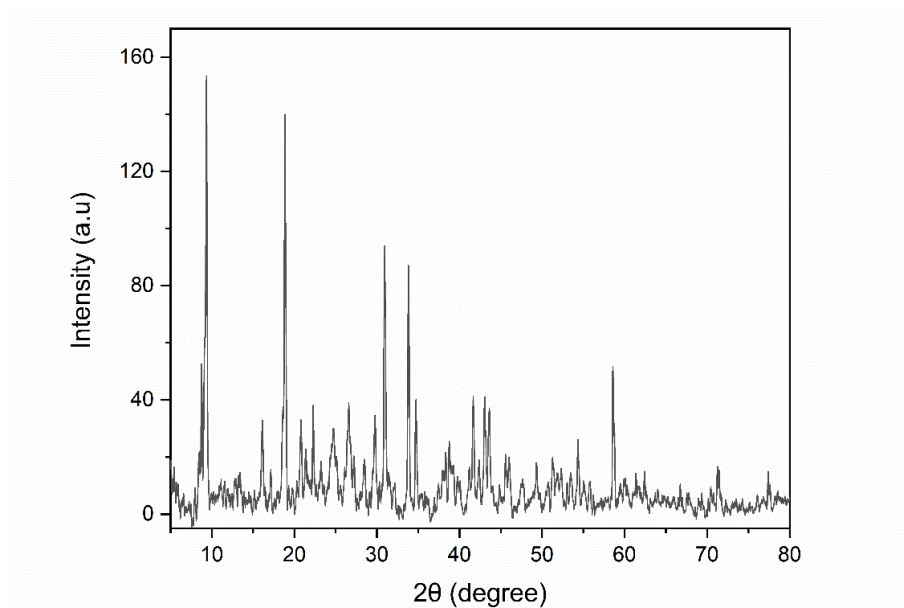


Fig. 5.3: XRD pattern of Pr(III):GSH complex.

Table 5.1: Powder XRD data praseodymium(III) complex with glutathione.

Position	d-obs	d-calc	hkl
8.757	10.088	10.104	200
9.337	9.463	9.453	101
16.103	5.499	5.514	010
18.852	4.703	4.726	202
22.250	3.991	3.963	311
24.691	3.602	3.588	212
26.574	3.351	3.368	600
30.932	2.888	2.874	610
33.804	2.649	2.647	121
34.7101	2.582	2.584	204
41.623	2.167	2.168	123
43.018	2.100	2.094	604
58.588	1.574	1.575	606

5.3.3 Scanning Electron Microscopy (SEM)

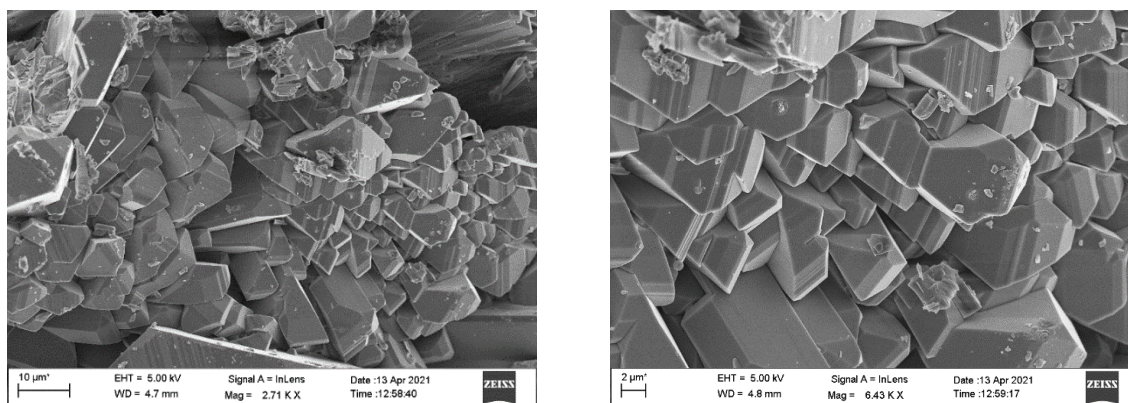


Fig. 5.4: SEM micrography for the praseodymium(III) complex.

Fig. 5.4 shows SEM images of the praseodymium(III):GSH complex. According to SEM observations, the powder obtained after precipitation is made up of large aggregates. These images emphasise the formation of micron-sized agglomerates with no discernible morphology. The sample is devoid of a defined morphology, irregular in shape and size. Smaller particles can also be seen visible between the grains as well as on their surfaces.

5.3.4 Thermogravimetric analysis (TGA)

The TGA curve of the praseodymium complex is shown in Fig. 5.5. The thermogram indicates that the praseodymium-glutathione complex is stable in air at room temperature and it starts to decompose when the temperature rises to 100°C. The degradation of the complex starts around 100°C and it takes place slowly at the initial stage; it continues and is found incomplete until 900°C with a total weight loss of about 55.4 %. The thermal decomposition of the complex undergoes two stages. From Fig. 5.5, it is seen that the first decomposition occurred between 100 and 298°C resulting in a loss of 7.38% weight. This weight loss is contributed to the loss of free and coordinated water and is an indication of the presence of free or coordinated water in the complex. This result is in accordance with the FTIR data. At a temperature of 330-890°C, the second stage of decomposition (48.01%

weight loss) was observed, which could be caused due to the loss of organic moiety from the praseodymium-GSH complex. The char yield of the sample was recorded to be approximately 44.6 wt% at 890°C. No stable intermediate is observed in the decomposition curve which could possibly suggest that no other ligand is attached to praseodymium(III). The slow decomposition of the complex may be a possible indication of the ligand's multidentate behaviour with varying thermal stability that corresponds to the different binding sites of GSH [14]. TGA analysis could provide important information about the thermal stability of the complex. The results indicate good thermal stability of the Pr(III):GSH complex with high decomposition temperature.

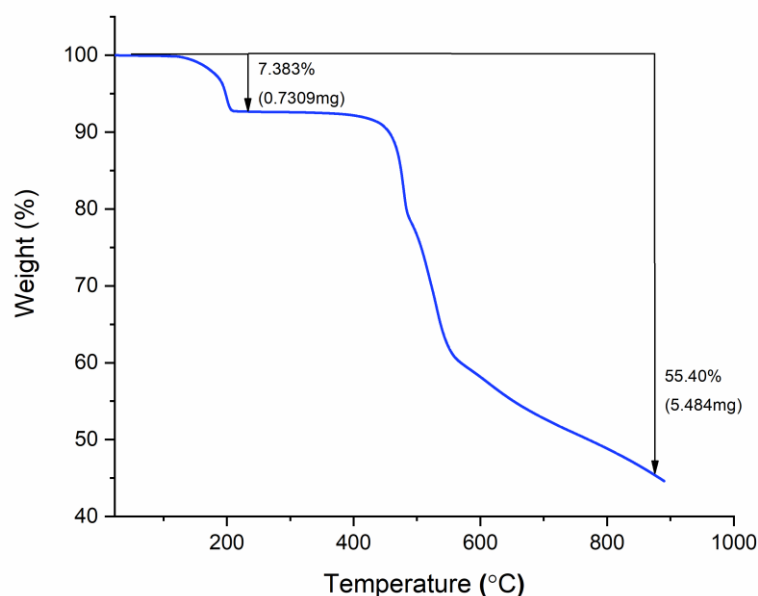


Fig. 5.5: TGA curve of the Pr(III):GSH complex.

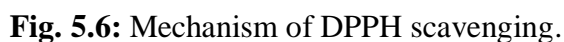
5.3.5 *In vitro* Antioxidant activity

(a) Radical scavenging assay (DPPH)

Reactive oxygen species (ROS) are highly reactive chemicals that are produced as part of the processes of aerobic metabolism in organisms. Excess production of ROS can cause

oxidative stress in the body. Oxidative stress is the imbalance between the production of ROS and the body's ability to counteract them with antioxidants. ROS like the hydroxy radical (OH^\bullet), peroxide (ROO^\bullet) and superoxide radical ($\text{O}_2^{\bullet-}$) can cause extensive damage to nucleic acid, lipids and proteins. Oxidative stress has been linked to ageing and development of diseases like cancer, diabetes and cardiovascular diseases [15,16]. The primary objective of antioxidant administration is the elimination of these radicals. Consequently, the antioxidant activity of Pr(III)-GSH complex has been investigated in this paper by the determination of its radical scavenging and reducing potentials, using DPPH and FRAP assay respectively.

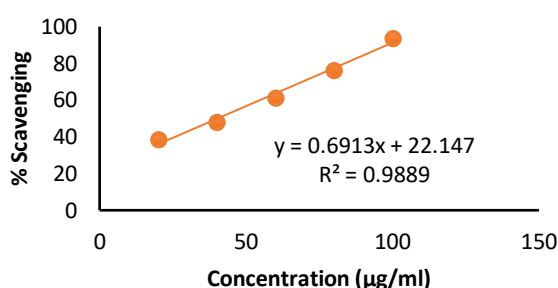
FRAP and DPPH assays are two of the most widely used assays for the determination of antioxidant activity. These assays provide rapid analysis, are easily standardizable and relatively simpler. DPPH is an N-centered free radical, stable at room temperature with an odd electron. DPPH gives off a purple colour in methanol solutions and exhibits a strong absorption at 517nm. The purple colour of DPPH changes from violet to yellow with the pairing of its odd electron by the donation of a hydrogen radical or an alkyl radical in the presence of a radical scavenger. This results in the formation of the reduced DPPH-H (Fig. 5.6) [17]. The change in colour from purple to yellow upon scavenging also results in subsequent lowering of absorbance at 517nm. Thus, such a lower absorbance in this case indicates a higher antioxidant activity. Antioxidant analysis using the DPPH free radical method works by quantifying the ability of antioxidants in quenching the DPPH radical. We have used Trolox as the standard for the assay.



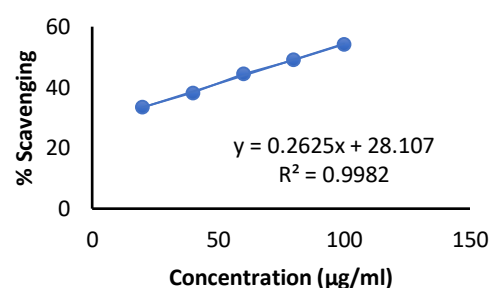
131

Table 5.2: DPPH radical scavenging activity, IC₅₀ values of the standard Trolox and the sample.

Concentration ($\mu\text{g/ml}$)	Trolox		Sample	
	% Inhibition	IC ₅₀ ($\mu\text{g/ml}$)	% Inhibition	IC ₅₀ ($\mu\text{g/ml}$)
20	38.6		33.41	
40	48.15		38.18	
60	61.4	40.29	44.38	83.40
80	76.32		49.11	
100	93.64		54.19	



A



B

Fig. 5.7: DPPH free radical scavenging activity in the presence of different concentrations of (A) Trolox and (B) sample.

(b) Reducing power assay

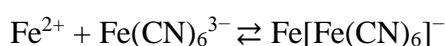
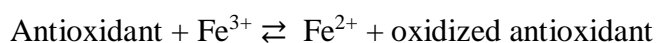
Another popular method for measuring antioxidant capacity is the FRAP assay. It is fast, simple and cheap. It is a nonradical method that depends on the reduction of ferric ion (Fe^{3+}) into ferrous ion (Fe^{2+}) [18]. The FRAP assay primarily assesses an antioxidant's reducing capacity when it reacts with Fe^{3+} ($\text{K}_3\text{Fe}(\text{CN})_6$) to produce a coloured Fe^{2+} ($\text{K}_3\text{Fe}(\text{CN})_6$) complex. Although tripyridyltriazine (TPTZ) was used in the original FRAP assay, other iron-binding ligand have been used in recent trends years, with potassium ferricyanide being the most popular ferric binding reagent. In this case, the end product is a blue coloured ferrous complex which is spectrophotometrically evaluated and reveals the

antioxidants' reducing power. Increased absorbance at 700 nm indicates antioxidant activity. The ability of any compound to donate an electron or hydrogen atom to a metal atom accounts for its reducing power. The sample compound is used as a reducing agent in a colorimetric reaction in the FRAP assay.

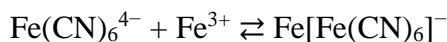
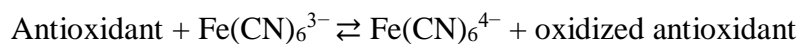
The test solution which is initially yellow in colour changes to various shades of green and blue depending on the reducing potential of the test compound. Consequently, the absorption at 700nm increases. The antioxidant activity is evaluated by measuring the change of absorbance at 700nm. Hence, the higher the absorbance value, higher is the antioxidant activity. The resultant blue colour of the Fe^{2+} complex can be produced in two ways, both of which yield the same result [19]. The two possible routes are

- (i) reduction of Fe^{3+} to Fe^{2+} , which binds to ferricyanide and produces a blue colour.
- (ii) ferricyanide reduction to ferrocyanide which binds to free Fe^{3+} to yield blue colour [20].

Following are the simplified schemes for the two reactions [20]:



Or



The results obtained using FRAP assay are shown in Fig. 5.8. Fig 5.8 presents a concentration vs absorbance graph of the sample and Trolox. Absorbance values obtained at 700nm have been plotted against their corresponding concentrations($\mu\text{g/ml}$). When compared with the standard Trolox, the sample was found to show a lower absorbance meaning that its antioxidant activity is lesser than Trolox. The FRAP assay followed a

similar trend shown by the DPPH assay. With increasing concentration, the sample's reducing power increased (Fig 5.8). The findings of this study clearly demonstrated that Pr(III):GSH possesses antioxidant activity.

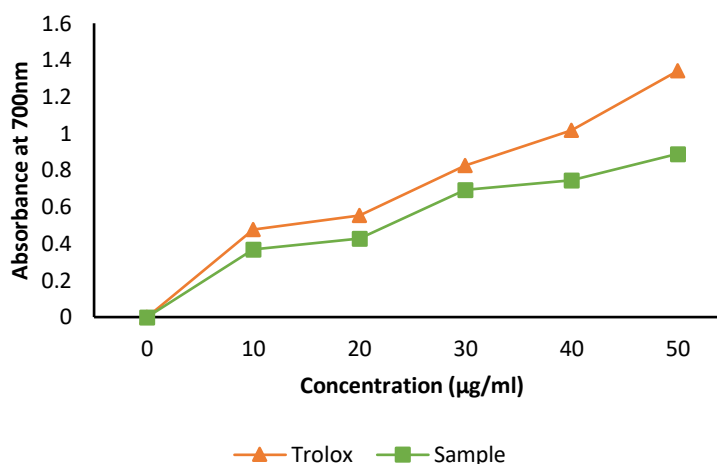


Fig. 5.8: Antioxidant activity of standard (Trolox) and the sample using FRAP assay.

5.3.6 *In vitro* Antibacterial activity

The *in vitro* antibacterial activities of Pr(III):GSH complex against *Escherichia coli*, *Bacillus subtilis*, *Klebsiella pneumoniae* and *Staphylococcus aureus* are summarised in Tables 5.3 and 5.4. The well diffusion method was used for antibacterial analysis of the sample and streptomycin. Both the sample and reference were taken in concentrations of 10mg/ml in sterilised water. The antibacterial efficacy was assessed by measuring the diameter of its zone of inhibition. The zone of inhibition is the clear circular area around the test compound where microbial growth is inhibited. Table 5.3 presents the zone of inhibition (mm) of the praseodymium complex against the different microbes. The results show that the praseodymium(III) complex exhibits potent antimicrobial activity against all the selected strains of microbes. The *in vitro* assay results show that the praseodymium complex has the highest activity against the gram -ve bacteria *Klebsiella pneumoniae* with

an inhibition zone of 14 mm. Fig. 5.9 shows images of antibacterial activity of the praseodymium complex against gram +ve and gram -ve bacteria.

Table 5.3: Zone of inhibition (mm) of Pr(III):GSH in comparison with the standard streptomycin.

Bacteria	<i>Bacillus subtilis</i>	<i>Escherichia coli</i>	<i>Klebsiella pneumoniae</i>	<i>Staphylococcus aureus</i>
Sample	11	12	14	10
Streptomycin	30	32	30	31

Table 5.4: Minimum inhibitory concentration of Pr(III):GSH in mg/ml in comparison with the standard streptomycin.

Bacteria	<i>Bacillus subtilis</i>	<i>Escherichia coli</i>	<i>Klebsiella pneumoniae</i>	<i>Staphylococcus aureus</i>
Sample	0.703	0.703	1.406	1.406
Streptomycin	0.0072	0.0029	0.0072	0.0058

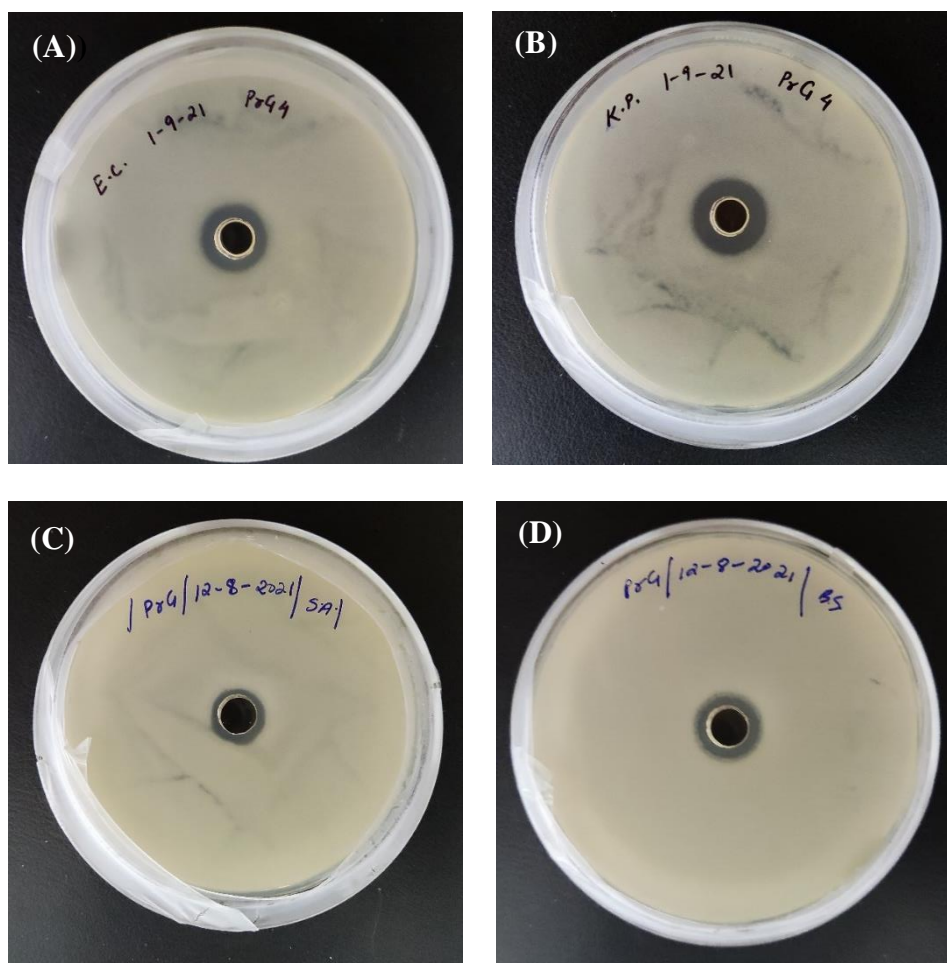


Fig. 5.9: Estimation of antimicrobial activity by agar plate diffusion experiment (A) *Escherichia coli* (B) *Bacillus subtilis* (C) *Staphylococcus aureus* and (D) *Klebsiella pneumoniae*.

The MIC of the compound was calculated against the four strains of bacteria to determine its bactericidal potency. MIC is the lowest concentration of an antimicrobial agent that completely inhibits visible microorganism growth. Compounds with lower MIC scores are more effective antimicrobial agents because lesser compound is required to inhibit the organism's growth. The MIC results of the sample and streptomycin are given in Table 5.4. The MIC values for the complex ranged from 0.7 to 1.4 mg/ml. The MIC values were used to determine the lowest concentration of the sample that inhibited visible growth of the bacteria under the given assay conditions. Hence, the MIC values represent the minimum concentration of the sample that is effective in promoting antibacterial

activity in the different bacterial strains tested. The MIC of the sample was found to be lowest against *Bacillus subtilis* (0.7 mg/ml) and *Escherichia coli* (0.7 mg/ml).

Since biological systems are so complex, determining the exact mechanism of antimicrobial activity of metal complexes is not feasible. However, the antibacterial behaviour of metal complexes can be explained using the Overton concept [21] and Tweedy's chelation theory [22]. According to the lipid membrane model of cells as proposed by C. E. Overton, the cell membrane is composed of a thin layer of lipid. This lipid layer only allows substances that are lipid soluble to pass through the cell membrane. As a result, liposolubility is an important determinant of antimicrobial activity. In this context, the correlation between liposolubility and antibacterial activity of metal complexes may be explained by the Tweedy chelation theory. According to Tweedy's chelation theory, on chelation of the metal ion with their corresponding ligand, the polarity of the metal is reduced. The main reason for this is because of the overlap of the ligand orbital and partial sharing of its positive charge with donor groups. Consequently, the delocalization of π -electrons is increased across the entire chelate ring, enhancing the lipophilicity of the metal complex. This would suggest that the chelation aids the permeation of the metal complex through the bacterial cell membrane by increasing its lipophilicity. Penetration of the lanthanide complex could result in cell wall disruption leading to cell lysis and subsequent cell death. The passage of the lanthanide complex through the cellular membrane could also result in the blockage of metal binding sites in the bacterial enzymes, obstructing normal cell functions such as metabolism, respiration and ATP production. This inhibits protein synthesis and cell processes, limiting the organism's growth and eventually leading to bacterial cell death.

*The work presented in this chapter has been accepted for publication in *Current Science*.

References

- [1] K. Bernot, C. Daiguebonne, G. Calvez, Y. Suffren, O. Guillou, A Journey in Lanthanide Coordination Chemistry: From Evaporable Dimers to Magnetic Materials and Luminescent Devices, *Acc. Chem. Res.* **207** (2021) 427–440. <https://doi.org/10.1021/acs.accounts.0c00684>.
- [2] N.S. Chundawat, S. Jadoun, P. Zarrintaj, N.P.S. Chauhan, Lanthanide complexes as anticancer agents: A review, *Polyhedron.* **207** (2021) 115387. <https://doi.org/10.1016/j.poly.2021.115387>.
- [3] A.L. Gassner, C. Duhot, J.C.G. Bünzli, A.S. Chauvin, Remarkable tuning of the photophysical properties of bifunctional lanthanide tris(dipicolinates) and its consequence on the design of bioprobes, *Inorg. Chem.* **47** (2008) 7802–7812. <https://doi.org/10.1021/ic800842f>.
- [4] H. Li, X. Wang, T.Y. Ohulchanskyy, G. Chen, Lanthanide-Doped Near-Infrared Nanoparticles for Biophotonics, *Adv. Mater.* **33** (2021) 2000678. <https://doi.org/10.1002/adma.202000678>.
- [5] J.C.G. Bünzli, Luminescence Bioimaging with Lanthanide Complexes, in: A. de Bettencourt-Dias (Ed.), *Lumin. Lanthan. Ions Coord. Compd. Nanomater.*, Wiley, 2014: pp. 125–196. <https://doi.org/10.1002/9781118682760.ch04>.
- [6] S.P. Fricker, The therapeutic application of lanthanides, *Chem. Soc. Rev.* **35** (2006) 524–533. <https://doi.org/10.1039/b509608c>.
- [7] M. Abdus Subhan, M. Saifur Rahman, K. Alam, M. Mahmud Hasan, Spectroscopic analysis, DNA binding and antimicrobial activities of metal complexes with phendione and its derivative, *Spectrochim. Acta - Part A Mol. Biomol. Spectrosc.* **118** (2014) 944–950. <https://doi.org/10.1016/j.saa.2013.09.110>.
- [8] G. Wu, Y.Z. Fang, S. Yang, J.R. Lupton, N.D. Turner, Glutathione Metabolism and

- Its Implications for Health, *J. Nutr.* **134** (2004) 489–492.
<https://doi.org/10.1093/jn/134.3.489>.
- [9] G. Noctor, G. Queval, A. Mhamdi, S. Chaouch, C.H. Foyer, Glutathione, *Tanpakushitsu Kakusan Koso.* **33** (1988) 1353–1654.
<https://doi.org/10.1199/tab.0142>.
- [10] K. Richa, R. Karmaker, T. Ao, N. Longkumer, B. Singha, U.B. Sinha, Rationale for antioxidant interaction studies of 4-bromo-1-isothiocyanato-2-methylbenzene – An experimental and computational investigation, *Chem. Phys. Lett.* **753** (2020) 137611. <https://doi.org/10.1016/j.cplett.2020.137611>.
- [11] S. Jain, M.S. Mehata, Medicinal Plant Leaf Extract and Pure Flavonoid Mediated Green Synthesis of Silver Nanoparticles and their Enhanced Antibacterial Property, *Sci. Rep.* **7** (2017) 15867. <https://doi.org/10.1038/s41598-017-15724-8>.
- [12] M. Selim, A. Saha, K.K. Mukherjea, Synthesis, characterization, and DNA binding of the biologically relevant novel cationic molybdenum(VI)-glutathione complex [Mo(GS)(Cl)(H₂O)]Cl₂, *Monatshefte Fur Chemie.* **143** (2012) 227–233.
<https://doi.org/10.1007/s00706-011-0601-8>.
- [13] G.C. Han, Y.N. Liu, Synthesis, characterization and fluorescent properties of cerium(III) glutathione complex, *Luminescence.* **25** (2010) 389–393.
<https://doi.org/10.1002/bio.1165>.
- [14] S. Ahmad, M. Hanif, M. Monim-Ul-Mehboob, A.A. Isab, S. Ahmad, Silver(I) complexation with glutathione in the presence of tetramethylthiourea, *Synth. React. Inorganic, Met. Nano-Metal Chem.* **39** (2009) 45–49.
<https://doi.org/10.1080/15533170802683172>.
- [15] A.M. Pisoschi, A. Pop, The role of antioxidants in the chemistry of oxidative stress: A review, *Eur. J. Med. Chem.* **97** (2015) 55–74.

<https://doi.org/10.1016/j.ejmech.2015.04.040>.

- [16] S.B. Nimse, D. Pal, Free radicals, natural antioxidants, and their reaction mechanisms, *RSC Adv.* **5** (2015) 27986–28006. <https://doi.org/10.1039/c4ra13315c>.
- [17] Y. Cai, M. Sun, H. Corke, Antioxidant activity of betalains from plants of the Amaranthaceae, *J. Agric. Food Chem.* **51** (2003) 2288–2294. <https://doi.org/10.1021/jf030045u>.
- [18] I.F.F. Benzie, J.J. Strain, The ferric reducing ability of plasma (FRAP) as a measure of “antioxidant power”: The FRAP assay, *Anal. Biochem.* **239** (1996) 70–76. <https://doi.org/10.1006/abio.1996.0292>.
- [19] Y. Zhong, F. Shahidi, Methods for the assessment of antioxidant activity in foods, in: F. Shahidi (Ed.), *Handb. Antioxidants Food Preserv.*, Woodhead Publishing, Cambridge, 2015: pp. 287–333.
- [20] K.I. Berker, K. Güllü, B. Demirata, R. Apak, A novel antioxidant assay of ferric reducing capacity measurement using ferrozine as the colour forming complexation reagent, *Anal. Methods.* **2** (2010) 1770–1778. <https://doi.org/10.1039/c0ay00245c>.
- [21] I. Cota, V. Marturano, B. Tylkowski, Ln complexes as double faced agents: Study of antibacterial and antifungal activity, *Coord. Chem. Rev.* **396** (2019) 49–71. <https://doi.org/10.1016/j.ccr.2019.05.019>.
- [22] B.G. Tweedy, Plant extracts with metal ions as potential antimicrobial agents, *Phytopatology.* **55** (1964) 910–918.

CHAPTER 6

SUMMARY AND CONCLUSIONS

Biological fluids are essentially multimetal-multiligand systems with an abundance of organic and inorganic species present in different concentrations, as well as variable lipophilicity and lipophobicity in physiological pH ranges. The biological fluids are fundamentally multimetal-multiligand systems in which a variety of endogenous metal ions compete with the coordinating sites of multidentate macromolecules, and multidonor sites also compete for different metal sites. Metal binding to a specific donor site of biomolecules is determined by a variety of factors such as donor capability, structure, conformation, orientation, physiological pH, the presence of similar types of metal ions and their relative abundance. Thus, it is deemed important to research the simultaneous coordination of two or three distinct metal ions with a multidentate biological molecule. We chose glutathione reduced (GSH), a tripeptide containing active carboxylate groups, a sulphydryl group, and peptide groups. GSH was chosen because it is easily available in its pure form, is biologically significant, and is an excellent ligand for simultaneous complexation by hard and soft metal ions. It has eight potential donor binding sites for complexation with endogenous metal ions and serves as an excellent multidentate ligand for metal ions. The coordination chemistry of glutathione is important for understanding a wide range of biological processes, as well as serving as an indicator for the chemistry of thiol-sulphide interchange interactions and the toxicology of numerous metals.

In an effort to mimic the *in vivo* complexation of glutathione (GSH) with endogenous metal Mg(II), we have used quantitative absorption spectral analysis involving

the 4f-4f transition absorption spectroscopy as a probe to follow the simultaneous multimetal coordination of Ln(III) and Mg(II) with GSH in different aquated organic solvents and pH. Additionally, we have investigated the kinetics of Pr(III):GSH complexation with Mg(II) in aquated DMF medium at 303K, 308K, 313K and 318K.

Ln(III) ions consist of 4f-4f transitions called hypersensitive transitions which are highly sensitive to their environment and are marked by enhanced intensities and oscillator strength. Transitions other than the hypersensitive transitions are generally insensitive to coordination changes, however, certain 4f transitions which are non-hypersensitive have also been found to show extreme sensitivity with changes in the coordination environment of Ln(III) ion. Such transitions are termed Pseudohypersensitive transitions. During our research involving Pr(III) and Nd(III) spectra, we found that Ln(III) complexes of GSH and Mg(II) caused significant sensitivity to the non-hypersensitive transitions. Such observations are termed 'Ligand Mediated Pseudohypersensitivity' and referred to as pseudohypersensitive transitions. The pseudohypersensitive transitions $^3\text{H}_4 \rightarrow ^3\text{P}_2$, $^3\text{H}_4 \rightarrow ^3\text{P}_1$, $^3\text{H}_4 \rightarrow ^3\text{P}_0$ for Pr(III) and $^3\text{H}_4 \rightarrow ^1\text{D}_2$, $^4\text{I}_{9/2} \rightarrow ^4\text{G}_{7/2}$, $^4\text{I}_{9/2} \rightarrow ^4\text{F}_{7/2}$, $^4\text{I}_{9/2} \rightarrow ^4\text{F}_{5/2}$, and $^4\text{I}_{9/2} \rightarrow ^4\text{F}_{3/2}$ for Nd(III) have been utilised in the comparative absorption spectrophotometric study for the complexation of GSH with Ln(III) and Mg(II). The presence of the 4f-4f electronic transitions of the lanthanides in the accessible spectral region and their sensitivity towards the coordination environment makes quantitative absorption spectroscopy through 4f-4f transitions a powerful tool for investigating the coordination chemistry and biochemistry of lanthanides, particularly in solution.

From our investigation using the UV-Vis spectra and computed energy interaction (Slater-Condon (F_k , $k = 2, 4, 6$), Lande spin-orbit interaction (ζ_{4f}), Racah (E^k), nephelauxetic ratio (β), bonding parameter ($b^{1/2}$) and percent covalency (δ)) and intensity parameters (Oscillator strength (P) and Judd-Ofelt T_λ , ($\lambda=2,4,6$)), maximum intensification for the

Ln(III) complexes were observed at pH 6. This information is supplemented by the decrease in the values of the inter-electronic repulsion parameters and the increase in the bonding parameter value and further supported by the increased oscillator strength and Judd-Ofelt parameter values T_{λ} ($\lambda = 2, 4, 6$). According to spectral and computed data obtained for the Ln(III) complexes in various solvents, DMF was found to induce the most intensification and red-shift, whereas methanol exhibits the least. This means that DMF has the greatest influence out of the four solvents on the complexation between Ln(III) and the ligands. From the kinetic studies of Pr(III):GSH:Mg(II) in DMF at different temperatures (303K, 308K, 313K and 318K), it was observed that the rate of complexation increases with temperature. The Rate constants (k), Activation energy (E_a), ΔH° , ΔS° and ΔG° for Ln(III):GSH:Mg(II) were calculated and the complexation process was found to be endothermic, entropy-driven, spontaneous and favourable in solution. We also report the synthesis of Pr(III):GSH complex. X-ray diffraction (XRD), infrared spectroscopy (FT-IR), scanning electron microscopy (SEM) and thermogravimetric analysis (TGA) were used to characterize the prepared complex. The prepared complex was tested for its *in vivo* antioxidant and antibacterial activity. The Pr(III):GSH complex was found to show potent antioxidant and antibacterial activity based on the biological investigations.



नागालैण्ड विश्वविद्यालय NAGALAND UNIVERSITY

(केंद्रीय विश्वविद्यालय) / (A Central University)

मुख्यालय : लुमामी, जिला : जुन्हेबोटो (नागालैण्ड) – 798 627

Hqrs: Lumami, Dist: Zunheboto, Nagaland – 798 627

Department of Chemistry

Ph.D. Thesis Certificate on Plagiarism check

Name of the research scholar	Mhasiriekho Ziekhru
Ph.D. registration number	786/2017
Title of Ph.D. thesis	Theoretical Analysis of the Complexation of Ln(III) with Glutathione/Mg(II): Its Thermodynamics and Biological Properties
Name & institutional address of the supervisor	Prof. M. Indira Devi Department of Chemistry Nagaland University, Lumami
Name of the department and school	Department of Chemistry, School of Sciences
Date of submission	16/12/2022
Date of plagiarism check	16/12/2022
Percentage of similarity detected by the URKUND software	2%

I hereby declare that/certify that the Ph.D thesis submitted by me is complete in all respect as per the guidelines of Nagaland University (NU) for this purpose. I also certify that the thesis (soft copy) has been checked for plagiarism using **URKUND** similarity check software. It is also certified that the contents of the electronic version of the thesis are the same as the final hard copy of the thesis. Copy of the report generated by the **URKUND** software is also enclosed.

Place: Lumami

Date: 16/12/2022


Indira Devi
Prof. M. Indira Devi
Name & signature of the Supervisor:

Mhasiriekho Ziekhru
(Name & signature of the Scholar)

Document Information

Analyzed document	Mhasiriekho Ph.D. Thesis.docx (D153607989)
Submitted	2022-12-16 10:37:00
Submitted by	Indira Devi
Submitter email	indira@nagalanduniversity.ac.in
Similarity	2%
Analysis address	indira.naga@analysis.arkund.com

Sources included in the report

SA	rare earths.docx Document rare earths.docx (D100556501)		1
W	URL: https://www.selfstudys.com/sitepdfs/PZHdGTHY0E0pp4Tg65lr Fetched: 2022-12-16 09:47:01		1
W	URL: http://www.anon.co.kr/wp-content/ynawd/3ef391-lanthanide-electronic-configuration Fetched: 2022-12-16 09:47:00		1
W	URL: https://www.sciencedirect.com/topics/chemistry/thulium Fetched: 2021-06-25 09:34:37		1
SA	25.10.2021_Truptiben_Chemistry.pdf Document 25.10.2021_Truptiben_Chemistry.pdf (D116280950)		2

Entire Document

The lanthanides are a series of fifteen chemical elements from lanthanum (La) to lutetium (Lu) with atomic number 57 to 71. The 15 elements, together with their chemical symbols,

100%

MATCHING BLOCK 1/6

SA rare earths.docx (D100556501)

are lanthanum (La), cerium (Ce), praseodymium (Pr), neodymium (Nd), promethium (Pm), samarium (Sm), europium (Eu), gadolinium (Gd), terbium (Tb), dysprosium (Dy), holmium (Ho), erbium (Er), thulium (Tm), ytterbium (Yb) and lutetium (Lu).

APPENDIX

a) Presentations

1. Poster presented at National Seminar on “*Chemistry in Interdisciplinary Research-2017*” (NSCIR-2017), Nagaland University, Lumami, 16-17 March, 2017.
2. Paper presented at *National Seminar on Chemistry in Interdisciplinary Research*, Department of Chemistry, Nagaland University, Lumami, 9-10 November, 2018.
3. Paper presented at the *2nd Convention of NEAST and International Conference on Recent Advances on Science & Technology (ISRAST)*, organized by NEAST, Mizoram University, Aizawl, 16-18 November, 2020.
4. Paper presented at the *National e-Seminar on Chemistry in emerging trends of Interdisciplinary Research (NeSCETIR)*, Department of Chemistry, Nagaland University, Lumami, 18-20 November 2020.
5. Paper presented at the *Global Web Conference on Impact of Engineering, Science & Management on Digital Transformation*, by National Foundation for Entrepreneurship Development (NFED), Coimbatore, Tamil Nadu, 29-30 January, 2021.

b) List of Publications

- 1) **Mhasiriekho Ziekhru**, Zevivonu Thakro, Chubazenba Imsong, Juliana Sanchu, M. Indira Devi, Computation of energy interaction and intensity parameters for the complexation of Pr(III) with glutathione at different pH in the presence/absence of Mg^{2+} : 4f-4f transition spectra as a probe, *Polyhedron*, 2021, 200, 115099, <https://doi.org/10.1016/j.poly.2021.115099>.

- 2) **Mhasiriekho Ziekhrrü**, Tovishe Phucho, M. Indira Devi, Theoretical computation of interaction parameters for the complexation of GSH with Pr(III) and Mg(II) in solution: Analysis of their reaction dynamics and thermodynamic characters, *Journal of the Indian Chemical Society*, 2021, 98, 100232, <https://doi.org/10.1016/j.jics.2021.100232>.
- 3) **Mhasiriekho Ziekhrrü**, Juliana Sanchu, Zevivonü Thakro, Chubazenba Imsong, M. Indira Devi, Computational study of multimetal complexation of Nd(III) with GSH and Mg(II) in solution at different pH through 4f-4f transition spectra, *Chemical Physics Impact*, 2022, 5, 100090, <https://doi.org/10.1016/j.chphi.2022.100090>.
- 4) Zevivonü Thakro, Moaienla T. Ao, Chubazenba Imsong, Juliana Sanchu, **Mhasiriekho Ziekhrrü**, M. Indira Devi, Absorption spectral and thermodynamic analysis for the complexation of Pr^{3+} with L-phenylalanine in the presence/absence of Mg^{2+} using 4f–4f transitions spectra as probe. *The European Physical Journal Plus*, 2022, 137, 608, <https://doi.org/10.1140/epjp/s13360-022-02765-w>
- 5) Putusenla Imchen, **Mhasiriekho Ziekhrrü**, Betokali K. Zhimomi, Tovishe Phucho, Biosynthesis of silver nanoparticles using the extract of *Alpinia galanga* rhizome and *Rhus semialata* fruit and their antibacterial activity, *Inorganic Chemistry Communications*, 2022, 142, 109599, <https://doi.org/10.1016/j.inoche.2022.109599>.
- 6) Juliana Sanchu, **Mhasiriekho Ziekhrrü**, Zevivonü Thakro, M. Indira Devi, , 4f-4f Transition Spectra of the Interaction of Pr(III) with L-Valine in Solution: Kinetics and Thermodynamic Studies, *Asian Journal of Chemistry*, 2022, 34, 2688–2696.

- 7) Juliana Sanchu, Chubazenba Imsong, Zevivonü Thakro, **Mhasiriekho Ziekhürü**, M. Indira Devi, Absorption spectral study for the interaction of Pr (III) with L-Aspartic acid in various aquated organic solvents through 4f-4f transition spectra : Analysis of reaction pathways and thermodynamic parameters, *Journal of Pharmaceutical Negative Results*, 2022, 13, 860–878, <https://doi.org/10.47750/pnr.2022.13.S01.105>

- 8) Chubazenba Imsong, **Mhasiriekho Ziekhürü**, Zevivonü Thakro, Juliana Sanchu, M. Indira Devi, Theoretical study of the heterometal complexation of Pr(III) with L-isoleucine in the presence/absence of Mg(II) in solution: 4f-4f transition spectra as probe. *Chemical Physics Impact*, 2022, 5, 100108, <https://doi.org/https://doi.org/10.1016/j.chphi.2022.100108>

- 9) **Mhasiriekho Ziekhürü**, Putusenla Imchen, Tavishe Phucho, M. Indira Devi, Synthesis, characterization, antioxidant and antimicrobial studies of praseodymium complex with glutathione, *Current Science*, 2022, Accepted, In press.